

MASS TRANSPORT PROCESSES ON THE SOUTHWESTERN NEWFOUNDLAND
MARGIN, EASTERN CANADA;
MECHANISMS FOR DEEP WATER SEDIMENT TRANSPORT

by

Michael K. Giles

Submitted in partial fulfilment of the requirements
for the degree of Master of Science

at

Dalhousie University
Halifax, Nova Scotia
June 2010

© Copyright by Michael K. Giles, 2010

DALHOUSIE UNIVERSITY
DEPARTMENT OF EARTH SCIENCES

The undersigned hereby certify that they have read and recommend to the Faculty of Graduate Studies for acceptance a thesis entitled "MASS TRANSPORT PROCESSES ON THE SOUTHWESTERN NEWFOUNDLAND MARGIN, EASTERN CANADA: MECHANISMS FOR DEEP WATER SEDIMENT TRANSPORT" by Michael K. Giles in partial fulfilment of the requirements for the degree of Master of Science.

Dated: June 7, 2010

Supervisors: Dr. David Mosher _____

Dr. Grant Wach _____

Readers: Dr. David Piper _____

Dr. Mladen Nedimovic _____

External Reviewer: Dr. Bruce Hart _____

Department Representative: Dr. David Scott _____

DALHOUSIE UNIVERSITY

DATE: June 7, 2010

AUTHOR: Michael K. Giles

TITLE: MASS TRANSPORT PROCESSES ON THE SOUTHWESTERN
NEWFOUNDLAND MARGIN, EASTERN CANADA: MECHANISMS
FOR DEEP WATER SEDIMENT TRANSPORT

DEPARTMENT OR SCHOOL: Department of Earth Sciences

DEGREE: M.Sc. CONVOCATION: October YEAR: 2010

Permission is herewith granted to Dalhousie University to circulate and to have copied for non-commercial purposes, at its discretion, the above title upon the request of individuals or institutions.

Signature of Author

The author reserves other publication rights, and neither the thesis nor extensive extracts from it may be printed or otherwise reproduced without the author's written permission.

The author attests that permission has been obtained for the use of any copyrighted material appearing in the thesis (other than the brief excerpts requiring only proper acknowledgement in scholarly writing), and that all such use is clearly acknowledged.

TABLE OF CONTENTS

LIST OF TABLES	vi
LIST OF FIGURES	vii
ABSTRACT	xvi
LIST OF ABBREVIATIONS USED.....	xvii
GLOSSARY OF TERMS USED	xviii
ACKNOWLEDGEMENTS	xx
Chapter One: Introduction	1
1.1: Objectives.....	3
1.2: Location and Physiography.....	3
1.3: Regional Geological Background.....	4
1.3.1: <i>Evolution of the Southern Grand Banks Margin</i>	4
1.3.2: <i>Glacial History of Atlantic Canada</i>	12
1.3.3: <i>Seismicity of the Eastern Canadian Margin</i>	14
1.3.4: <i>Salt Tectonics of the Laurentian and South Whale Sub-Basins</i>	17
Chapter Two: Methods.....	19
2.1: Seismic Reflection Methods.....	19
2.2: Seismic Stratigraphy	19
2.3: Data Sets	21
2.4: Age Control.....	29
2.5: Terminology and Classification of Mass Transport Processes and Deposits	29
2.6: Seismic Attribute Analysis	32
2.7: Uncertainty	33
2.7.1: <i>Biostratigraphic Control</i>	33
2.7.2: <i>Error Analysis</i>	34

Chapter Three: Seismic Facies and Stratigraphic Framework.....	37
3.1: Seismic Facies	37
3.2: Key Reflections.....	38
3.3: Seismic Units.....	56
3.4: Stratigraphic Framework.....	65
Chapter Four: Discussion	70
4.1: Seismic Stratigraphic Units and Mass Transport Deposits	70
4.1.1: <i>Interpretation of Seismic Units</i>	70
4.1.2: <i>Comparison to the Scotian and NE Newfoundland margin</i>	83
4.1.3: <i>Identifying Components of Mass Transport Deposits</i>	90
4.1.4: <i>Styles of Mass Transport Deposits</i>	93
4.1.5: <i>Case Study of the late Miocene MTD</i>	93
4.2: Factors Influencing Mass Transport Deposit Location	104
4.3: Classification of MTDs	115
4.4: Channels.....	119
4.5: Impacts of Mass Transport Processes	122
4.5.1: <i>Hydrocarbon Exploration and Production Impacts</i>	122
4.5.2: <i>Societal Impacts</i>	125
Chapter Five: Conclusions	127
References	132

LIST OF TABLES

Table 4.1	The dimensions of the nine MTDs mapped in Unit 2. Thicknesses in km are calculated using a velocity of 2000 m/s. The dimensions of the MTDs are likely larger as the MTDs typically extend outside of the coverage of the Laurentian East 3D volume. The numbering of the MTDs begins with 2 in order to correspond to Figure 4.28.	80
Table 4.2	Classification of MTDs identified in the study area on the southwestern Newfoundland slope (modified from Mulder and Cochonat, 1996; Frey-Martinez et al., 2006; and Moscardelli and Woods , 2008).	117

LIST OF FIGURES

- Figure 1.1** The study area is located 225 km southwest Newfoundland on Canada's continental margin (orange box). The Laurentian Channel is a major glacial feature on the margin. The dashed grey line is the inferred location of the Cobequid-Chedabucto/SW Grand Banks transform margin (modified from Shaw et al., 2002). 5
- Figure 1.2** A multibeam sonar bathymetry map of the study area shows the highly erosive nature of the southwestern Newfoundland margin as depicted by several large scale valley systems. The St. Pierre Slope and Whales Slope represent the boundaries of the study area along the margin. 6
- Figure 1.3** Location of the Scotian Basin and its five sub-basins (SB) shown in yellow: Shelburne, Sable, Abenaki, Laurentian and South Whale. Lahave Platform, Canso Ridge and Burin Platform are structural highs in the region (modified from Wade et al., 1995). 8
- Figure 1.4** Stratigraphy for the Scotian Basin was first proposed by McIver (1972) and further modified by Jansa and Wade (1975a), Wade and MacLean (1990) and Kidston et al. (2007). The stratigraphy for the stratigraphic chart (above) is modified from Wade et al., 1995. The eustatic sealevel curve is from Haq et al. (1987) (from Kidston et al., 2007). 9
- Figure 1.5** Glacier ice extended to the edge of the continental shelves at 20 000 years BP where major ice channels were established in the Bay of Fundy, Laurentian Channel and northeast Newfoundland. Thick dashed lines are ice divides and the thin blue lines represent ice-flow lines. Final retreat of the glacier occurred between 16000 to 10000 years BP (from Shaw et al., 2002 and 2006). 15
- Figure 1.6** The Laurentian Slope Seismic Zone is an area that covers the Cobequid-Chedabucto Fault system and is the location of an increased amount of seismicity. It is estimated that 450 earthquakes occur each years in Atlantic Canada. Yellow circles represent earthquake location with the green circle representing the 1929 Grand Banks Earthquake (from Mosher et al., 2010). 18
- Figure 2.1** Seismic facies are acoustic characteristics based on

	reflection configuration, continuity of reflections, amplitude and frequency content. Continuous, medium-high amplitude; continuous, low-medium amplitude; discontinuous, low-medium amplitude; and chaotic are examples of seismic facies from the southwestern Newfoundland margin.	22
Figure 2.2	Reflection configurations are elements of seismic facies that assist in interpretation of depositional environments (modified from Mitchum et al., 1977).	23
Figure 2.3	Reflection geometries are another component of reflection-character analysis which provides information on the depositional style of the seismic unit (modified from Mitchum et al. 1977).	24
Figure 2.4	Data used for this study cover the continental shelf and slope of the southwestern Newfoundland margin and includes multibeam sonar bathymetry, high resolution 2D seismic reflection, 2D seismic reflection, 3D seismic reflection, and two industry wells (Hermine E-94 and Emerillon C-56).	27
Figure 2.5	Classification of submarine, gravity driven mass transport deposits (modified from Moscardelli and Wood, 2008).	31
Figure 2.6	Confidence map for the seafloor pick of the Laurentian East 3D volume created in SMT Kingdom Suite. Areas in blue (colour bar top right) shows that there is a high degree of confidence in the autopick option of the software, whereas areas represented by white and red show a lower confidence in the software autopick.	36
Figure 3.1	Six seismic facies are identified from the Laurentian East data set and are used to gain insight about the depositional environment and direction of sediment transport of the depositional sequences.	39
Figure 3.2	Inline 7700 from the Laurentian East 3D data set displays six of the eight key seismic reflections mapped across the study area. Five of these key seismic reflections (K99, O50, M70, Q50 and the seafloors) are used to establish the stratigraphic framework for the southwestern Newfoundland Slope.	40
Figure 3.3	Surface render of the K99 horizon from the Laurentian	42

East 3D data set shows that erosional processes occurred at this time, creating erosional scours that run perpendicular (northwest – southeast) to the slope (northeast – southwest). A dendritic morphology is seen in the paleo-topographic highs. In the lower southeast corner, the K99 reflection could not be mapped due to deformation of strata by Argo Salt.

- Figure 3.4** Dip map for the K99 horizon of the Laurentian East 3D data set. Dip angles between the paleo-topographic highs and erosional features range between 3° and 25°. 43
- Figure 3.5** The Z reflection from the Laurentian East 3D data set is the base of a chaotic seismic facies package. In the upper slope of this horizon, erosional features are present and run northwest-southeast. In the lower southeast corner of the data set, diapirism from the Argo Salt is apparent. 45
- Figure 3.6** Surface render of the M70 horizon from the Laurentian East 3D data set. Paleo-topographic highs appear in the northeast corner as well as along the upper slope of the Newfoundland Margin. Erosional scours dissect topographic highs along the upper slope. In the western region of the data set, the top corners of rotated reflection packages are ridges that run north-south. In the southeast (black circle) region of the data set, the M70 reflection could not be mapped as result of Argo Salt diapirism. 46
- Figure 3.7** The dip map for M70 horizon from the Laurentian East 3D data set shows that the paleo-topographic highs in the northeast corner and along the western region of the data set have dip angles between 15° and 30°. The centre region of this horizon is relatively flat. 47
- Figure 3.8** Inline 7590 from the Laurentian East 3D data set show the other two key seismic reflections (C Base and C Top) above the M70 reflection. The red arrow shows where the C base reflection cuts into parallel reflections before “stepping up” in the strata and continuing seaward. Faults are represented by dashed black lines that terminate at the base of the chaotic package below M70. 49
- Figure 3.9** Surface render of the C Base horizon from the Laurentian East 3D data set. The C Base horizon is erosive in nature as seen by the occurrence of erosional cuts in the eastern and southwestern regions. 50

Figure 3.10	Surface render of the C Top horizon from the Laurentian East 3D data set. The geomorphology of this surface is affected mostly by the chaotic sediment package deposited below it and results in a rugose surface.	51
Figure 3.11	Surface rendering of the Q50 horizon from the Laurentian East 3D data set. The Q50 reflection is missing from the western region of the data set and probably has been removed by recent erosional processes. Erosional features are seen between paleo-topographic highs in this surface as well as having similar characteristics of the modern seafloor.	52
Figure 3.12	Dip map for the Q50 horizon from the Laurentian East 3D data set. There is little change in the degree of dip in this horizon. In the northeast and western sections of this horizon line features that run northeast – southwest are artifacts created from missed picks in the data.	53
Figure 3.13	Seafloor render from the Laurentian East 3D data set displaying the dendritic nature of the modern geomorphology of the southwestern Newfoundland Margin. The modern seafloor of the southwestern Newfoundland Slope lies in water depths of between 400 and 3000 mbsl (using an average velocity of 1500 m/s).	54
Figure 3.14	Dip map for the seafloor render of the Laurentian East 3D data set showing that the walls of inter-canyon ridges have dip angle of between 10° and 25°. Although the southeast corner of the study area has erosional features, it is not as complex as the western portion of the study area.	55
Figure 3.15	Seismic profile 34 from the Geological Survey of Canada – Atlantic Research cruise 2007_020 showing 300 m of relief (using a velocity of 1500 m/s) on Whale Slope. The amphitheatre shape of the erosional feature is seen in the multibeam bathymetry map (inset top left). The location of seismic profile 34 is represented by the blue on the inset map.	57
Figure 3.16	The Laurentian East 3D data set was divided into three seismic units numbered 1 through 3 with 1 being the oldest. Inline 7700 from the data set shows the four key seismic reflections used to define the lower and upper limit of each unit. Unit 1 is bounded by the K99 and M70	

	57 reflections, Unit 2 is between M70 and Q50, and Unit 3 is defined by Q50 and the seafloor.	58
Figure 3.17	Line drawing of Inline 7700 showing the three seismic units defined in the Laurentian East 3D data set. The lower section of Unit 1 consists of parallel reflections that were offset by faults (dashed black lines). In the upper portion of Unit 1, reflections are rotated in the upper slope while further seaward reflections are chaotic in nature. Unit 2 consists mostly of stacked packages of chaotic reflections. Parallel reflections interbedded with thin chaotic reflection packages define Unit 3.	59
Figure 3.18	Thickness map for Unit 1 shows that the unit is of a uniform thickness as shown by the green. Blues in the northeast and southwest indicate thicker sedimentary sections.	60
Figure 3.19	Inline 7950 from the Laurentian East 3D data set shows the deformation caused by Argo Salt diapirism in Units 1 and 2. The Argo Salt prevents correlation of some reflections within the data set. Faulting occurs through Unit 1 with faults terminating at the base of the thick chaotic package or at the M70 reflection.	61
Figure 3.20	Inline 7695 from the Laurentian East 3D data set shows 300 to 450 m thick rotated blocks of reflections that are located on the upper Newfoundland Slope. The inset in the top right corner is a line drawing representing the interpretation of the rotated reflections.	63
Figure 3.21	Thickness map for Unit 2 shows that the thickest section in this unit is about 450 m and runs from the northwest to the southeast (represented by the blue).	64
Figure 3.22	Unit 3 is relatively thin compared to Units 1 and 2. The thickest section for Unit 3 is found in the eastern region of the data. The unit is thinnest where presumed recent erosional processes removed material on the modern seafloor.	66
Figure 3.23	Age control diagram for Hermine E-94 well. Comparison of wiggle plot and seismic section to synthetic seismogram calculated from Sonic log.	67
Figure 4.1	This rendering of the K99 horizon shows Late Cretaceous	71

canyons (the area of which are represented by white arrows) and inter-canyon ridges.

- Figure 4.2** The Laurentian East amplitude volume shows formation of mini basins in response to the diapirism of the Argo Salt Formation in the southeast corner of the study area. The yellow outlined MTD is late Miocene in age. The salt diapirs are outlined in green. 72
- Figure 4.3** Seaward dipping faults present in Unit 1 are shown in a “similarity volume” of the Laurentian East data set. (A) Laurentian East Inline 7193 shows that the seaward dipping faults extend across the data set. (B) An enlargement from (A) represented by the black rectangle shows these faults extend from the red K99 reflection event and terminate at either the Z reflection event (yellow horizon) or the M70 event reflection. 73
- Figure 4.4** Wavy concordant reflections below the Late Miocene MTD (represented by the purple) from the Laurentian East Crossline 5435 are interpreted to be sediment waves formed in response to bottom currents. 75
- Figure 4.5** The mid-late Miocene MTD: (A) In areas of the Laurentian East data set, the MTD has thickness up to 500 ms. (B) Shows the mid-late Miocene MTD in the similarity volume as well as other small MTDs above it. MTDs are represented differently (darker and not continuous) compared to the surrounding sediments which are interpreted as parallel and continuous bedding. (C) This MTD covers an estimated area of 900 km² as mapped in the Laurentian East and TGS-NOPEC data sets. It is represented as a translucent outline over the M70 surface render. 76
- Figure 4.6** Sediment waves from the St. Pierre Slope. (A) An un-interpreted section of Line 03 from Cruise 2007020. (B) Undulating reflections above M70 are interpreted to be sediment waves (purple package). A fault extends from the seafloor and soles in this package. 78
- Figure 4.7** (A) Represents an un-interpreted profile from Inline 7656 of the Laurentian East data set. (B) Stacks of recurring MTDs (coloured polygons) are interpreted between M70 (blue) and Q50 (orange) with volumes ~ 60 km³ and covering areas ≤ 400 km². 79

Figure 4.8	The Q50 and Seafloor rendered surfaces have canyon systems located in similar positions as denoted by canyon incisions (A, B, C, E, and G) and topographic highs (D and F). This observation suggests that the process responsible for the Q50 surface recurs through the evolution of the margin.	82
Figure 4.9	Location map of the studies used for comparison with the southwestern Newfoundland margin: 1 – MacDonald (2005), 2 – Brake (2009), 3 – this study, and 4 – Deptuck (2003).	84
Figure 4.10	Comparison chart to show how different areas of the Canadian’s eastern margin are related in terms of estimated sediment thickness and sedimentary processes. The yellow, purple, and blue represent Units 1 to 3 on the southwestern Newfoundland margin. Time scale is modified from the International Stratigraphic Chart proposed by the International Commission on Stratigraphy (Gradstein et al., 2004).	86
Figure 4.11	Time slice of coherency volume of the Laurentian East data set showing the incoherent nature of the late Miocene MTD. The MTD is represented by the orange polygon where the incoherent reflections as seen in both cross section and plan views.	91
Figure 4.12	MTDs are broken into three domains: headwall, translational, and toe domains (Frey-Martinez et al., 2006; and Bull et al., 2009). In each domain certain components are typically found (e.g. headwall domains have head scarps and extensional ridges and blocks). (A) An un-interpreted section from Laurentian East Inline 7226. (B) The line drawing of the mid-late Miocene MTD shows the different domains and components of a MTD as well as an example of frontally emergent MTD.	92
Figure 4.13	Inline and crossline profiles of the late Miocene MTD showing the N to S direction of travel.	95
Figure 4.14	The basal surface of the late Miocene MTD showing. Locations of the seismic profiles (black lines) in figures are shown.	96
Figure 4.15	(A) Examples of rotated blocks in Laurentian East Inline	97

7687. (B) Deformed blocks which have moved from the headwall domain into the translational domain are preserved in the failure deposit.

- Figure 4.16** Rotated slump blocks from the upper central slope of the late Miocene MTD. A section between the blocks and the debris flow where the deposit is not preserved is represented by either a zone of bypass, or the failure has been removed by subsequent failures. 98
- Figure 4.17** The top of the Late Miocene MTD has a rugose topography created by slumping. The black outlines represent specific regions where expression of these block are most prominent. Outside the black polygons, the deposit is represented by a debris flow style of failure. The yellow arrows indicate the source and transport direction of the rotated and deformed blocks. The larger orange arrows show the location of two Miocene-aged channels. 99
- Figure 4.18** The blocky nature of the late Miocene MTD is shown in this arbitrary seismic profile from the Laurentian East 3D volume. 100
- Figure 4.19** The large gouge seen in the base of late Miocene MTD on Laurentian East Inline 7130. The gouge deeply cuts the underlying stratigraphy indicating it was highly erosive in nature. 102
- Figure 4.20** The late Miocene MTD is penetrated by syndepositional salt tectonics, evident in Crossline 2815 from the Laurentian East data set. A ramp landward of the salt diapirs is over steepened as a result of the salt movement. From this profile at the lower slope, the MTD has travelled some distance and the failure can be described as a debris flow. 103
- Figure 4.21** The similarity volume of the Laurentian East data set show the seaward dipping faults in both in plan view and in cross section. These faults are typically found mid slope and are Miocene in age. Inset A is a detailed plan view of the faults and shows their polygon shape. Inset B shows the relationship of these faults going from the cross section to the plan view. Faults extend to the M70 horizon event or are cut by the late Miocene MTD shown here as the orange polygon. 107

Figure 4.22	Sedimentary bedforms identified at the base of the late Miocene MTD are interpreted to be sediment waves. The sediment waves are only mapped in a small area as they have been eroded in the upper slope by the overlying late Miocene MTD.	108
Figure 4.23	The sediment waves have influenced the morphology of the late Miocene MTD as seen in crossline 5435 from the Laurentian East data set. Rotated blocks located in the western edge of the deposit occur on the flank or in the trough of the sediment waves.	110
Figure 4.24	Comparison of global sealevel of Zachoes et al., 2001; Miller et al., 1996; Haq et al., 1987; and Miller et al., 2005 (image modified from MacDonald, 2006).	113
Figure 4.25	The late Miocene MTD is classified as a frontally emergent MTD but it is also laterally confined at the western edge of the deposit as seen in crossline 4698 and the surface render from the Laurentian East data set.	116
Figure 4.26	After the late Miocene (~M70), MTDs became smaller but their frequency increased. Between M70 and Q50, at least nine other MTDs are mapped (1 represents the top of the late Miocene MTD) with areas between 30 and 400 Km ² . Plio-Pleistocene MTDs are represented by the numbers 2-10 and different coloured polygons which overlay the M70 surface render.	118
Figure 4.27	A broad v-shaped erosional feature seen in the top of a Plio-Pleistocene MTD with high amplitudes is interpreted to be a channel. Other high amplitude, concave reflections at the top of the same MTD are also interpreted to be channels. The presence of these channels suggests that sediment was transported across the top of these MTDs and deposited further downslope.	120
Figure 4.28	Amplitude map of the top of a Plio-Pleistocene MTD. The high amplitudes (yellow-orange-red) indicate sediment infill of sinuous channels that run north south. Sediment from the shelf bypassed the upper and middle slope as it was transported through these channels to the lower slope.	121

ABSTRACT

The importance of sediment mass failure processes in the evolution of passive continental margins is increasingly recognized amongst the scientific community. The southwestern Newfoundland margin is the location of the tsunami-inducing 1929 Grand Bank's Landslide and today is an active exploration frontier. Seismic reflection data from the slope provides evidence of successive mass failures at a variety of scales. The occurrence of stacked, regionally extensive mass transport deposits (MTDs) with volumes up to 150 km³ indicates that sediment mass transport was a significant process in the evolution of the margin during the Cenozoic. Initiation of failures on the southwestern Newfoundland margin is attributed to earthquakes. Frequency of earthquakes and pre-conditioning factors explain differences in size of MTDs on the margin. Late Miocene MTDs were larger due to high sedimentation rates and low frequency earthquakes. Younger sediment failures on the margin were smaller due to high sedimentation rates and higher frequency earthquakes which prevented thick sediment accumulation between failures. This study shows the prevalence of MTD's in the Cenozoic stratigraphic succession of the southwestern Newfoundland continental margin. Clearly, sedimentation and exploration models of continental slope environments must take better account of the mass failure processes for sedimentation distribution of source/reservoir/trap development.

LIST OF ABBREVIATIONS USED

CCGS	Canadian Coast Guard Ship
CMP	Common mid point
cm³	Centimetre cubed
Hz	Hertz
kHz	Kilohertz
km	Kilometres
km²	Kilometre squared
m	Metres
mbsf	Metre below seafloor
ms	Milliseconds
m/s	Metres per second
MTD	Mass transport deposit
STP	St. Pierre Slope data set
TWTT	Two-way travel time

GLOSSARY OF TERMS USED

<u>Aggradation:</u>	The vertical build up of a sedimentary sequence (Posamentier and Allan, 1999).
<u>Attached MTD:</u>	Regional extensive (100s to 1000s km ²) mass sediment failure triggered by regional events such as earthquakes, long shore currents, or hydrate dissociation (Moscardelli and Wood, 2008).
<u>Canyon:</u>	Steep-sided, erosional features that are typically linear and are directed down gradient to the base of continental slopes. They typically originate in two ways: 1) turbidity currents and 2) slope failures (Pratson et al., 2007).
<u>Debris Flow:</u>	Failure that is mainly muddy in composition and have disturbed and/or indistinct structures characterized by acoustically transparent and chaotic facies (Mulder and Cochonat, 1996).
<u>Detached MTD:</u>	Smaller scaled (≤ 10 km ²) mass sediment failure that is triggered by local mechanisms such as gravitational instabilities (Moscardelli and Wood, 2008).
<u>Highstand:</u>	The interval of time during a cycle or cycles of relative change of sealevel when sealevel is above the shelf edge in a given local area (Mitchum, 1977).
<u>Lowstand:</u>	The interval of time during a cycle or cycles of relative change of sealevel when sealevel is below the shelf edge (Mitchum, 1977).
<u>Mass Transport Deposit (MTD):</u>	The resulting deposit of a mass sediment failure event which can be composed of many different styles of failures including: slides, slumps, and debris flows.
<u>Mass Transport Process:</u>	Is the mass movement of failed material driven directly by gravity or other body forces, rather than tractive stresses associated with fluid motion (Lee et al., 2007).
<u>Pre-conditioning Factor:</u>	Sedimentological and structural feature responsible for weakening the sediment column and preparing

the sediment for failure.

<u>Progradation:</u>	The lateral outbuilding, or progradation, of strata in a seaward direction (Posamentier and Allan, 1999).
<u>Regression:</u>	A seaward movement of the shoreline indicated by the seaward migration of the littoral facies (Mitchum, 1977).
<u>Seismic Attribute:</u>	A measure of seismic data that visually enhances or quantifies features of interpretational interest (Chopra and Marfurt, 2007).
<u>Seismic Facies Analysis:</u>	Reflection patterns that provide insight into depositional environments (Sangree and Widmier, 1977) where seismic facies units are based on reflection configuration, continuity of reflections, amplitudes and frequency content (Veeken, 2007).
<u>Similarity Attribute:</u>	The lateral continuity or discontinuity of bedding based on the degree of dip (Chopra and Marfurt, 2007).
<u>Slide:</u>	The movement of essentially rigid, internally undeformed masses along discrete slip planes (Lee et al., 2007).
<u>Slump:</u>	A type of slide in which blocks of failed material rotate along curved slip surfaces (Lee et al., 2007).
<u>Transgression:</u>	A landward movement of the shoreline indicated by the landward migration of a given stratigraphic unit (Mitchum, 1977).
<u>Trigger Mechanism:</u>	An external factor that either increases the stress acting on the seafloor sediment, reduces the strength of the sediment (increased pore pressure), or a combination of the two, that results in the triggering of a slope failure (Lee et al., 2007).

ACKNOWLEDGEMENTS

I would like to extend my greatest thanks and appreciation to my supervisors Dr. David Mosher (Geological Survey of Canada – Atlantic (GSC-A)) and Dr. Grant Wach (Dalhousie University). They provided a project that was truly captivating and thought-provoking and allowed me to investigate new ideas as this thesis developed. I would also like to thank the remainder of my committee, Dr. David Piper (GSC-A) and Dr. Mladen Nedimovic (Dalhousie University) for their many discussions during this work. John Jenson of ConocoPhillips Canada is thanked for his assistance and effort during the course of this project.

Thanks are extended to my family who have always supported me through my endeavours and have provided the support and motivation to allow me to achieve my goals. To all the friends I have made over the last few years, you have truly made my experience at Dalhousie University unforgettable - Thank you. To the “team”, Shawn Goss, Calvin Campbell, and Ginny Brake, without our many discussions, late nights at B.I.O. and coffee breaks this thesis would not be what it is. I wish you all the best in your future endeavours.

Research for this study was funded by the Nova Scotia Offshore Energy Technical Research Association grant No. 51834 to Drs. G. Wach and D. Mosher and a Pengrowth-Nova Scotia Petroleum Innovation Grant and Lew King Endowment to M. Giles. The three-dimensional Laurentian East data set was donated by ConocoPhillips Canada to the Geological Survey of Canada – Atlantic. Two-dimensional seismic reflection data (St. Pierre Slope and TGS-NOPEC) and multibeam data were available through the GSC-A. SMT Kingdom Suite licenses for seismic interpretation supplied by Seismic Micro Technologies Inc. and were available through the GSC-A and Dalhousie University.

Chapter One: Introduction

Continental margin slopes cover an estimated area of 28.7 million km² or 15% of the Earth's surface (Drake and Burk, 1974; Nardin et al., 1979), and host the thickest sections of unconsolidated sediment of any other deposition environment. Sediment mass failures are as a significant process along continental slopes and are a key mechanism for transporting sediments to the deep ocean. The upper continental slope often acts as a temporary storage for land-derived sediments. However, when the stability of the slope deposits decrease, periodic failure occurs and sediments are transported downslope. Sediment mass failures have occurred on continental margins with varying slopes, tectonic regimes, and sediment distribution patterns, such as the volcanic islands of the Canary Island's (Masson et al., 1998); passive glaciated margins such as Storegga, Norway (Haflidason et al., 2004); Trinity Peninsula, Antarctica (Imbo et al., 2003); Svalbard margin, Arctic Ocean (Vanneste et al., 2006); and the Gulf of Alaska (Schwab and Lee, 1988). Sediment mass failures result in mass transport deposits (MTD) and these MTDs can represent a significant proportion of the sedimentary column of continental margins from around the world. Studies from the Scotian margin (Campbell et al., 2004), Egyptian margin (Garziglia et al., 2008), and the Gulf of Mexico (Weimer and Slatt, 2006) show that MTDs represent 35 to 60 % of the sedimentary columns in those regions. This suggests that mass transport processes occur globally and are important mechanisms for deep water sediment transport.

Over the past two decades more than 20 oil/gas bearing basins that extend off the shelf into the slope and rise regions of continental margins have been discovered. It is

estimated that nearly 9% of the World hydrocarbon supplies now come from these environments (Khain and Polyakova, 2004). The currently developed deep water (500 m or more below sea level - bsl) oil and gas fields are restricted to passive margins of the Atlantic Ocean (Khain and Polyakova, 2004). As the demand for hydrocarbons increases and exploration expands into deeper waters, it also brings with it further development of the offshore in terms of platform and pipeline infrastructure and an increasing number of submarine cables. The ability to recognize portions of the World's continental margins that are more susceptible to failure is important as today's demand for hydrocarbons is steadily increasing. Submarine failure processes are also a societal concern because as coastal areas become increasingly more populated, the impact of a possible tsunami caused by an underwater landslide is greatly magnified. Therefore, it is critical to understand the geological processes of slope environments and recognize the depositional patterns, structural controls and geohazards associated with these complex regions.

The southwestern Newfoundland margin is an active area for hydrocarbon exploration and is the location of historic submarine landslide with a known trigger. The 1929 Grand Banks Landslide occurred in the study area on the upper St. Pierre Slope and was triggered by a M7.2 earthquake (Doxsee, 1948; Heezen and Ewing, 1952; Piper and Aksu, 1987). The occurrence of a recent submarine landslide with a known trigger in the study provides insight into the mechanisms responsible for MTDs present in the Cenozoic section of the region and helps quantify the importance of these processes in the evolution of the margin.

1.1: Objectives

It is the purpose of this study to assess the significance of mass transport processes in the evolution of the southwestern Newfoundland margin. This objective will be achieved by evaluating the volume and seismic character of mass transport deposits (MTDs) and the stratigraphic interval within which they occur. In this context, this study will address the potential triggering mechanisms and pre-conditioning factors that lead to mass failures. These objectives will be accomplished by establishing a late Cenozoic stratigraphic framework for the southwestern Newfoundland margin incorporating published stratigraphic markers (Piper and Normark, 1989; Piper et al., 2005) and through the use of seismic sequence stratigraphy, seismic facies analysis, and geomorphologic analysis of 2D and 3D seismic reflection data.

1.2: Location and Physiography

The southwest Newfoundland Slope strikes east – west and lies off the coast of Newfoundland on the passive continental margin of the western North Atlantic Ocean. The shelf break lies between 400 and 500 mbsl with the transition to the Sohm Abyssal Plain at 5000 mbsl (Piper et al., 1984; Mosher and Piper, 2007). The slope gradient along the southwest Newfoundland Slope varies between a gradient of 2° and 5° with the steepest angles at the shelf break (Mosher and Piper, 2007). The morphology of the southwest Newfoundland margin is highly incised by canyon and valley systems with numerous failure escarpments present on the modern slope (Mosher and Piper, 2007). The study area is located on Newfoundland's southwestern continental slope, extending

from the St. Pierre Slope in the west, to the Whale Slope in the east (44°04'N to 45°09'N and 54°20'W to 56°14'W) (Figure 1.1 and 1.2).

1.3: Regional Geological Background

1.3.1: Evolution of the Southern Grand Banks Margin

The southern margin of the Grand Banks is a transform margin that formed during the earliest rifting between North America and Africa. This rifting began in the Late Triassic affecting the eastern Canadian margin from the northern Grand Banks to the Gulf of Maine and continued to create rift basins until the Cretaceous. Unlike the Grand Banks, rifting on the Scotian margin ended with seafloor spreading during the Early to Middle Jurassic. The southern margin of the Grand Banks continued to be an active transform margin as the eastern margin experienced continental rifting between Iberia and North America. This rifting created a complex margin offshore of Newfoundland with the development of several rift basins (Jansa and Wade, 1975a; Keen et al., 1990). Verhoef and Jackson (1991) show that the isostatic compensation of the southwest Newfoundland transform margin is essentially local and implies that the mechanical weakness of the transform boundary at the time of formation is parallel to lithospheric flow. On the rifted Scotian margin, by comparison, isostatic compensation is regional, indicating flexural coupling of the oceanic and continental lithosphere due to extension (Verhoef and Jackson, 1991). The southwestern region of the Grand Banks experienced a similar rift-drift history as the Scotian margin in which a series of connected Mesozoic-Cenozoic depo-centres formed as a result of horst-and-graben formation and salt tectonism (Wade and MacLean, 1990). This series of depo-centres is collectively called the Scotian Basin

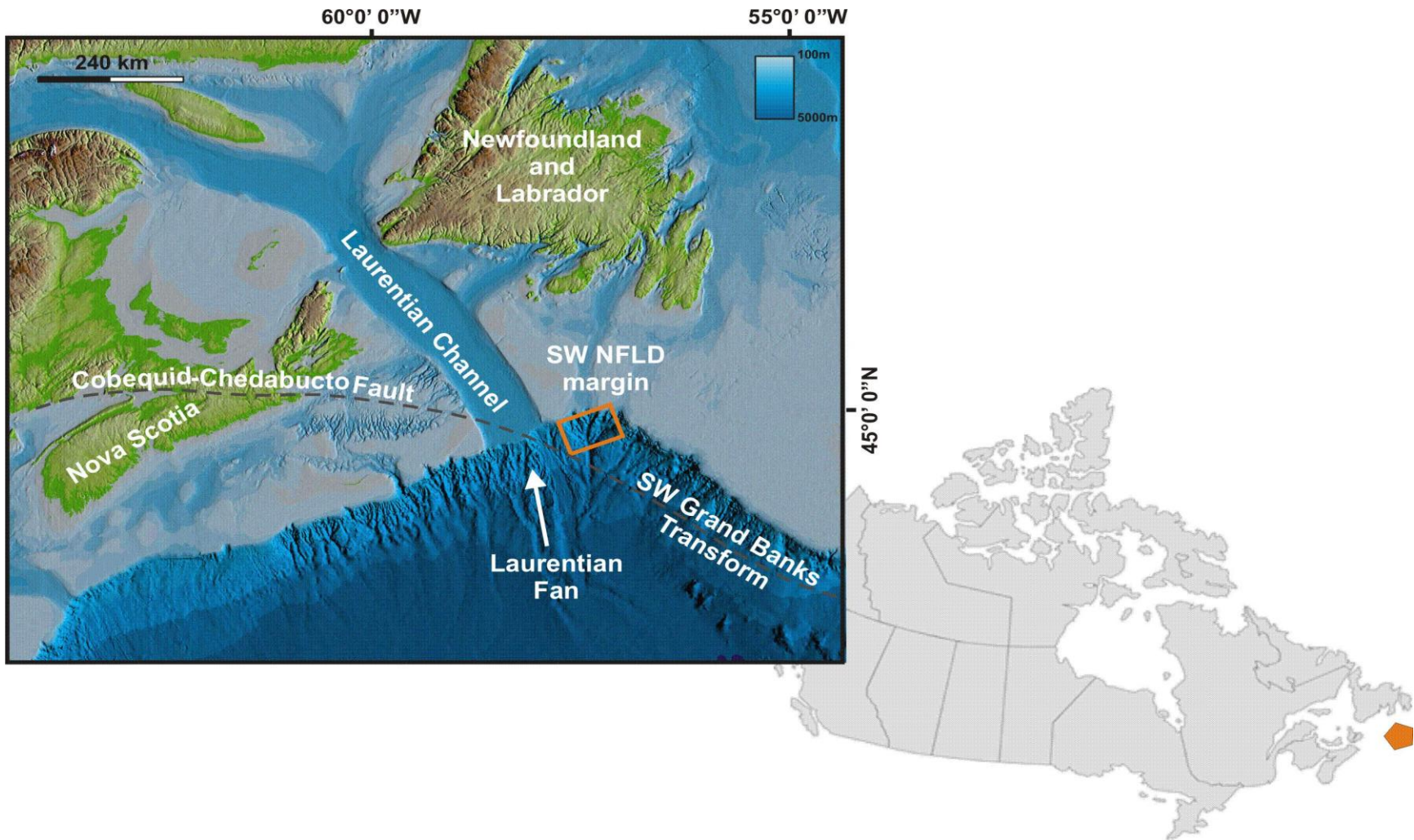


Figure 1.1: The study area is located 225 km southwest of Newfoundland on Canada's continental margin (orange box). The Laurentian Channel is a major glacial feature on the margin. The dashed grey line is the inferred location of the Cobequid-Chedabucto/SW Grand Banks Transform margin (modified from Shaw et al., 2002).

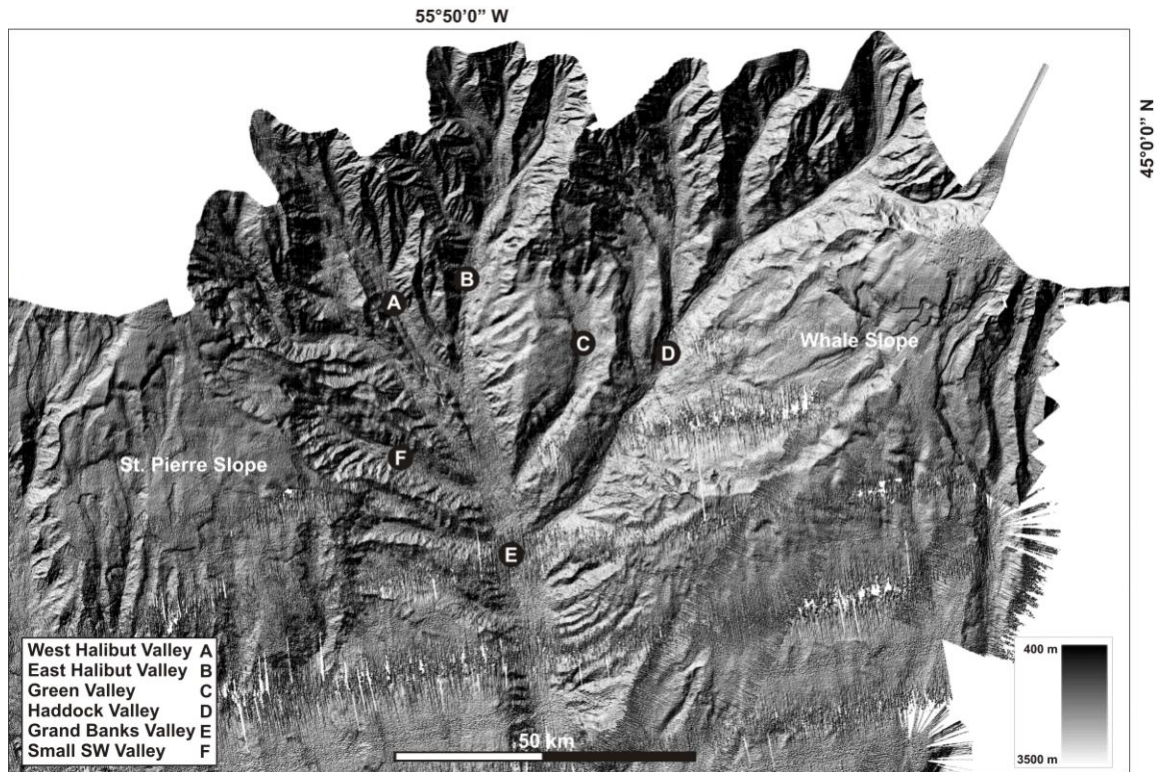


Figure 1.2: A multibeam sonar bathymetry map of the study area shows the highly erosive nature of the southwestern Newfoundland margin as depicted by several large scale valley systems. The St. Pierre Slope and Whales Slope represent the boundaries of the study area along the margin (modified from Mosher and Piper, 2007).

and is divided into five sub-basins (Fig.1.3). From southwest to northeast, these sub-basins are: Shelburne SB, Sable SB, Abenaki SB, Laurentian SB, and South Whale SB. The southwestern Newfoundland margin is found in the South Whale SB, northeast of the Scotian margin. Periods of post-rifting subsidence occurred during the Jurassic, Cretaceous and the Cenozoic, which deepened the connected sub-basins (Louden, 2002), and resulted in the accumulation of over 12 km of sediments (Wade and MacLean, 1990).

The stratigraphy of the Scotian Basin was initially proposed by McIver (1972) and further modified by the work of Jansa and Wade (1975a), Wade and Maclean (1990), and Kidston et al. (2002; 2007) through investigation of industry wells and seismic data from the Scotian Shelf and Slope. Mesozoic, and in part Cenozoic, sedimentary rocks of the Scotian Basin overlie a crystalline basement consisting mostly of Paleozoic metasedimentary rocks and plutonic granites except in the Burin Platform (Fig. 1.3 and 1.4) where they are locally deposited on upper Paleozoic sedimentary strata. During the Triassic phase of continental breakup, the formation of horsts and grabens and shallow marine conditions allowed the accumulation of thick continental sediments of the Eurydice Formation to occur in the Scotian Basin. Overlaying these continental sediments are the evaporate deposits of the Argo Formation (Jansa and Wade, 1975b). Accumulation of these thick extensive evaporite deposits (salt gypsum, and anhydrite), perhaps 1 – 2 km in thickness, was driven by a hot, dry climate and margin uplift. Deposition of the Argo Formation continued into the Early Jurassic as a shallow sea covered the basin during marine transgression (Kidston et al., 2002). Sediments of the Iroquois and Mohican formations completed the process of infilling the rift grabens and

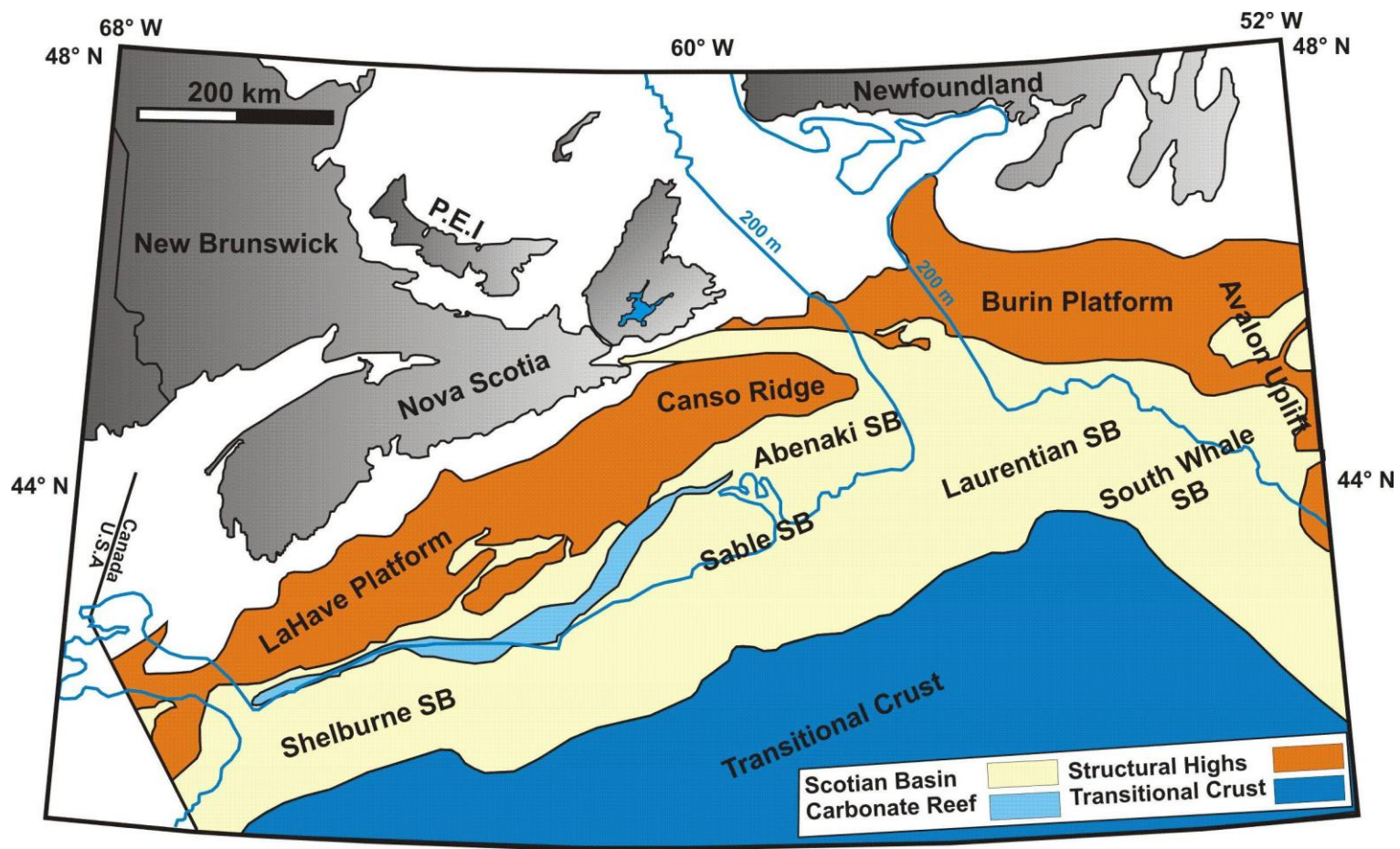


Figure 1.3: Location of the Scotian Basin and its five sub-basins (SB) shown in yellow: Shelburne, Sable, Abenaki, Laurentian and South Whale. LaHave Platform, Canso Ridge and Burin Platform are structural highs in the region (modified from Wade et al., 1995).

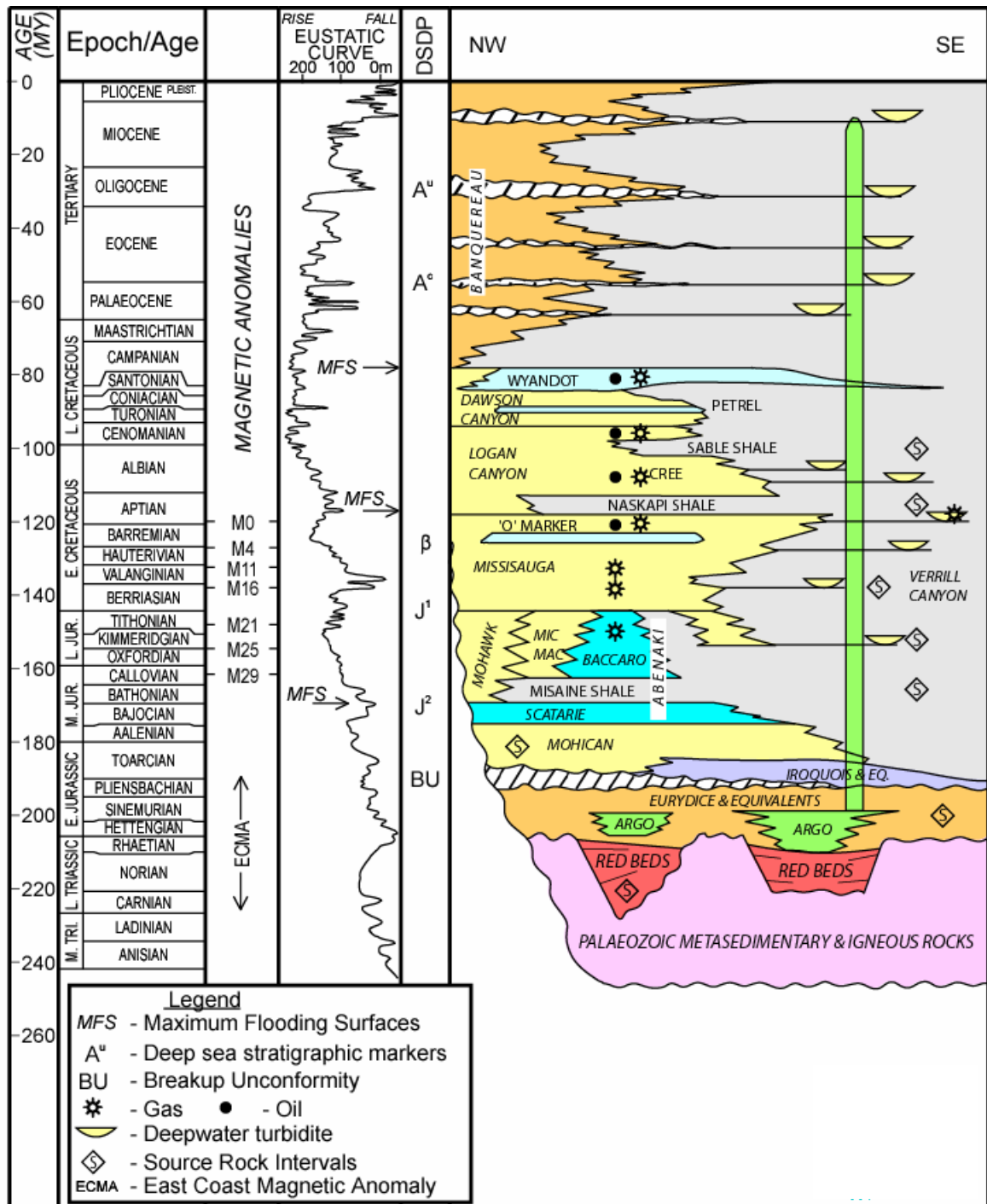


Figure 1.4: Stratigraphy for the Scotian Basin was first proposed by McIver (1972) and further modified by Jansa and Wade (1975a), Wade and MacLean (1990) and Kidston et al. (2007). The stratigraphy for the stratigraphic chart (above) is modified from Wade et al., 1995. The eustatic sealevel curve is from Haq et al. (1987) (from Kidston et al., 2007).

overlap the basement highs of the post-breakup surface (Wade and MacLean, 1990). During the Middle and Upper Jurassic, marine conditions were established across the Scotian Basin as represented by the deposition of continental clastics, shallow marine sediments, a shelf carbonate facies (McIver, 1972) and a basinal shale facies (Wade and MacLean, 1990). Sedimentation continued during this period and initiated the mobilization of deeply buried Jurassic salt resulting in vertical and lateral intrusion into overlying sediment that continues to the present day (Wade and MacLean, 1990; Kidston et al., 2002).

The eastern margin of Canada was highly affected by the breakup of the Iberian and North American plates during the Late Jurassic. The Grand Banks south of Newfoundland was the most strongly affected area, experiencing uplift, deformation and extensive erosion of Jurassic sediments (Jansa and Wade, 1975b). This breakup unconformity is known as the Avalon Unconformity and is observed across the inner part of the Canso Ridge, the Orpheus Graben, Burin Platform, the western flank of the Laurentian Subbasin and eastern flank of the South Whale Subbasin of the Scotian Basin (Fig. 1.3) (Wade and MacLean, 1990).

During the Early Cretaceous, the Scotian Basin was characterized by the deposition of the fluvial-deltaic Missisauga and Logan Canyon formations. The Missisauga Formation was deposited by a major river system which probably drained much of the northeastern part of the Canadian Shield (McIver, 1972). Deltaic successions of this formation are best known in subsurface of the Sable Island area. They probably also occur in parts of the

Laurentian and South Whale Subbasins. A marine transgression during the early Late Cretaceous resulted in the transition from deltaic sands to a succession of marine sediments of the Logan Canyon and Dawson formations (McIver, 1972; Kidston et al., 2002).

The Late Cretaceous experienced a period of sea level rise and basin subsidence resulting in the deposition of marine sediments of the Wyandot Formation (Jansa and Wade, 1975b; Kidston et al., 2002). Cretaceous sediments and the entire Cenozoic sedimentary section above the Wyandot Formation are assigned to the Banquereau Formation (McIver, 1972). The Scotian Basin experienced several major unconformities relating to sea level lowering during the Tertiary. These unconformities are prominent during the Paleocene, Oligocene and Miocene as fluvial and deep-water currents eroded unconsolidated sediments and transported them to the continental slope and abyssal plain (Kidston et al., 2002; Brake, 2009; Campbell and Deptuck, in press).

The Miocene and Pliocene evolution of the Scotian Basin is generally not well known. Thick, predominantly muddy Miocene successions developed both on the Scotian and southwestern Newfoundland slopes (Wade et al., 1995; Wielens et al., 2004). During the Miocene, major channelling of the existing continental shelf occurred (Wade and MacLean, 1990) and sediment distribution was influenced by the Western Boundary Undercurrent while periods of intensified bottom current activity also influenced Late Pliocene sedimentation (Myers and Piper, 1988; Piper 2005). Beginning in the Early Pliocene and continuing into the mid Pliocene, a pronounced change in sedimentation

style occurred when turbidites began to accumulate on the Laurentian Fan (Uchupi and Austin, 1979; Piper and Normark, 1989) and turbidity currents formed leveed channels on the St. Pierre Slope (Piper et al., 2005).

Quaternary evolution of the Newfoundland margin was dominated by alternating glacial and inter-glacial processes. Several hundred metres of glacial and marine sediments were deposited on the outer shelf and upper slope of the region (Piper, 2005; Piper et al., 2005). Prior to the Laurentian Channel supplying material to the greater Laurentian Fan region, the ancestral St. Lawrence River delivered coarse grained material to the Laurentian Fan during the Late Pliocene to Early Quaternary (Skene and Piper, 2006). The morphology of the Laurentian Fan during that time was typical of a deep-sea fan (Piper and Normark, 1982; Skene 1998). Sediment accumulation on the St. Pierre Slope was principally prodeltaic muds seaward of deltas (Piper and Normark, 1982). Salt deformation of shallow strata in the Laurentian Subbasin (Shimeld, 2004) resulted in substantial offsets in Quaternary strata on the continental shelf (Piper and Gould, 2004) as well as in the deep basin (Ledger-Piercey and Piper, 2005).

1.3.2: Glacial History of Atlantic Canada

During the Tertiary, both the Scotian and southwestern Newfoundland margins experienced major episodes of sea level lowstands (Piper and Normark, 1989). These periods resulted in the basinward progradation and accumulation of prodeltaic shales and of large scale canyon incision along the outer shelf. The onset of Pliocene terrestrial glaciations induced rapid sedimentation on the Laurentian Fan as well as southwestern

Newfoundland and Scotian slopes. The first shelf-crossing glaciations occurred during the mid-Pleistocene (about 0.5 Ma) and since that time, the continental slope has been dominated by proglacial sediment deposition, with little sediment accumulated at sealevel highstands (Mosher et al., 2004).

During the Wisconsinan glaciation, eastern Canada was affected by the retreats and advances of the Laurentide ice sheet and local ice caps of the Appalachians. The general pattern of major glacial fluctuations in eastern Canada led to subdivision of the Wisconsinan glacial stage into three substages: Early Wisconsinan (~120000 years – 65000 years BP), Mid-Wisconsinan (65000 years – 23000 years BP) and Late Wisconsinan (23000 years – 10000 years BP) (King and Fader, 1986). During the Early Wisconsinan (70000 years to 50000 years BP), the continental shelf was covered by a dry-based continental ice sheet that extended to the shelf edge and was predominately an erosional phase. Following this erosional phase, the Mid-Wisconsinan saw the beginning of glacial recession (50000 years to 45000 years BP) with deposition of the upper slope till, development of lift-off moraines, and deposition of early glaciomarine sediments on the shelf. At this time, ice remained grounded on the banks. The maximum recession of the Laurentide ice sheet occurred between 45000 years and 32000 years BP and was characterized by minor surges and retreats and deposition of till tongues along the main moraine. The end of the Mid-Wisconsinan represents the general retreat of the ice sheet from the continental shelf. During Late Wisconsinan, the Laurentian Channel acted as a major ice corridor for the Laurentide ice sheet (King and Fader, 1990; and Hughes 1998). The Laurentian Channel Ice Stream drained an extensive catchment extending north into

Quebec and Labrador as well as eastern New Brunswick, Prince Edward Island and northern Nova Scotia (Shaw et al., 2006). Ice from western Newfoundland converged with Labrador ice and flowed southwest to the Gulf of St. Lawrence. Along the southwestern Newfoundland coast, ice drained down Hermitage Channel converging with the Laurentian Channel Ice Stream (Shaw et al., 2006). Between 20000 years and 18000 years BP, the Laurentian Channel Ice Stream terminated at the shelf edge and formed the largest calving margin for the region (Fig. 1.5). Compared to the Scotian and southwestern Newfoundland shelves where ice had retreated from the shelf edge at around 18000 years BP, ice persisted at the shelf edge of the Laurentian Channel, indicated by evidence from the Laurentian Fan (Skene and Piper, 2003). Between 14000 and 13000 years BP the ice sheet began a rapid calving retreat through the Gulf of St. Lawrence into the St. Lawrence Estuary. At around 12000 years BP a small ice cap was still present on some shelf banks while ice continued to retreat else-where along the Nova Scotia and Newfoundland margins (Shaw et al., 2006).

1.3.3: Seismicity of the Eastern Canadian Margin

Eastern Canada is located within a stable area of the North American Plate where there is a relatively low rate of recorded seismic activity. Intraplate earthquakes are most commonly explained by concepts based on lithospheric weakness and local stress concentration compared to a typical intraplate state of strength and stress. Local reduction of crustal and/or upper mantle strength can be a mechanism to initiate seismic activity where thermal, mechanical, or chemical anomalies can be major factors in reducing the strength of the mantle (Mazzotti, 2007). Local increases in differential stresses can be

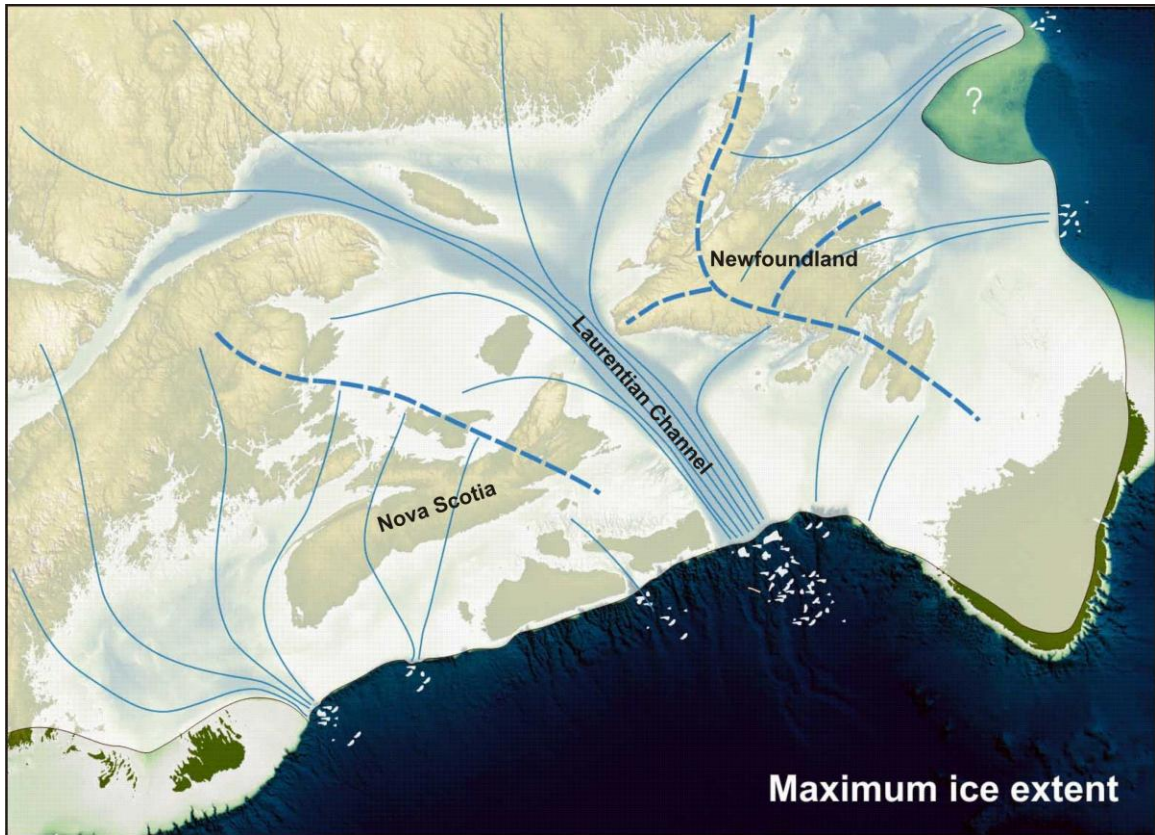


Figure 1.5: Glacier ice extended to the edge of the continental shelves at 20 000 years BP where major ice channels were established in the Bay of Fundy, Laurentian Channel and northeast Newfoundland. Thick dashed lines are ice divides and the thin blue lines represent ice-flow lines. Final retreat of the glacier occurred between 16000 to 10000 years BP (from Shaw et al., 2002 & 2006).

caused by density contrasts, local topography, or kinks and intersections in a fault system. Ultimately, the underlying assumption is that seismicity is promoted by local physical perturbations in an otherwise less seismic intraplate environment (Mazzotti, 2007). There are four geodynamic models suggested by Mazzotti (2007) for the intraplate in North America: the random seismicity and low strain model; the plate boundary zone model; the localized weak zone model; and the large scale weak zone model. The seismicity documented on the eastern Canadian margin can be described by either the random seismicity model or the plate boundary zone model (Mazzotti, 2007). The random seismicity model is characterized by a lack of or paleotectonic structures, a low uniform intraplate strain rate, a random distribution of earthquakes in space and time. In other words, large earthquakes can occur anywhere, but their magnitudes and recurrence intervals are limited by the low strain rate. According to the plate boundary model, intraplate earthquakes are associated with large scale lithospheric structures (Cobequid-Chedabucto Fault?) and are symptomatic of deformation of the entire lithosphere section, as in a plate boundary zone. The major difference between a typical plate boundary region and a plate boundary zone is that seismic events are several orders of magnitude smaller than typical plate boundaries (Mazzotti, 2007). Similar models (random distribution and focused distribution) are also suggested by Basham et al., (1983) and Adams (1986) to explain the occurrence of seismicity across the Canadian eastern margin. Natural Resources Canada estimates that 450 earthquakes occur each year in Eastern Canada with the majority having a magnitude of between two and three. Earthquakes that affect Eastern Canada typically occur in clusters and at depths ranging from the surface to 30 km. Seismicity occurs more-or-less randomly along the Scotian

and Grand Banks margins except for a concentration of events in the greater Laurentian Channel area known as the Laurentian Slope Seismic Zone (Fig. 1.6).

1.3.4: Salt Tectonics of the Laurentian and South Whale Sub-Basins

Salt structures present in the Scotian Basin were divided into five tectonostratigraphic subprovinces by Shimeld (2004) based on interpretation of distinct differences in style of salt and sediment deformation. Shimeld's (2004) subprovince V incorporates the Laurentian and South Whale subbasins (Fig. 1.3) and is the least well imaged and understood subprovince in the Scotian Basin. Structures in this subprovince have a complex 3D morphology influenced by significant extension during the Cretaceous and contraction during the latest Cretaceous through Neogene. Diapirs beneath the upper slope of the southwestern Grand Bank margin in subprovince V have a thinner post-kinematic cover compared to other subprovinces, while the crests of several diapirs are within 100 m of the seafloor (Shimeld, 2004).

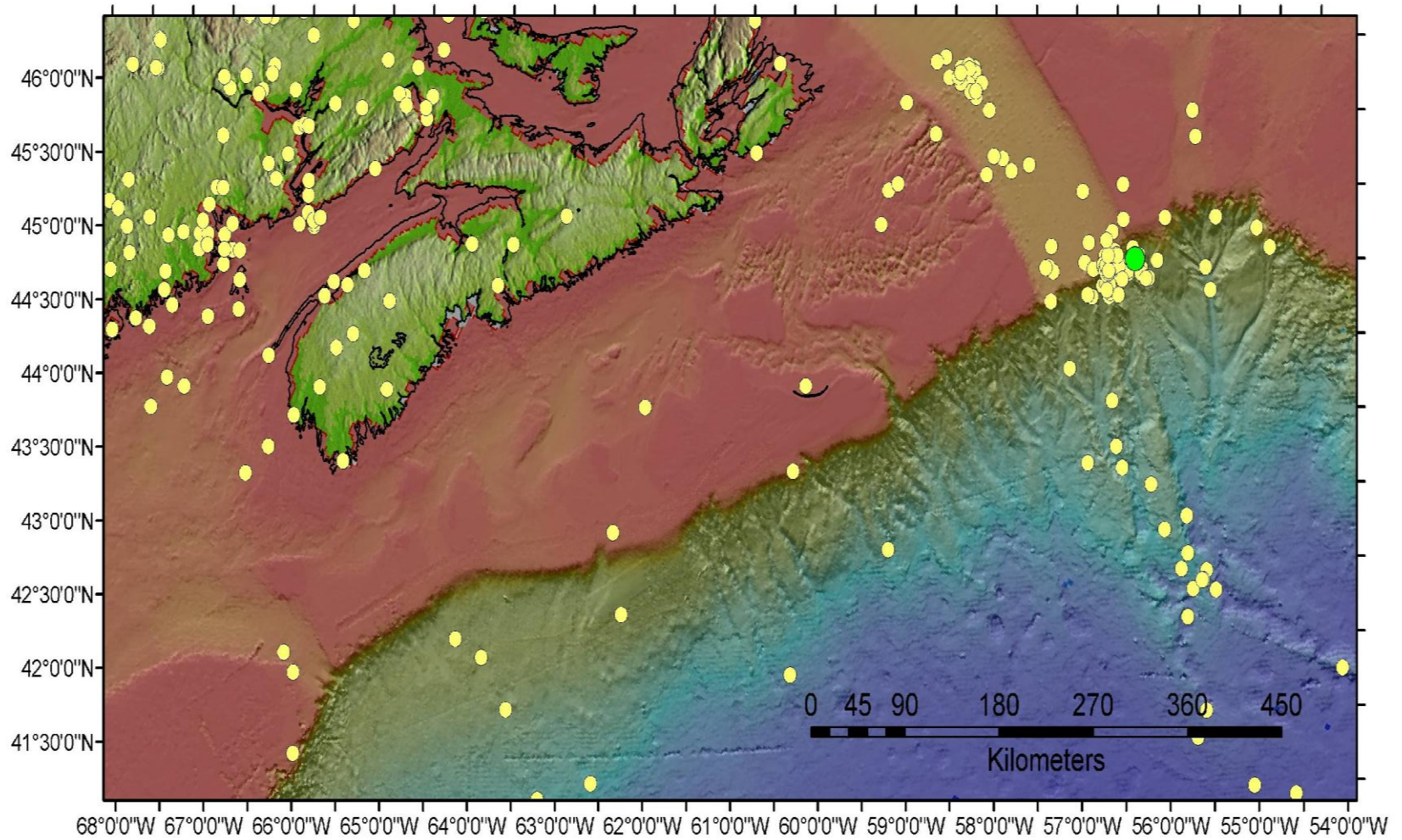


Figure 1.6: The Laurentian Slope Seismic Zone is an area that covers the Cobequid-Chedabucto Fault system and is the location of an increased amount of seismicity. It is estimated that 450 earthquakes occur each year in Atlantic Canada. Yellow circles represent earthquake location with the green circle representing the 1929 Grand Banks Earthquake (from Mosher et al., 2010).

Chapter Two: Methods

The primary method of geologic investigation during this study was interpretation of industry and government collected seismic reflection and bathymetry data. These data included multibeam sonar bathymetry, 2D seismic reflection data collected by the Geological Survey of Canada – Atlantic (GSC-A), and industry acquired 2D and 3D seismic reflection survey data. These data were tied to industry well data to establish a seismic stratigraphic framework for the study area. Seismic Micro Technologies Kingdom Suite was the interpretation seismic software used in this study.

2.1: Seismic Reflection Methods

Reflection seismology is an important technique used in the investigation of subsurface geology in both continental and marine settings. Many textbooks discuss the physics and practical applications of marine seismic reflection techniques (for example: Claerbout, 1976; Claerbout, 1985; Yilmaz, 1987; Sheriff and Geldart, 1995; Brown, 1999; Yilmaz, 2001; Sheriff, 2002; Brown, 2003; and Veeken, 2007) and these principles and applications are not discussed here except when specifically relating to the individual data sets used in this study.

2.2: Seismic Stratigraphy

Seismic stratigraphy is a technique used in seismic interpretation that combines seismic reflection geometries and basic stratigraphic concepts to infer depositional architecture (Vail et al., 1977). The unique properties of seismic reflections allowed the direct application of geologic concepts based on physical stratigraphy (Vail et al., 1977).

Stratigraphic interpretation of seismic reflection geometries provide insights into post depositional structural deformation and thickness changes, geologic time correlations, definition of genetic depositional units, depositional environments based on depositional topography, paleobathymetry, and geologic history. Seismic reflections (often resembling geologic bedding) are generated at acoustic impedance contrasts (Z); impedance being the product of changes in the bulk rock properties of velocity and density. Assuming normal incidence, seismic reflections are explained through the Zoeppritz equation, and when reduced it is the equation for the normal reflection coefficient (Sheriff and Geldart, 1995):

$$R = \frac{Z_{layer\ 2} - Z_{layer\ 1}}{Z_{layer\ 2} + Z_{layer\ 1}}$$

R = reflection coefficient (ratio between reflected and transmitted energy).

Z = acoustic impedance (product of the material bulk density and its seismic velocity).

The equation states that the reflection amplitude is a function of the magnitude of change of acoustic impedance. A reflection coefficient is generated at each change in acoustic impedance and collectively the sequence of reflection coefficients are referred to as the Earth's reflection series. The seismic source wavelet convolves with the Earth's reflection coefficient series to produce a series of seismic reflections. Seismic facies analysis and seismic stratigraphic concepts are used in the interpretation of these seismic reflections to infer depositional and tectonic evolution of sequences (Sheriff and Geldart, 1995).

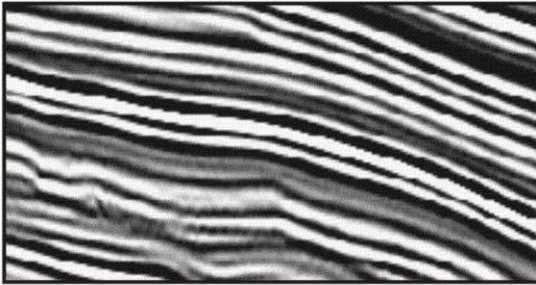
Seismic reflection data consists of several attributes including amplitude, phase, frequency and coherency. When these “attributes” are used in combination with reflection character, reflection configuration and external geometry, they form the basis of seismic interpretation (Stoker et al., 1997). Seismic reflections are grouped into seismic facies or intervals of similar reflection characteristics (Fig. 2.1). Seismic facies are further grouped into seismic units based on patterns of occurrence or associations. Seismic facies and units are then used to interpret the distribution of sediments and environments of deposition based on internal reflection organization, bounding relationships, external geometry and lateral changes (Fig. 2.2 and 2.3) (Mitchum et al., 1977a; Mitchum et al., 1977b; Catuneanu, 2002; Veeken, 2007). Seismic facies are then grouped into seismic units to describe the overall reflection character of specified interval or succession of seismic facies.

2.3: Data Sets

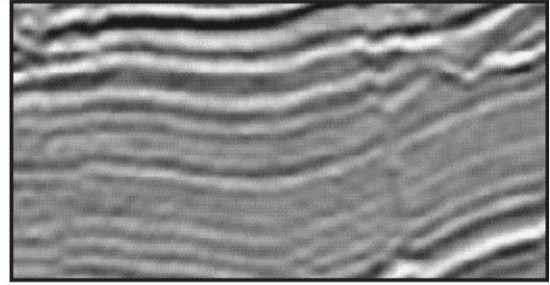
Seismic reflection data are the primary data used in this study and were collected by both the Geological Survey of Canada and Industry. These data were collected by various systems with different parameters and therefore have different resolutions. For the 2D and 3D seismic data in the region, the vertical (temporal) resolution is approximated by the Rayleigh criteria and horizontal (spatial) resolution of the 3D seismic data is determined by the first Fresnel zone (Mosher et al., 2006).

Vertical resolution of seismic data is determined by the frequency of the seismic signal, its bandwidth, the interval velocity of the investigated rocks, and the acoustic impedance

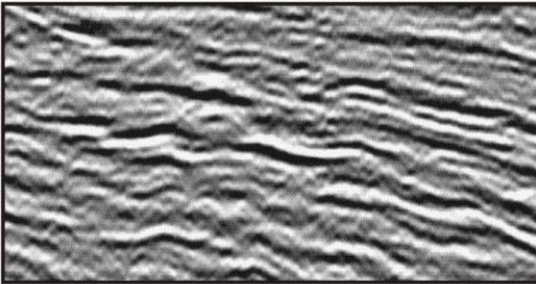
Seismic Facies



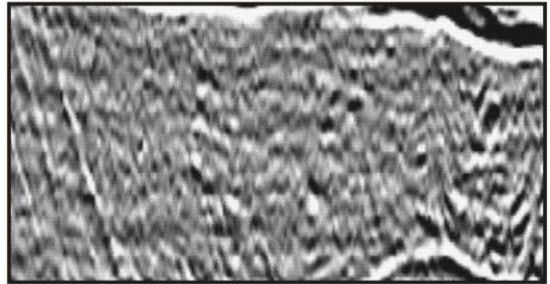
Continuous, Medium-High Amplitude



Continuous, Low-Medium Amplitude



Discontinuous, Low-Medium Amplitude



Chaotic

Figure 2.1: Seismic facies are acoustic characteristics based on reflection configuration, continuity of reflections, amplitude and frequency content. Continuous, medium-high amplitude; continuous, low-medium amplitude; discontinuous, low-medium amplitude; and chaotic are examples of seismic facies from the southwestern Newfoundland margin.

Reflection Configuration

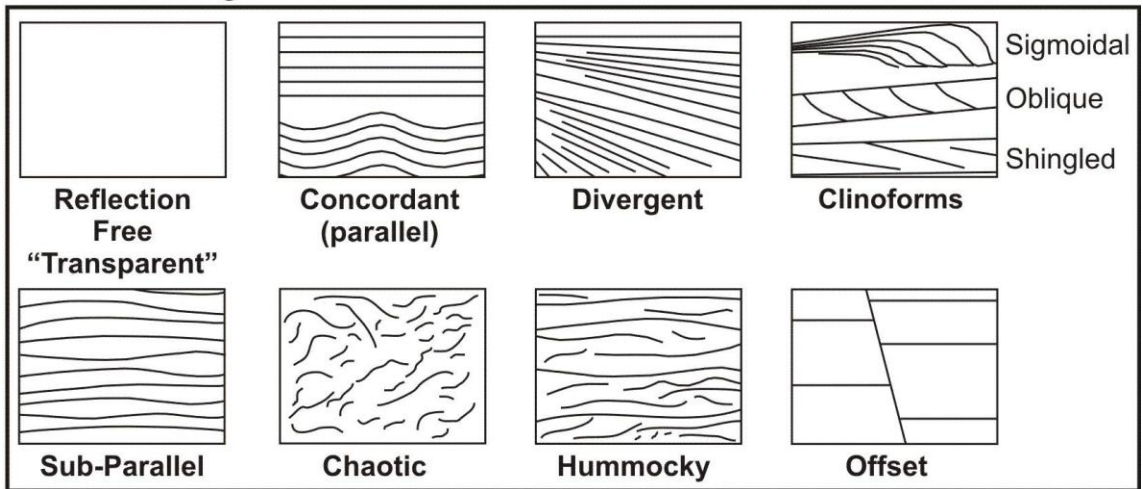


Figure 2.2: Reflection configurations are elements of seismic facies that assist in interpretation of depositional environments (modified from Mitchum et al., 1977).

Reflection Geometries - Cross Section View

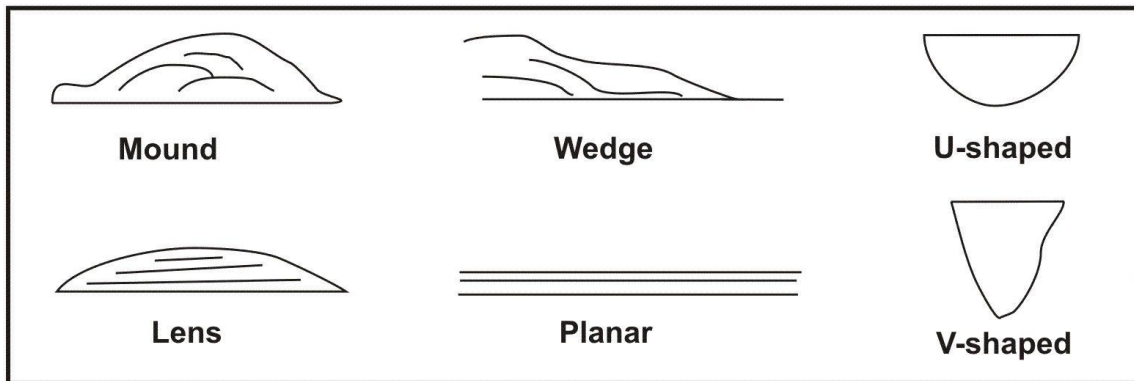


Figure 2.3: Reflection geometries are another component of reflection-character analysis which provides information on the depositional style of the seismic unit (modified from Mitchum et al., 1977).

contrast (Veeken, 2007). To approximate the vertical resolution for seismic reflection data, the Rayleigh criteria states that one quarter of the wavelength ($\frac{1}{4}\lambda$) of a seismic signal can be resolved and is shown by the equation (Eq. 2.1):

$$\Delta R_z \approx \frac{v}{4 f_{\max} \cos i}$$

For the above equation, the variables v = velocity, f_{\max} is the maximum frequency, and i is the angle of incidence. The use of Eq. 2.1 will provide the smallest resolvable target but in order to resolve a range of targets, a range of frequencies known as a temporal bandwidth is required. Water depth is another function that affects vertical resolution due to its dependency on the angle of incidence. As water depths increase, the angle of incidence decreases for the same shot-receiver spread which makes $\cos i$ smaller (Mosher et al., 2006).

Spatial resolution is controlled by the subsurface sampling points or bin size (CMP) and is a function of the Fresnel zone size. Bin size dimensions, stacking fold, and errors associated with CMP positioning are all issues that affect spatial resolution. Typically for 3D surveys, the bin size dimensions are larger than the acoustic resolution, and therefore bin size determines the resolvable target size and lateral resolution. In order to resolve a target in seismic reflection data it is generally accepted that 2 – 3 samples are required (Nyquist sampling theory indicates 2 samples per waveform) (Mosher et al., 2006).

In 2006, a 32,150 km² multibeam sonar bathymetry data set, covering the upper slope from the Laurentian Fan to Whale Slope was collected by Fugro Jacques GeoSurveys Inc.

under contract to the Geological Survey of Canada. The data were acquired by the vessel Kommandor Jack with a Kongsberg Simard EM120 multibeam system that operates at a frequency of 12 kHz. Data density is approximately 2300 soundings per km² in a 1000 m of water depth and 84 soundings per km² in 3000 m. This concentration of values implies a horizontal resolution of about 40 m in shallower depths and 400 m at greater depths (Mosher and Piper 2007) (Fig. 2.4).

In 2006-2007, 1844 line-km of digital seismic data were acquired over the Laurentian Fan and southwestern slope of the Grand Banks by the Geological Survey of Canada – Atlantic by the research vessel CCGS Hudson. These data were collected to improve the understanding of geohazards in the region in response to recent industry interest. These high resolution data were collected with a 2x3440 cm³ GI gun array and a single channel Teledyne streamer (Mosher and West, 2007) (Fig. 2.4). The central frequency for the airgun data is ~ 180 Hz and spans from 0 to 400 Hz, meaning that vertically resolution of

$$1/4 = 180 \text{ Hz} \times 1 \text{ sec} / 1500 \text{ m/s} = 2.1 \text{ m}$$

the data is in the order of 2 m, using a near surface velocity of 1500 m/s.

In 1998-1999, TGS-NOPEC collected 34 000 line km of multichannel 2D seismic reflection data across the Scotian and SW Newfoundland Margins. The grid spacing for the survey is 8 km by 8 km. The data were collected with a 130 litre tuned airgun array and streamer lengths of 6 km or 8 km. Data collected in 1998 had a normal stack fold of 80 and data collected in 1999 had a stack fold of 106 fold and CMP spacing of 12.5 m. The data were collected at a 4 ms sample rate. The central frequency of the data is 65 Hz

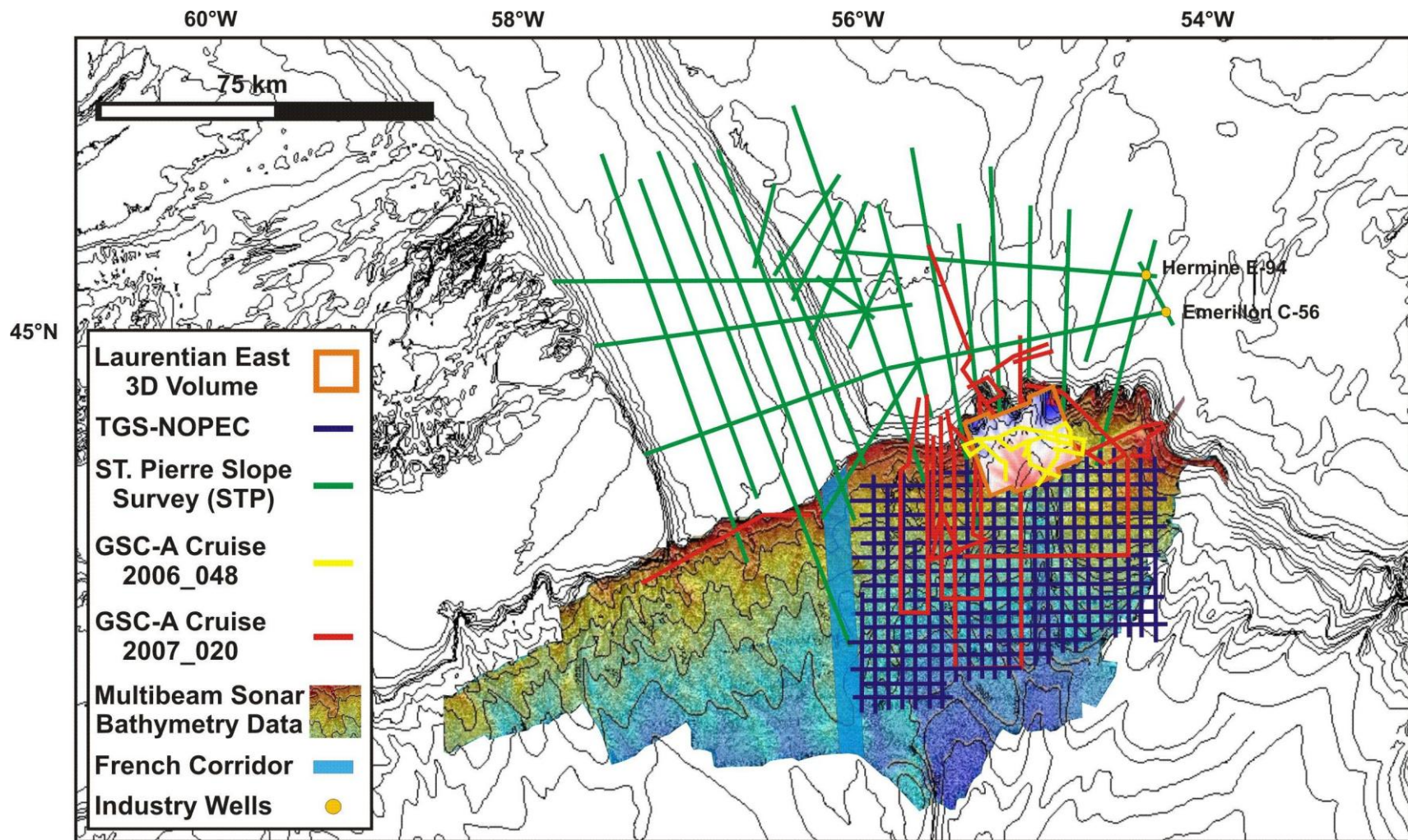


Figure 2.4: Data used for this study cover the continental shelf and slope of the southwestern Newfoundland margin and includes multibeam sonar bathymetry, high resolution 2D seismic reflection, 2D seismic reflection, 3D seismic reflection, and two industry wells (Hermine E-94 and Emerillon C-56).

and spans from 0 to 110 Hz. Using a near surface sediment velocity of 1500 m/s, the vertical resolution of the data is in the order of ~ 6-7 m.

The St. Pierre Slope 2D seismic data set (STP) was acquired for the Geological Survey of Canada in 1984 and 1985 by Geophysical Services Inc. and Western Geophysical. The survey consists of 3100 km of 2D multichannel seismic reflection data collected at a 2 ms sample rate (Fig. 2.4). These data have a central frequency of 50 Hz and therefore a vertical resolution of ~ 7.5 m.

In 2005, approximately 1200 km² of 3D seismic data were collected over the southwestern Newfoundland margin for ConocoPhillips Canada by WesternGeco. The upper 5.5 seconds were donated to the GSC-A at the Bedford Institute of Oceanography for scientific research. The Laurentian East 3D data set is located on the continental slope of Haddock Channel and was acquired using a multisource, multi-streamer 3D configuration to obtain up to 60-fold data. The recording configuration typically consisted of 10 streamers of 6000 m active length, with 12.5 m group intervals, 240 channels per streamer and 100 m streamer separation and streamer depths of 8 – 9 m. The survey consists of 1720 strike-lines oriented NW-SE and 5601 cross-lines orientated NE-SW. Received data were sampled at a 2 ms rate, and processed to a bin spacing of 25 x 6.25 m (Fig. 2.4). To estimate the temporal resolution of the Laurentian East 3D volume, a central frequency of 50 Hz and a near surface sediment velocity of 1500 m/s results in a vertical resolution of ~ 7.5 m; anything less than 7.5 m thick is theoretically not distinguishable according to the Rayleigh Criteria. Horizontal resolution for this data set

would be determined by the sounding density and therefore at best would be ~ 50 m by 13 m.

2.4: Age Control

The regional Cenozoic framework for the southwestern Newfoundland margin was established with ties to the Pliocene section of the Laurentian Fan by Piper and Normark (1989) and Piper et al. (2005) and on the established seismic stratigraphic framework of the St. Pierre Slope (MacLean and Wade, 1992). MacLean and Wade (1992) correlated STP-11 to industry wells Emerillon C-65 and Hermine E-94 located on the continental shelf, southwest of Newfoundland, both of which encountered a thick Miocene succession. New palynological analysis of Hermine E-94 industry well presented in Piper et al. (2005) allowed the correlation of a mid and late Miocene marker through STP-18 and STP-22 to slope dip lines STP-10 and STP-11. The correlation completed by Piper et al. (2005) confirms the interpretation presented by MacLean and Wade (1992) but the ages were improved with the new biostratigraphy. Age control established by this previous work was correlated down the St. Pierre Slope and east into the study area using STP and TGS-NOPEC 2D seismic data.

2.5: Terminology and Classification of Mass Transport Processes and Deposits

For this study, the classification system for gravity driven flows as proposed by Mulder and Cochonat (1996) are coupled with the classifications developed by Frey-Martinez et al. (2006) and Moscardelli and Woods (2008) to assign a descriptive nomenclature to MTDs preserved on the southwestern Newfoundland margin.

Plastic flows are frequent on continental slopes and are usually the movement of mass, underconsolidated sediments. The head scarps of these failures are indistinct or non-identifiable, and the only information about the event is provided by the shape and nature of the deposit. The internal structure of a plastic flow deposit is typically disorganized in nature. If the composition of the debris flow is mainly mud, then the yield resistance of the flow and its velocity are the main factors controlling its flow characteristics. For all other flows, the motion of the sediment is a result of the presence of interstitial fluid. The main body of the deposits typically consists of disturbed and indistinct structures characterized by acoustically transparent and chaotic facies (Fig. 2.5) (Nardin et al., 1979; and Mulder and Cochonat, 1996).

Based on the compressional toe domain of submarine landslides, failure deposits are divided into two styles: frontally emergent and frontally confined. A frontally emergent landslide is defined by the material ramping out of the basal shear surface onto the seafloor and is free to travel considerable distances over the undeformed slope. In comparison, a frontally confined submarine landslide is buttressed against a frontal ramp and is not able to detach from the original basal shear surface (Frey-Martinez et al., 2006).

Submarine landslides are further classified as attached or detached MTDs based on their geomorphological and morphometric dimensions, location of source area and the relationship of the MTD to its source area. Attached MTDs are typically regionally extensive and occupy hundreds to thousands of square kilometres in area, whereas





Gravity Induced Deposits			Genetic Classification Transport Mechanism (Dott, 1963)	Descriptive Classification Sedimentary Structures (Nardin et al., 1979)	Seismically Recognizable Features (Moscardelli et al., 2006; Moscardelli and Wood, 2008)
Mass Transport Deposits	Slide		Shear failure along discrete shear planes with little or no internal deformation or rotation.	Essentially undeformed, continuous bedding.	Continuous blocks without apparent internal deformation. High-amplitude, continuous reflections.
	Slump		Shear failure accompanied by rotation along discrete shear surfaces with various degrees of internal deformation.	Plastic deformation particularly at the toe or base. Plow structures, folds, tension faults, joints, slickensides, groves, rotational blocks	Compressional ridges, imbricate slides, irregular upper bedding contacts, duplex structures, contorted layers. Low and high amplitude reflections geometrically arranged as though deformed through compressive stresses.
	Debris Flow		Shear distributed throughout the sediment mass. Strength is principally from cohesion due to clay content. Additional matrix support may come from buoyancy.	Matrix supported, random fabric, clast size variable. Rip ups, rafts, inverse grading and flow structures possible.	Mega rafted and/or detached blocks, irregular upper bedding contacts, lateral pinch-out geometries, oriented ridges and scours. Low amplitude, semitransparent chaotic reflections.
Turbidity Current	Turbidite		Supported by fluid turbulence.	Normal size grading, sharp basal contacts, gradational upper contacts.	Lobate features and laterally continuous.

Figure 2.5: Classification of Submarine, gravity driven mass transport deposits (modified from Moscardelli and Wood, 2008).

detached MTDs are smaller and typically only occupy areas less than ten square kilometres. Establishing the differences between shelf attached and slope detached MTDs is determined by the geomorphological features in the upslope part of the deposits. Shelf attached MTDs have paleocanyons proximal to their sources that have funnelled sediments downslope, as well as aggradational or progradational clinofolds near the paleoshelf break. Slope attached MTDs have head scarps that are regionally extensive for tens of kilometres and are hundreds of metres deep that occur in the shelf break/upper slope region.

Several other terms including canyons, valleys and gullies are used to describe the morphology of both the paleo and the modern seafloor. Canyons and valleys are large scale erosional features that dissect the continental margin. They are typically ~50-100 m deep and 1-2 km wide and have “U” or “V” shaped profiles (Mountain, 1987; Pratson et al., 1994; and Mountain et al., 1996). In general, canyon walls have steeper angles compared to valley walls. Gullies are the smaller counterparts of submarine canyons. These downslope trending, channel-like features range from 5-10 m wide and 1-2 m deep to broader features that are 50-300 m wide and 10-40 m deep (Farre et al., 1983).

2.6: Seismic Attribute Analysis

Seismic attributes are characteristics or derivatives of characteristics of seismic signals, including time, amplitude, frequency and phase. These attributes assist in studies of structure, stratigraphy and rock properties of seismic data (Brown, 2003) and are extracted along a time surface, a horizon, or from a pre-defined vertical window

encompassing any number of reflections. In addition to these conventional attributes, derivative attributes of similarity and coherency were computed for the Laurentian East volume. The similarity and dip of maximum similarity attributes are computed together and stored differently by scanning adjacent traces within a user defined range of dips as indicated from a time window. Areas of high similarity indicate a high degree of lateral signal similarity interpreted as a similar depositional environment. Coherency is a measure of lateral changes in the seismic response caused by variation in structure, stratigraphy, lithology, or porosity. It is particularly useful in the identification of faults. Data are viewed in profile to identify changes in dip, thickness, and fault offsets. Viewing data as a time slice identifies changes in lateral and vertical attribute changes. A similarity time window of 0.04 s and a variance time window of 0.08 s were used to generate two 3D similarity volumes from the Laurentian East data set.

2.7: Uncertainty

2.7.1: Biostratigraphic Control

For this study, the largest source of uncertainty is associated with the stratigraphic framework used for the southwestern Newfoundland margin. Biostratigraphy from two industry wells (Hermine E-94 and Emerillon C-56) located on the adjacent continental shelf were tied to STP-18 and correlated across the shelf to slope trending STP seismic lines. Limited sediment preservation at the shelf break complicates correlation of biostratigraphic ties to the slope environment as reflections exhibit variable reflection strength and preservation. Seismic character and continuity of units are used to extend ties down slope and as a result, the confidence of the age control used in the stratigraphic

framework is low. Until an industry well is drilled on the slope where the Cenozoic section is sampled, improvement of the biostratigraphy for the southwestern Newfoundland slope is difficult.

2.7.2: Error Analysis

Uncertainty and errors arise during acquisition and processing of the data as well as during interpretation. The Laurentian East 3D volume, TGS-NOPEC and St. Pierre Slope 2D seismic data were processed before being received by the GSC-A. 2D seismic data acquired by the GSC-A were processed in-house. For the 3D seismic volume, SMT Kingdom Suite provides the ability to assess the correlation of manual picks made through the data with a confidence map. Confidence is calculated in SMT Kingdom Suite by the Equation 2.2 and by the assumption that the manual picks have the highest confidence (confidence = 1).

Eq. 2.2:

$$c(pt) = X_t e^{-k(pt+\delta t)}$$

Where X_t is a measure of affinity between two traces within a cross correlation window, p is the maximum vertical shift between all picks in the neighbourhood of p_t , δ is the shift to the best cross-correlation sample within the correlation window, and k is a smoothing factor of 0.5. A confidence map created for the seafloor horizon of the Laurentian East 3D volume (Fig. 2.6) shows that areas represented by blue have a strong degree of confidence in the autopick. White and red represent areas where confidence in the autopick is reduced. Confidence is lowered in these areas as a result of rapid changes in bathymetric highs and lows in the modern seafloor caused by canyon and channel

incision. The complexity of the subsurface geology can force a lower confidence of the autopicker.

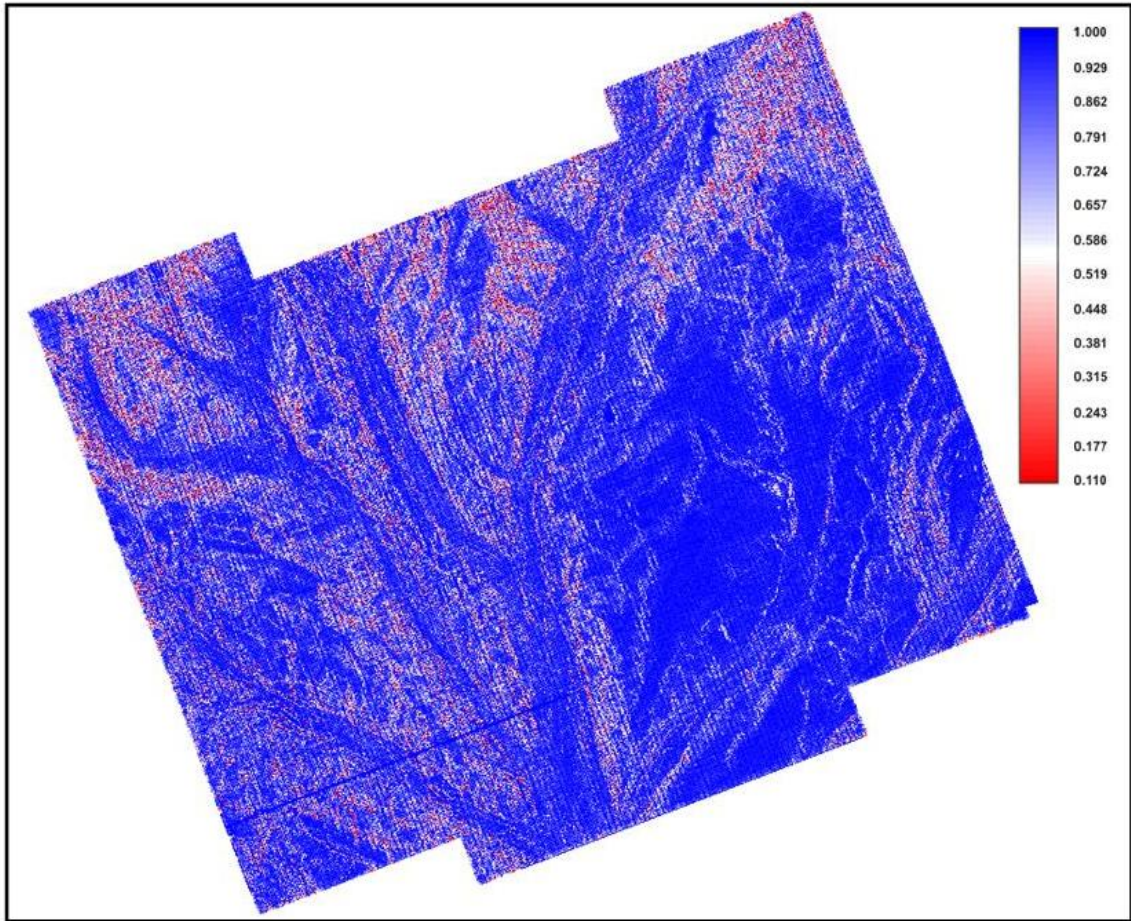


Figure 2.6: Confidence map for the seafloor pick of the Laurentian East 3D volume created in SMT Kingdom Suite. Areas in blue (colour bar top right) shows that there is a high degree of confidence in the autopick option of the software, whereas areas represented by white and red show a lower confidence in the software autopick.

Chapter Three: Seismic Facies and Stratigraphic Framework

Identification of seismic facies, reflection configurations, and reflection geometries coupled with stratigraphic context provides the basis to infer depositional history in a region. Mapping dominant reflectors throughout the study area establishes the seismic stratigraphic framework and interpretation of seismic facies permits one to surmise the mechanisms responsible for the transport of sediment from the shelf to the abyssal plains.

3.1: Seismic Facies

The use of seismic facies follows the definitions of Mitchum et al., (1977b) and Sangree and Widmier (1977; 1979). Seismic facies analysis is the process that involves the delineation and interpretation of reflection geometry, continuity, amplitude, frequency and interval velocity, as well as the external form and three-dimensional associations of groups of reflections (Sangree and Widmier, 1977). Reflection geometry or configuration reveals the overall stratification patterns from which depositional processes, erosion, and paleo-topography can be interpreted. Reflection continuity is associated with the continuity of strata while reflection amplitude is interpreted to represent a change in lithology (Mitchum et al., 1977b). Seismic facies identification and analysis is used to determine the geometry, lithology, and depositional environment of depositional sequences as well as identify the direction of sediment transport.

Reflection geometries are sub-divided into packages of reflections which compose a unit and are described as parallel (concordant), sub-parallel (discordant), divergent, clinoform

(sigmoidal, oblique, or shingled), reflection free, wavy, chaotic or contorted. Seismic packages are also described in terms of their external morphology and three-dimensional character as sheets, lenses, wedges, mounds and drapes (Mitchum et al., 1977b).

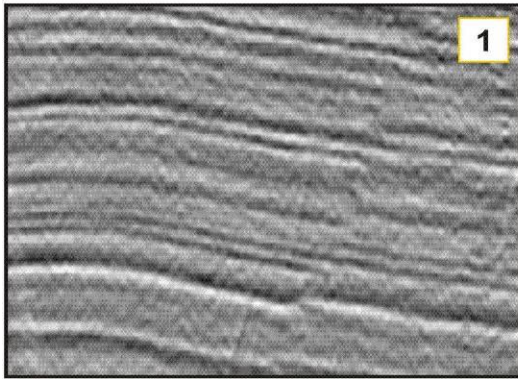
Six seismic facies are identified from the Laurentian East data set (Fig. 2.1 and 2.2). Facies 1 is composed of low to moderate amplitude parallel continuous reflections. Facies 2 consists of moderate to high amplitude parallel to sub-parallel continuous reflections. The nature of these two facies suggests the associated sediment is well stratified. Facies 3 is composed of chaotic and contorted reflections. Facies 4 consists of moderate to high amplitude wavy and concordant reflections. Facies 5 is described as reflection free and may represent homogenous or nonstratified sediment. Facies 6 is composed of low to high amplitude discontinuous to incoherent reflections (Fig. 3.1)

3.2: Key Reflections

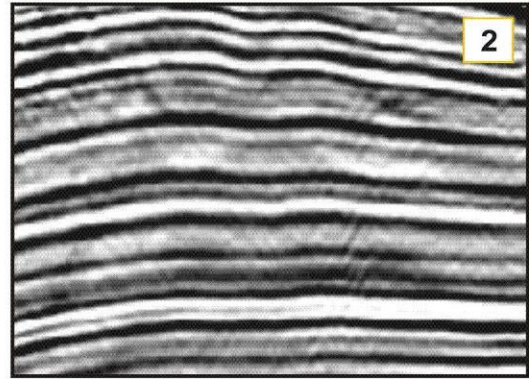
Five key reflections were identified and mapped across the study area. Key reflections were chosen based on their reflection amplitude and continuity across the study area. Reflections were named based on the type of geological feature mapped and its location or by age and location of the reflection within the stratigraphic sequence. In areas where reflection amplitude decreased, reflection geometry and continuity of seismic units were used to continue correlations across the study area.

Reflection event **K99** (Fig. 3.2) is the deepest reflection mapped in the study area and is represented by a high amplitude continuous peak. Correlation and interpretation of the reflection became problematic in eastern seaward regions as a result of deformation of

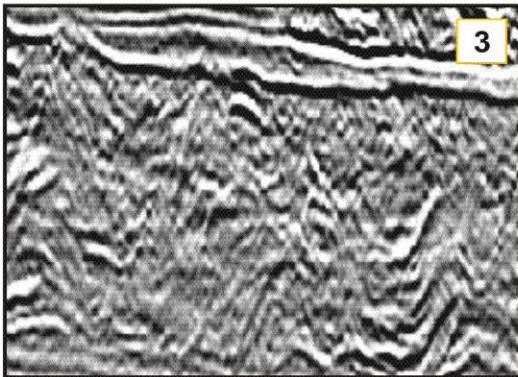
Seismic Configurations and Facies



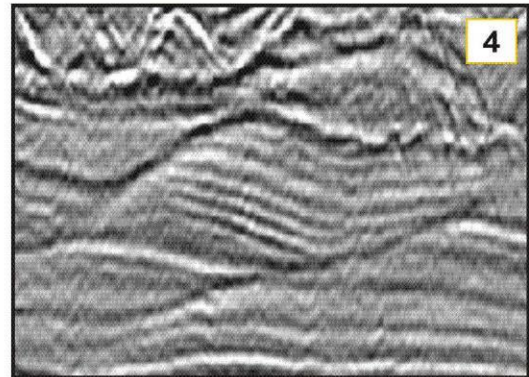
**Low to Moderate Amplitude
Parallel Continuous**



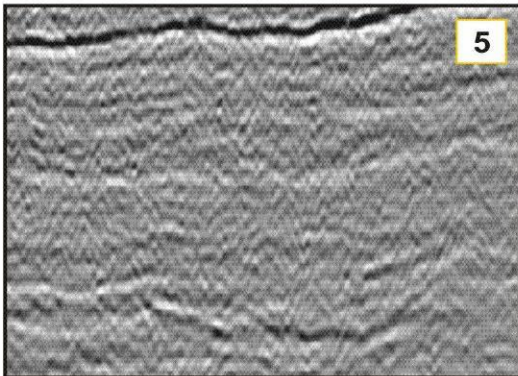
**Moderate to High Amplitude
Parallel to Sub-parallel**



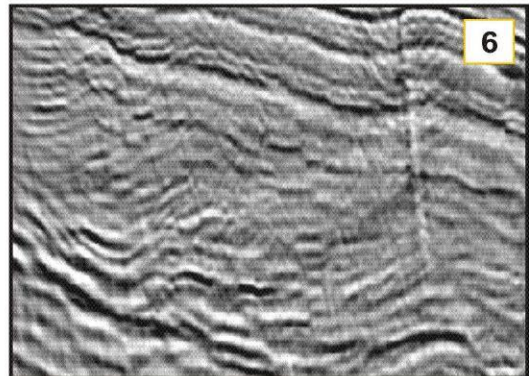
Chaotic & Contorted



**Moderate to High Amplitude
Wavy to Concordant**



**Reflection Free
"Transparent"**



**Low to Moderate Amplitude
Discontinuous**

Figure 3.1: Six seismic facies are identified from the Laurentian East data set and are used to gain insight about the depositional environment and direction of sediment transport of the depositional sequences.

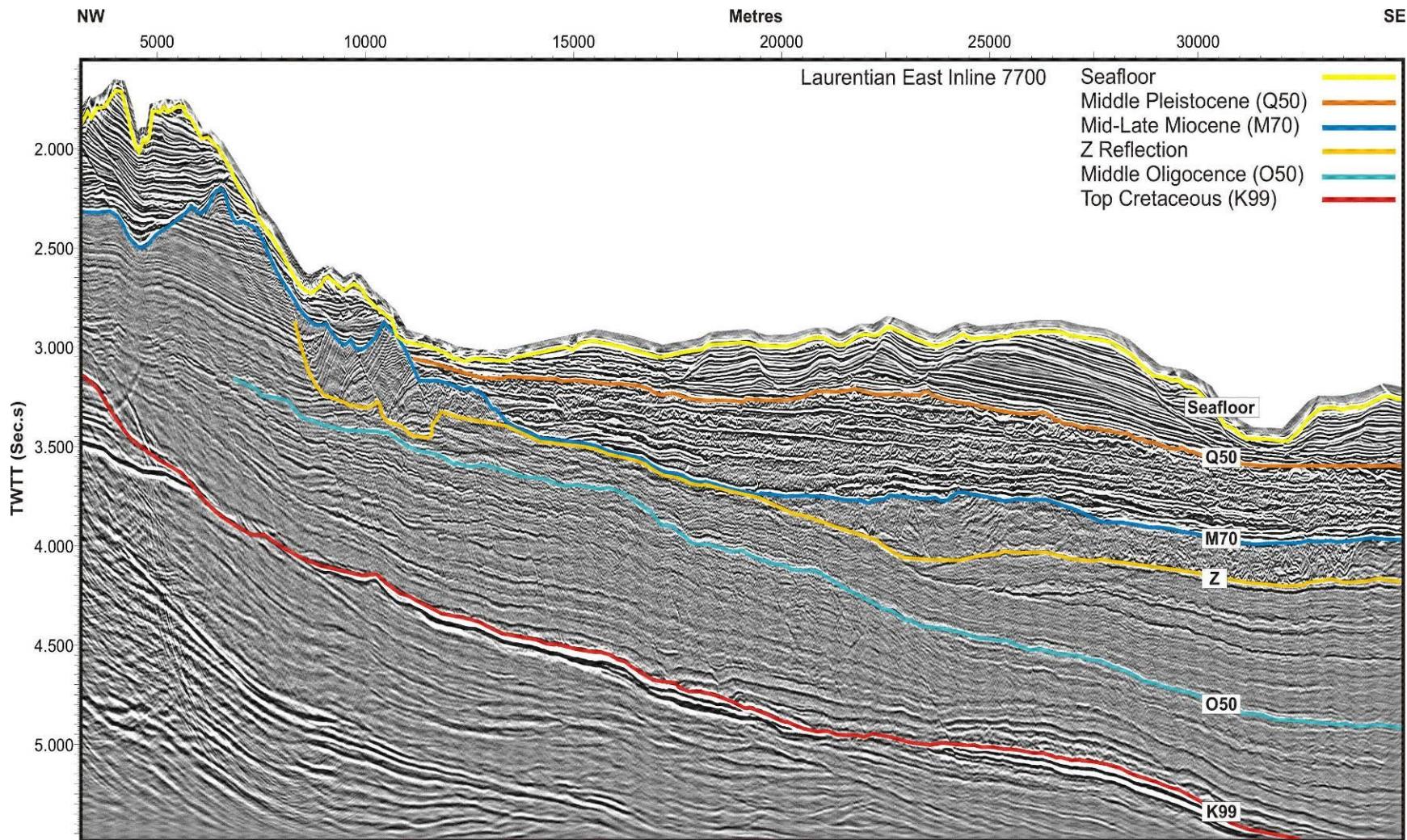


Figure 3.2: Inline 7700 from the Laurentian East 3D data set displays six of the eight key seismic reflections mapped across the study area. Five of these key seismic reflections (K99, O50, M70, Q50 and the seafloors) are used to establish the stratigraphic framework for the southwestern Newfoundland Slope.

underlying Late Triassic-Early Jurassic Argo salt. Erosional scours that run NW-SE are present on the upper slope of the K99 surface where paleo-ridges separate these scours and have dendritic morphologies (Fig. 3.3). The alternating high elevations areas and erosional features have slope angles varying between 3 and 25 degrees (Fig. 3.4). In the subsurface of the small SW Valley region, **K99** cannot be mapped as it becomes deeper than the seismic record depth.

Reflection event **O50** (Fig. 3.2) is a peak wavelet of variable amplitude. It is not mappable in all areas of the study region. Its amplitude is low in the upper slope region and increases to a moderate strength in the seaward direction. The **O50** reflection has poor continuity as result of seaward dipping fault offsets. Offsets are greatest in the upper slope, making correlation difficult. Towards the mid slope, faults have smaller offsets permitting correlation of the horizon seaward. In the subsurface of the area where the West and East Halibut Channels coalesce, keystone faults caused by Argo Salt deformation reduce the continuity of the reflection and cause uncertainties in the correlation. In the eastern seaward region of the study area, shallow diapirism of the Argo Salt prevents correlation of the horizon. Geomorphological variability of the **O50** is similar to **K99** except that there is not as much relief between the scours and ridges

Reflection event **Z** (Fig. 3.2) is a medium amplitude continuous peak that is mapped across the majority of the Laurentian East 3D data set. This reflection represents an erosive event as it truncates underlying reflections. It is easily identified by a chaotic reflection facies deposited above it. Argo Salt deformation in the eastern seaward portion

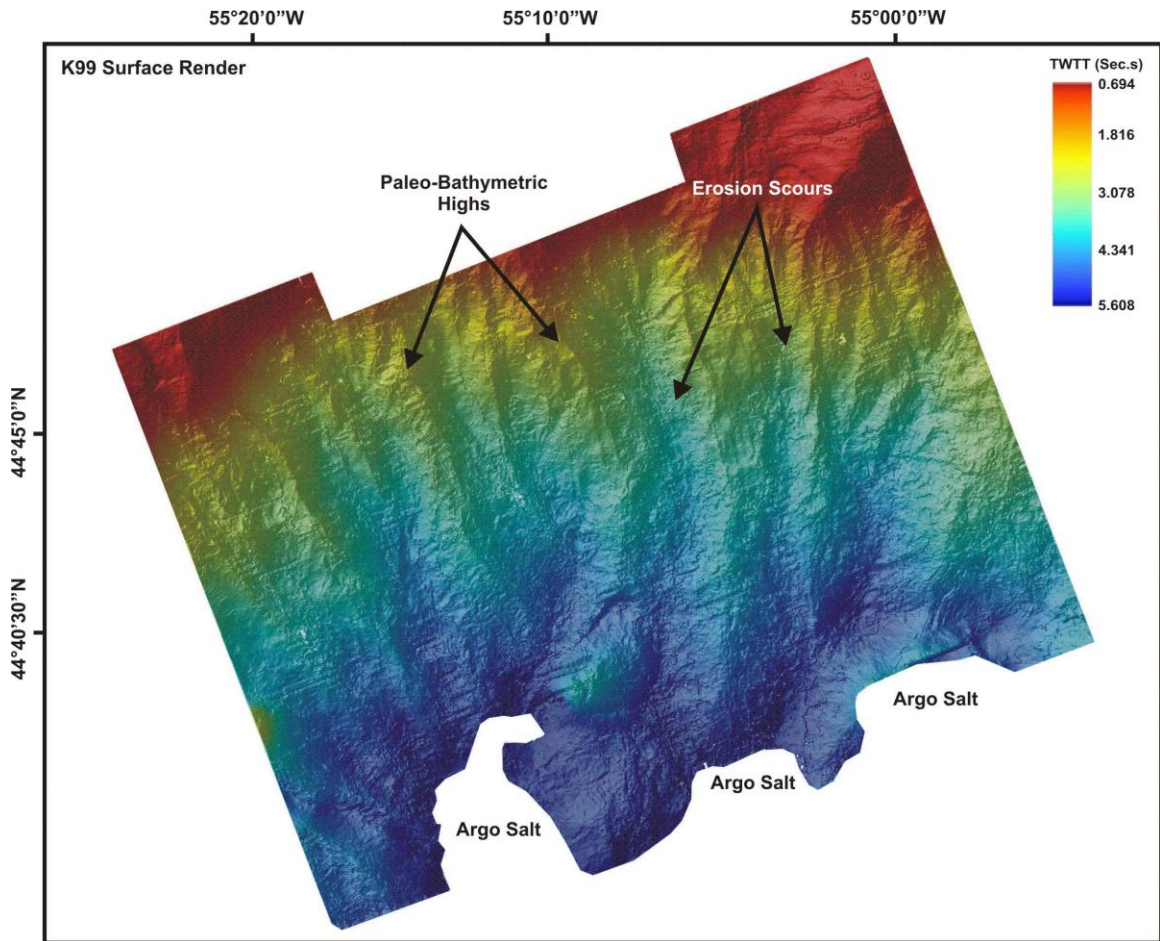


Figure 3.3: Surface render of the K99 horizon from the Laurentian East 3D data set shows a canyon surface morphology. A dendritic morphology is seen in the paleo-topographic highs. In the lower southeast corner, the K99 reflection could not be mapped due to deformation of strata by Argo Salt.

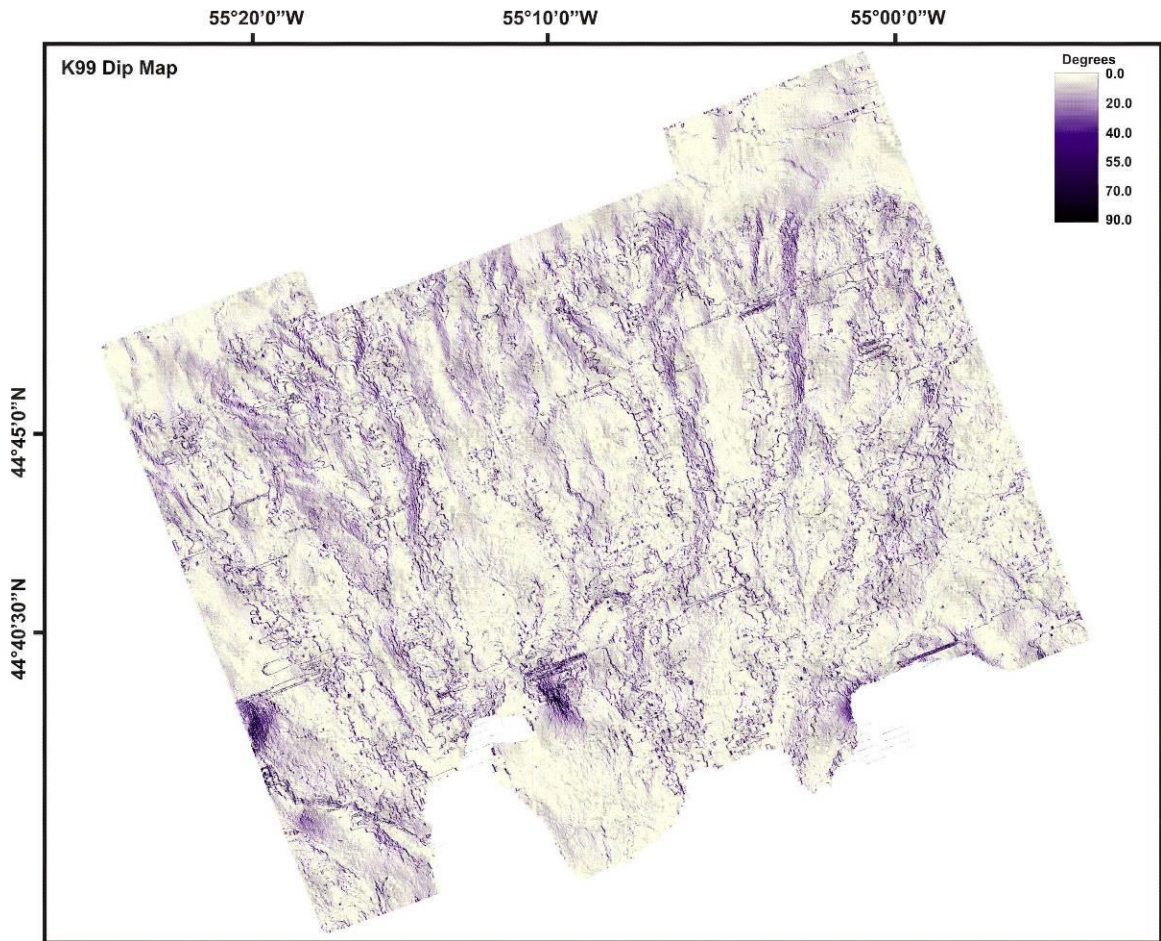


Figure 3.4: Dip map for the K99 horizon of the Laurentian East 3D data set. Dip angles between the paleo-topographic highs and erosional features range between 3° and 25°.

of the study area affects the **Z** reflection in a small area but does not impede the correlation. Seaward dipping faults that affect reflection **O50** terminate at the **Z** reflection. In the upper slope region, NW-SE erosional scours are present as shown in the horizon map of the **Z** reflection (Fig. 3.5). Seaward of the erosional scours, the **Z** reflection deepens abruptly and continues to deepen towards the centre and in the seaward direction of the Laurentian East 3D data area.

Reflection event **M70** (Fig. 3.2) is represented as a high amplitude continuous peak present across the Laurentian East data set, except for in the northeast corner. Correlation of the reflection becomes problematic in this region as a result of dramatic changes in local bathymetry and its proximity to the modern upper slope/shelf break. Paired with the **M70** reflection is a high amplitude, continuous trough which aids in correlation. The morphology of **M70** is mostly controlled by morphology of underlying sediments resulting in an irregular architecture. For example, the blocky nature of the underlying deposit is reflected in the **M70** surface rendering (Fig. 3.6). There is relatively little change in dip in this horizon with the exception of the northeast corner, where there is an apparent paleo-bathymetric high (Fig. 3.7). Through the use of TGS-NOPEC and the STP data sets, reflection **M70** is mapped across part of the St. Pierre Slope.

Above **M70**, reflections **C Base** and **C Top** are high amplitude peaks mapped in the western half of the data set. Correlation of the **C Base** reflection becomes difficult in the seaward direction due to the discontinuous and chaotic nature of reflections between these events. The **C top** reflection is difficult to correlate in the seaward section of the

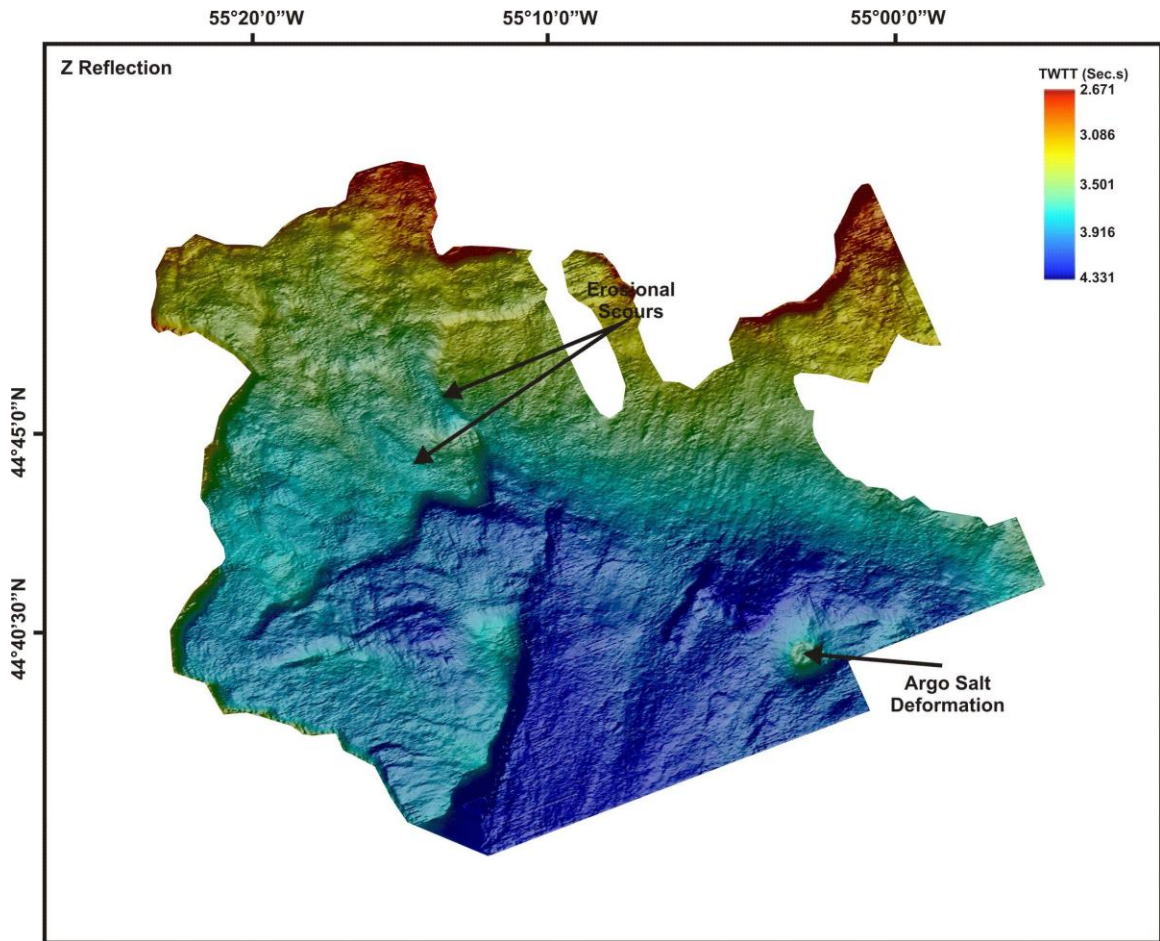


Figure 3.5: The Z reflection from the Laurentian East 3D data set is the base of a chaotic seismic facies package. In the upper slope of this horizon, erosional features are present and run northwest-southeast. In the lower southeast corner of the data set, diapirism from the Argo Salt is apparent.

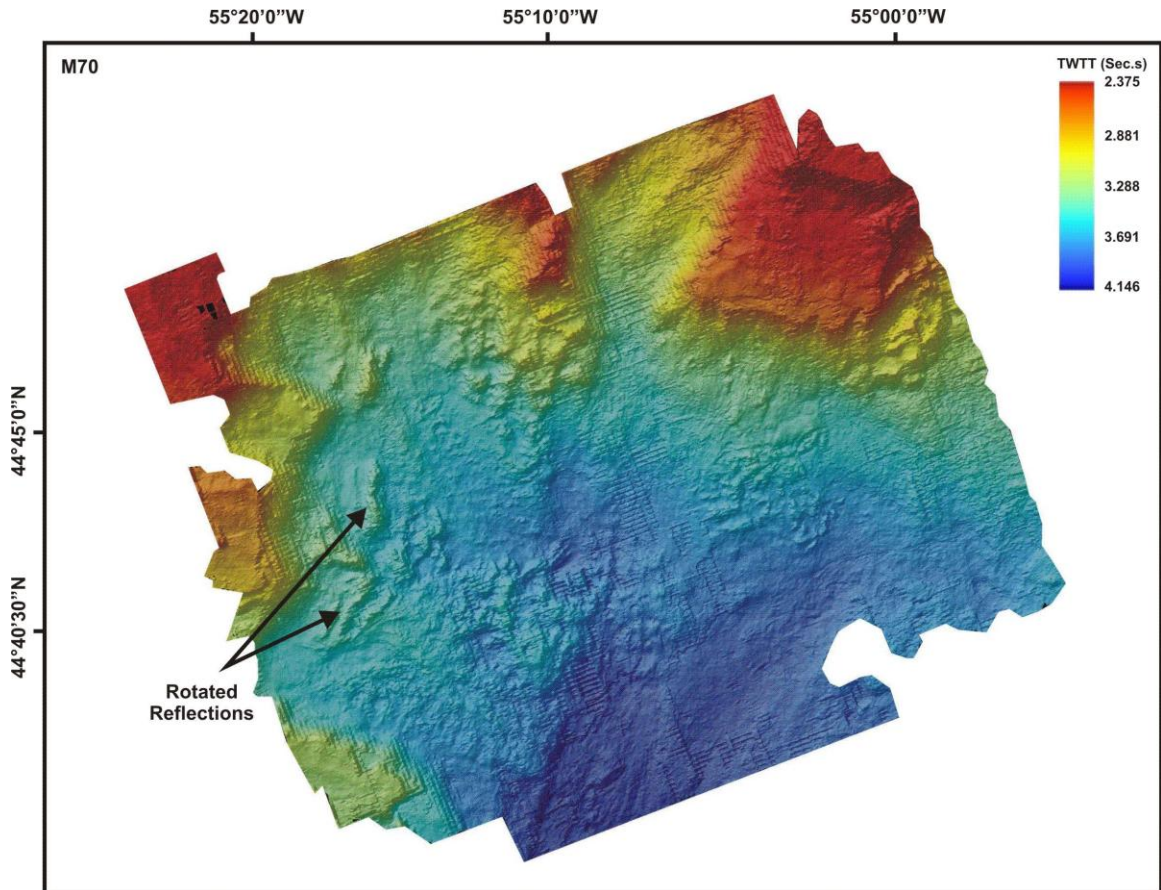


Figure 3.6: Surface render of the M70 horizon from the Laurentian East 3D data set. Paleotopographic highs appear in the northeast corner as well as along the upper slope of the Newfoundland Margin. Erosional scours dissect topographic highs along the upper slope. In the western region of the data set, the top corners of rotated reflection packages are ridges that run north-south. In the southeast (black circle) region of the data set, the M70 reflection could not be mapped as result of Argo Salt diapirism.

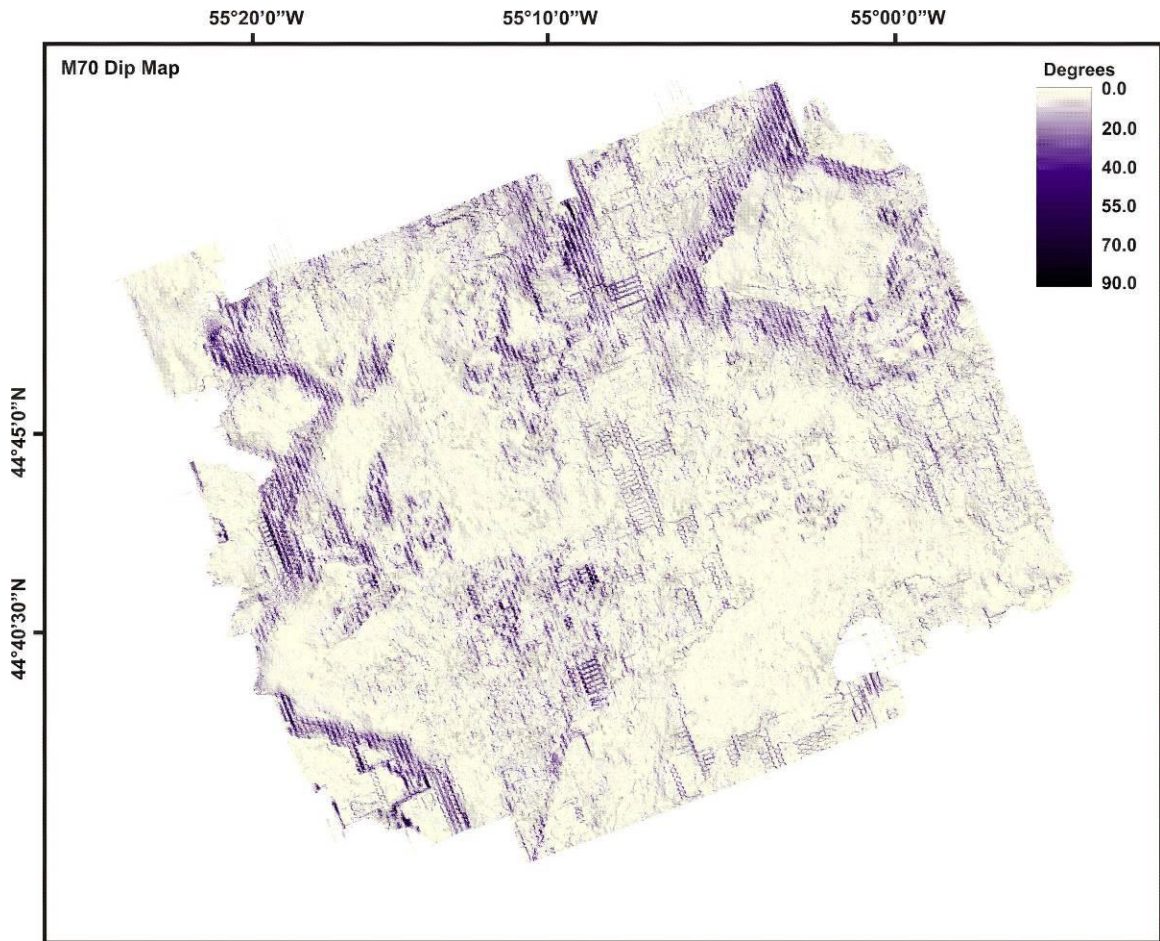


Figure 3.7: The dip map for M70 horizon from the Laurentian East 3D data set shows that the paleo-topographic highs in the northeast corner and along the western region of the data set have dip angles between 15° and 30°. The centre region of this horizon is relatively flat.

data as younger events have eroded this area. The **C Base** reflection is also erosive as it cuts into underlying subparallel – parallel reflections creating “step-like” features (Fig. 3.8) and erosional cuts (Fig. 3.9). Both **C Base** and **C Top** (Fig. 3.10) are absent in the central area of the Laurentian East 3D data area due to canyon incision of the southwestern Newfoundland margin.

Reflection event **Q50** (Fig. 3.2) is a high amplitude continuous peak that is present across the Laurentian East data volume. The **Q50** reflection is only absent where modern day canyon incision removed it (Fig. 3.11). Correlation of **Q50** also becomes difficult to correlate around an inter-canyon ridge in the eastern section of the area. In the upper slope region, **Q50** has minor erosional scours which become unidentifiable in the seaward direction. There is little change in dip throughout the **Q50** horizon (Fig. 3.12). The geomorphology of this reflection may control the deposition of the overlying strata which influences the bathymetry of the modern seafloor.

The seafloor is the upper most horizon event mapped and is represented by a high amplitude peak which is correlatable across the study area. The seafloor lies in water depths varying between 400m and 3000m where canyon incision has created a complex dendritic morphology with pinnate intercanyon ridges in the continental slope (Fig. 3.13). The walls of these ridges have dip angles between 10° and 25° (Fig. 3.14). Canyon heads cut the continental shelf at approximately 300 metres below sealevel (mbsl). Three large canyon systems, the West Halibut Valley, East Halibut Valley, and Haddock Valley converge at approximately 2600 mbsl in the southern region of the study area to form the

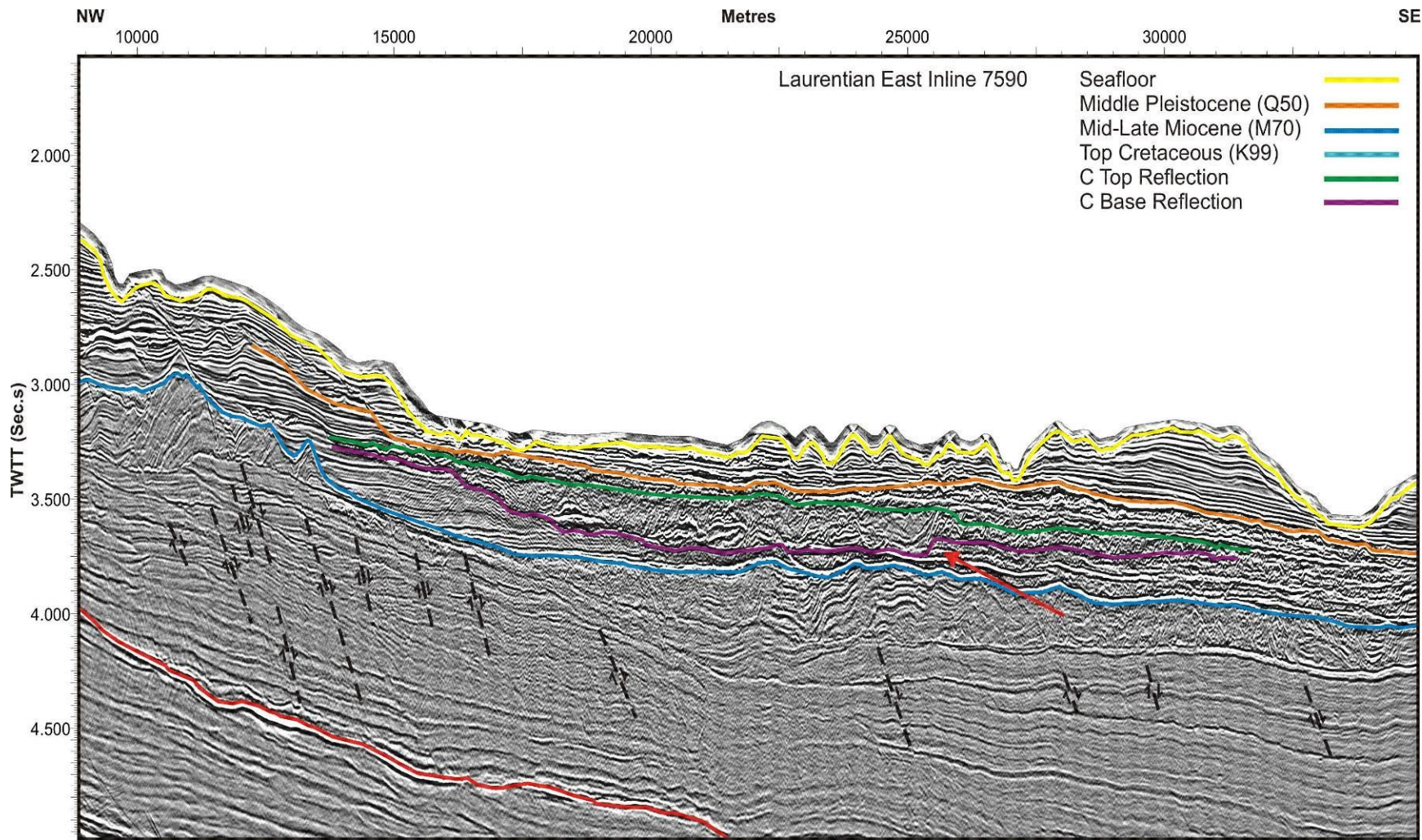


Figure 3.8: Inline 7590 from the Laurentian East 3D data set show the other two key seismic reflections (C Base and C Top) above the M70 reflection. The red arrow shows where the C base reflection cuts into parallel reflections before “stepping up” in the strata and continuing seaward. Faults are represented by dashed black lines that terminate at the base of the chaotic package below M70.

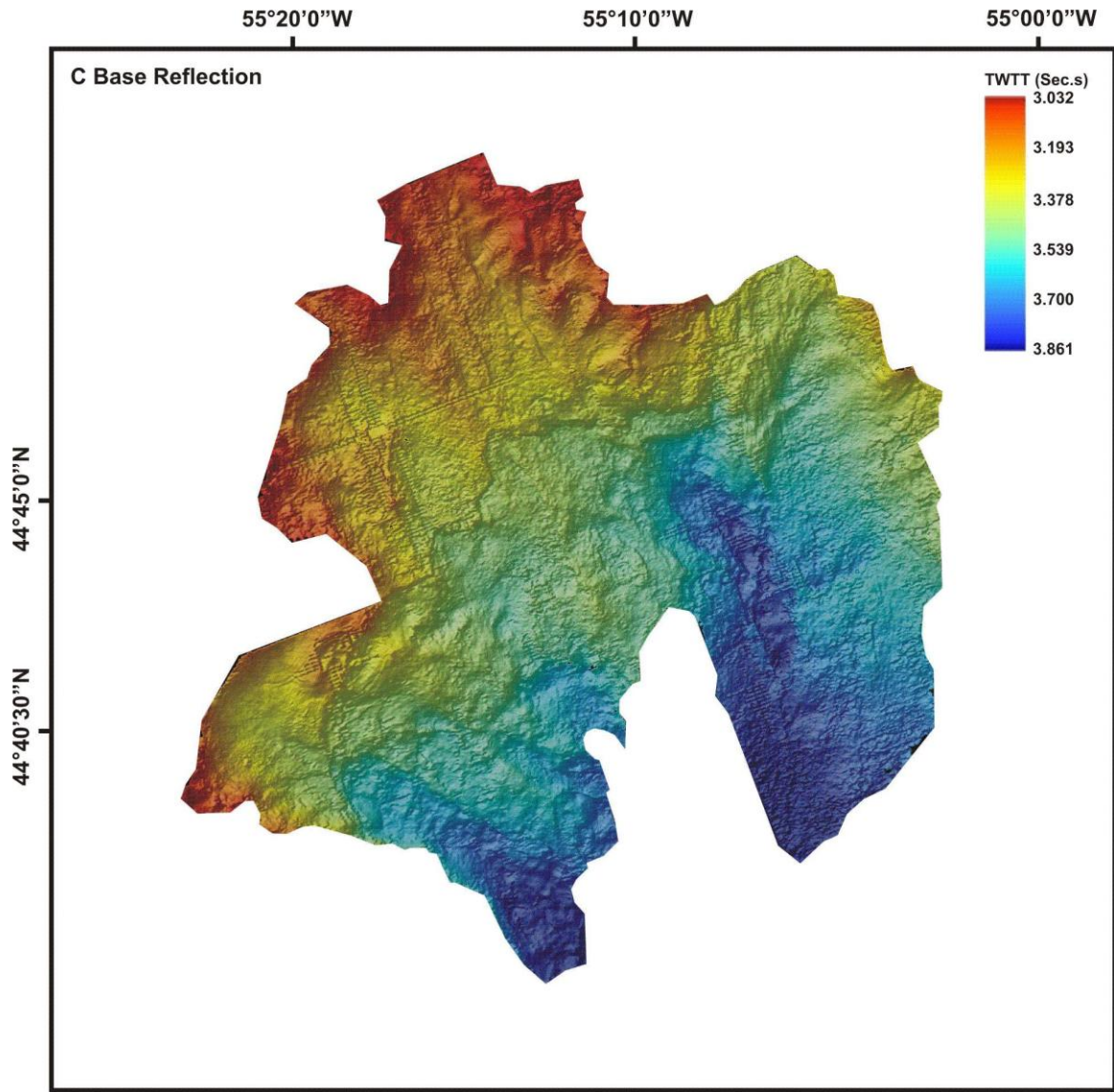


Figure 3.9: Surface render of the C Base horizon from the Laurentian East 3D data set. The C Base horizon is erosive in nature as seen by the occurrence of erosional cuts and remnant escarpments in the eastern and southwestern regions.

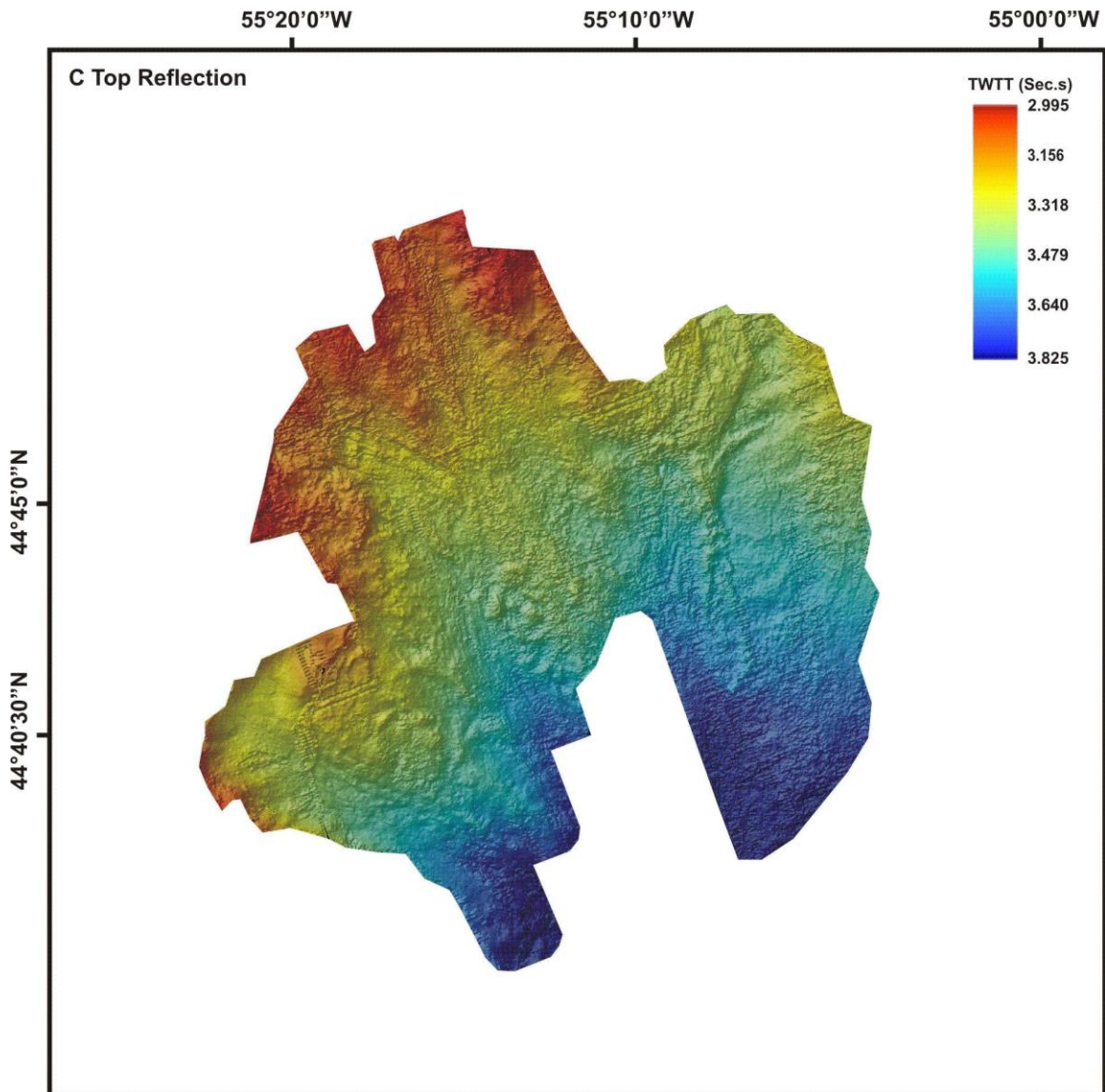


Figure 3.10: Surface render of the C Top horizon from the Laurentian East 3D data set. The geomorphology of this surface is affected mostly by the chaotic sediment package deposited below it and results in a rugose surface.

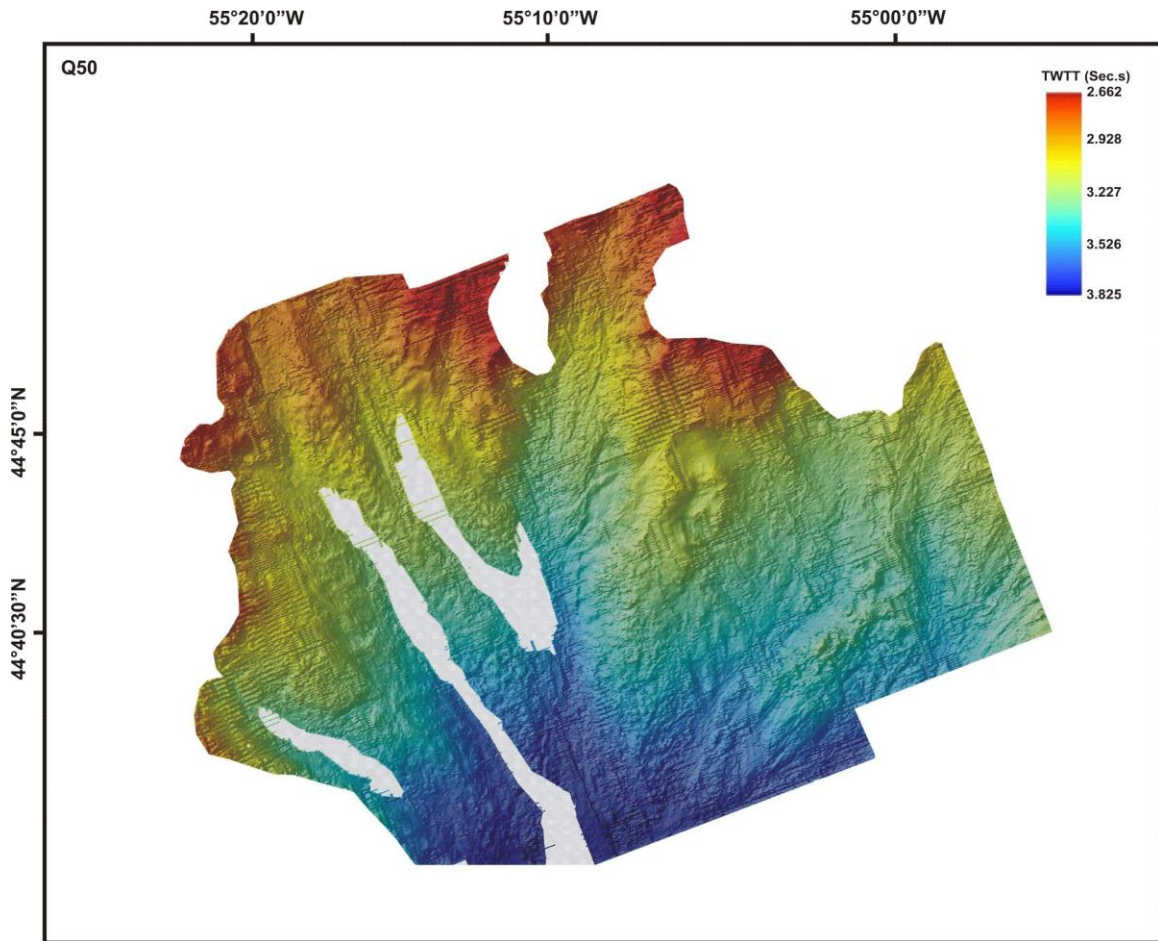


Figure 3.11: Surface rendering of the Q50 horizon from the Laurentian East 3D data set. The Q50 reflection is missing from the western region of the data set and probably was removed by recent erosional processes. Erosional features are seen between paleo-topographic highs in this surface as well as having similar characteristics of the modern seafloor.

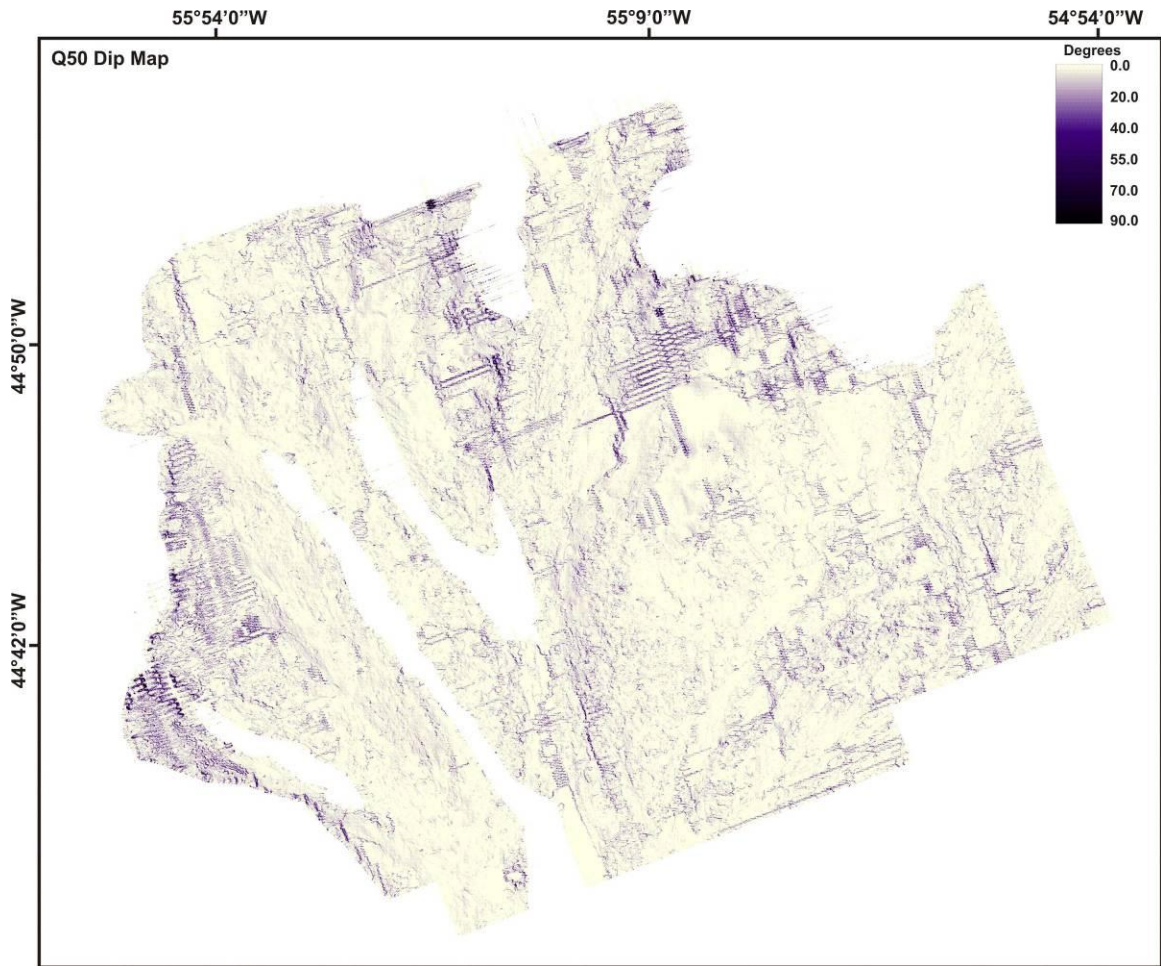


Figure 3.12: Dip map for the Q50 horizon from the Laurentian East 3D data set. There is little change in the degree of dip in this horizon. In the northeast and western sections of this horizon line features that run northeast – southwest are artifacts created from missed picks in the data.

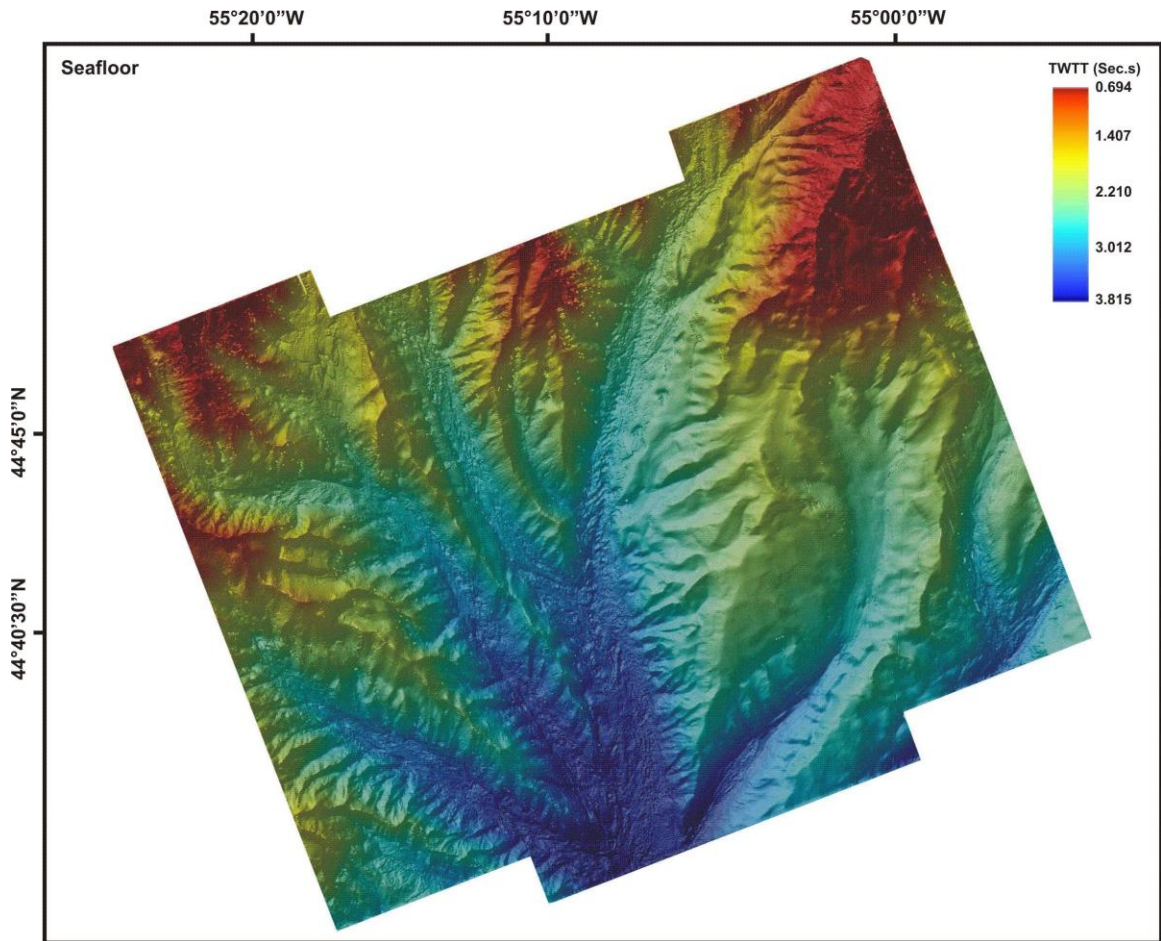


Figure 3.13: Seafloor render from the Laurentian East 3D data set displaying the dendritic nature of the modern morphology of the southwestern Newfoundland Margin. The modern seafloor of the southwestern Newfoundland Slope lies in water depths of between 400 and 3000 mbsl (using an average velocity of 1500 m/s).

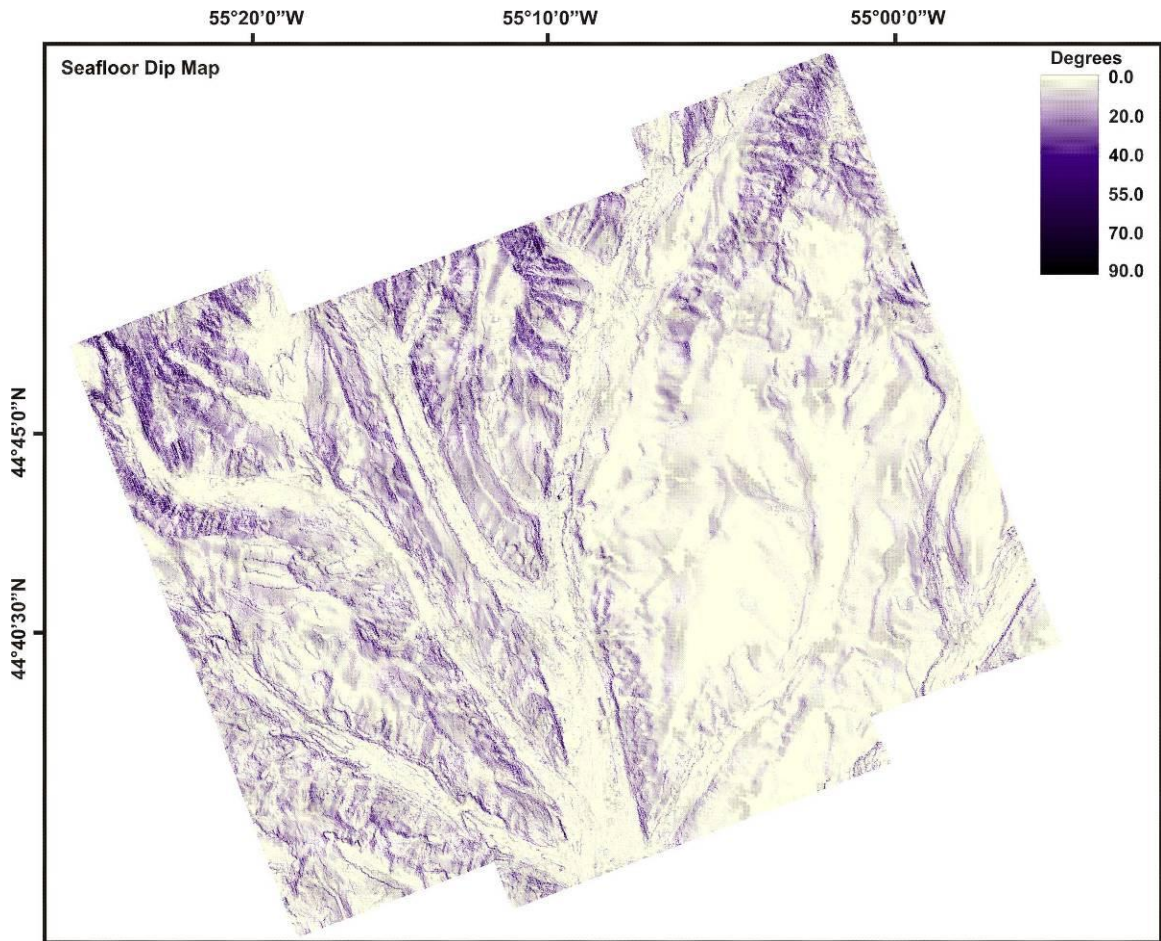


Figure 3.14: Dip map for the seafloor render of the Laurentian East 3D data set showing that the walls of inter-canyon ridges have dip angle of between 10° and 25°. Although the southeast corner of the study area has erosional features, it is not as complex as the western portion of the study area.

Grand Banks Valley. To the west and east of the dendritic morphology are the St. Pierre and Whale slopes respectively. Both the St. Pierre Slope and Whale Slope lie in water depths of 800 to 2500 mbsl and seaward of their respective banks on the continental shelf. The morphology of these two slopes is relatively smooth in comparison to the West Halibut, East Halibut, and Haddock Valley regions. There are amphitheatre shaped escarpments on these two banks that are 10's of kilometres long with 100's of metres of vertical relief (Fig. 3.15).

3.3: Seismic Units

The seismic data used in this study are divided into three units based on the stratigraphic framework established for the southwestern Newfoundland margin from the previous work completed by Piper and Normark (1989), MacLean and Wade (1992), and Piper et al. (2005). These units are labelled 1, 2 and 3 from the oldest to the youngest (Fig. 3.16 and 3.17). Unit 1 is the interval between the **K99** and **M70** reflections. This unit is present across the study area and is approximately 270 to 335 ms (~325 m to 400 m based on a 2400 m/s velocity) m below the present seafloor. It has a variable thickness ranging from 375 to 835 ms (~450 to 1000 m based on a 2400 m/s velocity), with thicker sections in the southwestern and northeastern regions of the study area (Fig. 3.18). Reflections above **K99** are sub-parallel to parallel with low to moderate amplitudes (Facies 1) and are laterally extensive. Seaward of the upper slope, reflections in Unit 1 are repeatedly offset as a result of the seaward dipping faults as well as keystone faults created by Argo Salt deformation (Fig. 3.19). In the upper slope of this unit, reflections are characterized as moderate to high amplitude and discontinuous with some having a

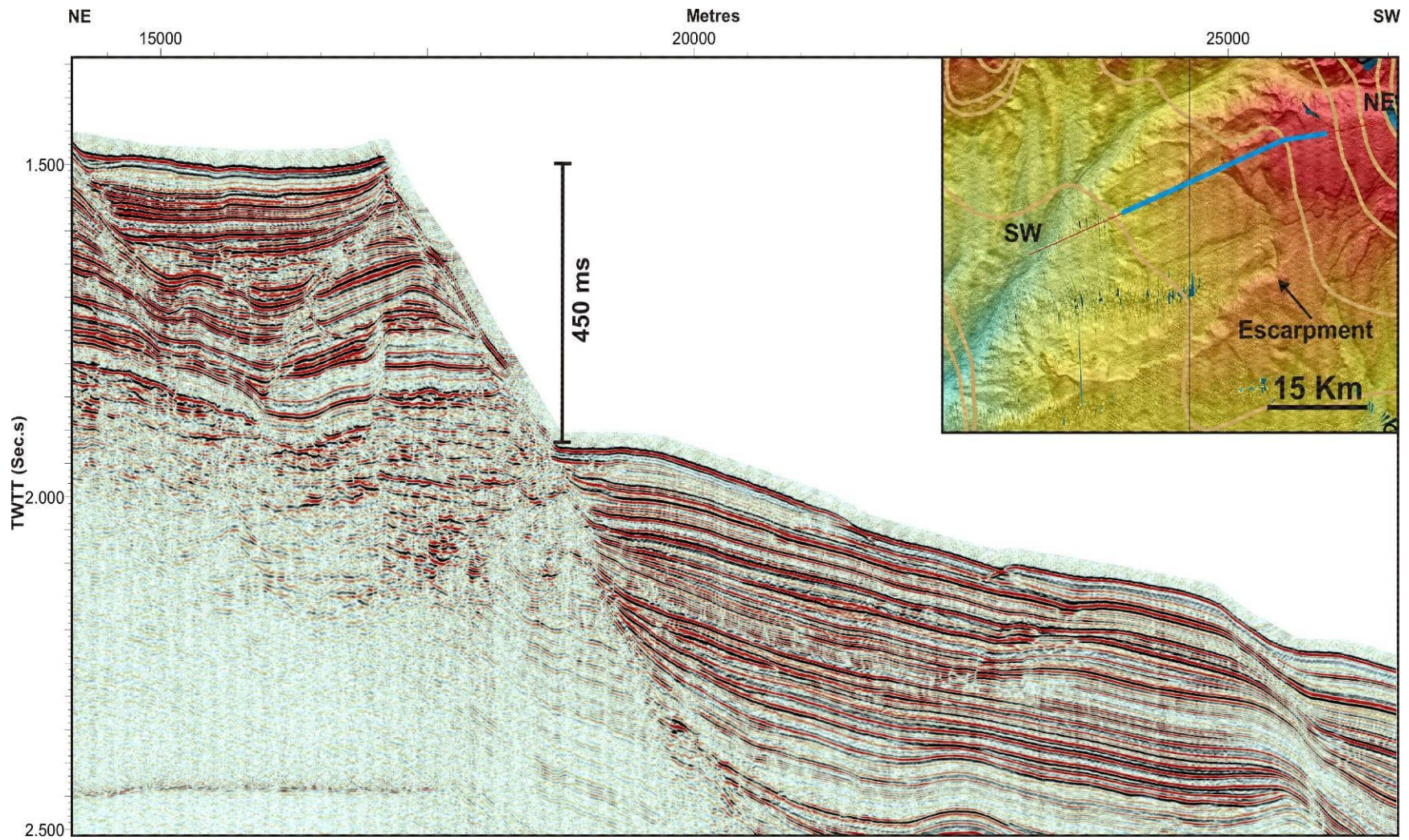


Figure 3.15: Seismic profile 34 from the Geological Survey of Canada – Atlantic Research cruise 2007_020 showing 300 m of relief (using a velocity of 1500 m/s) on Whale Slope. The amphitheatre shape of the erosional feature is seen in the multibeam bathymetry map (inset top left). The location of seismic profile 34 is represented by the blue on the inset map.

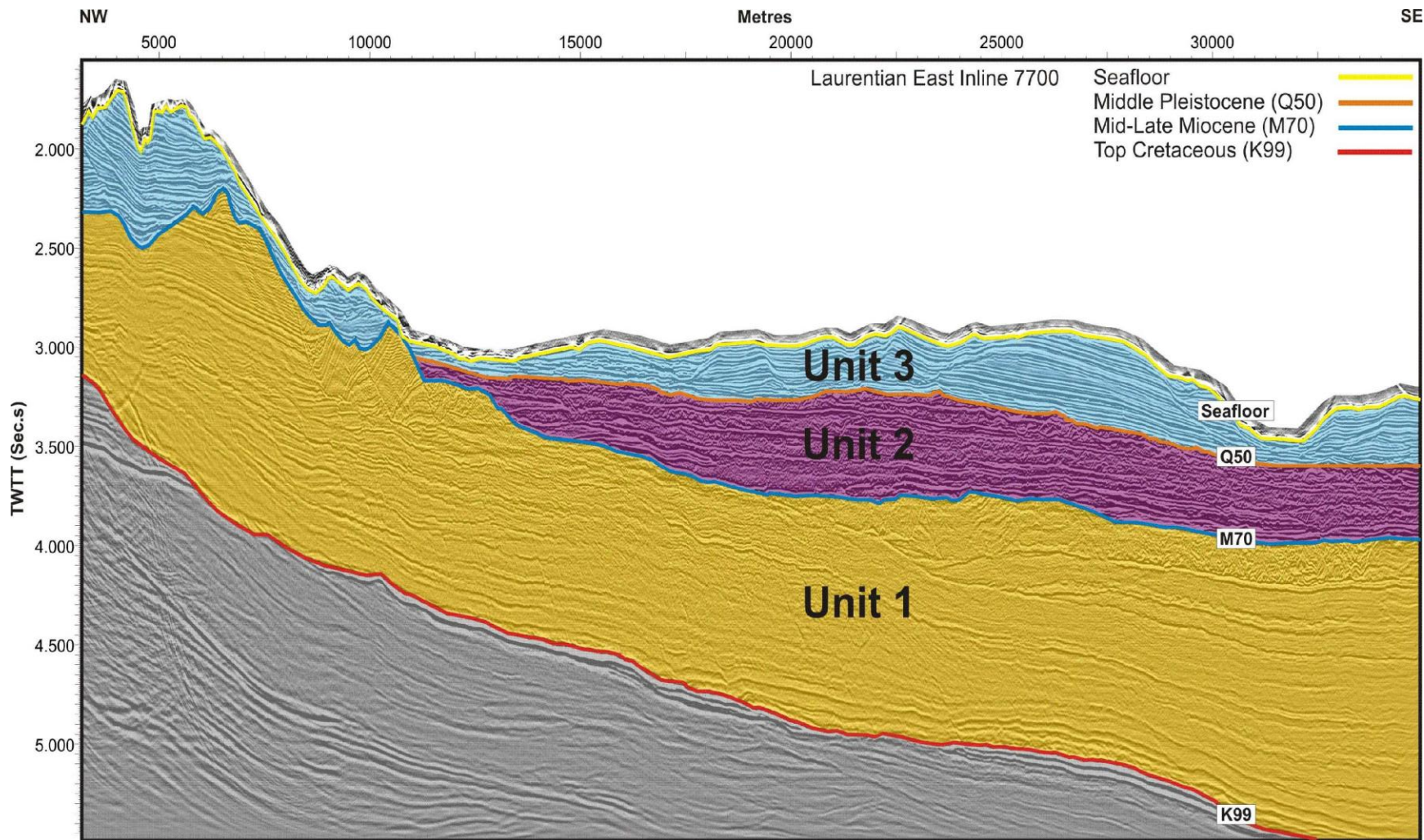


Figure 3.16: The Laurentian East 3D data set was divided into three seismic units numbered 1 through 3 with 1 being the oldest. Inline 7700 from the data set shows the four key seismic reflections used to define the lower and upper limit of each unit. Unit 1 is bounded by the K99 and M70 reflections, Unit 2 is between M70 and Q50, and Unit 3 is defined by Q50 and the seafloor.

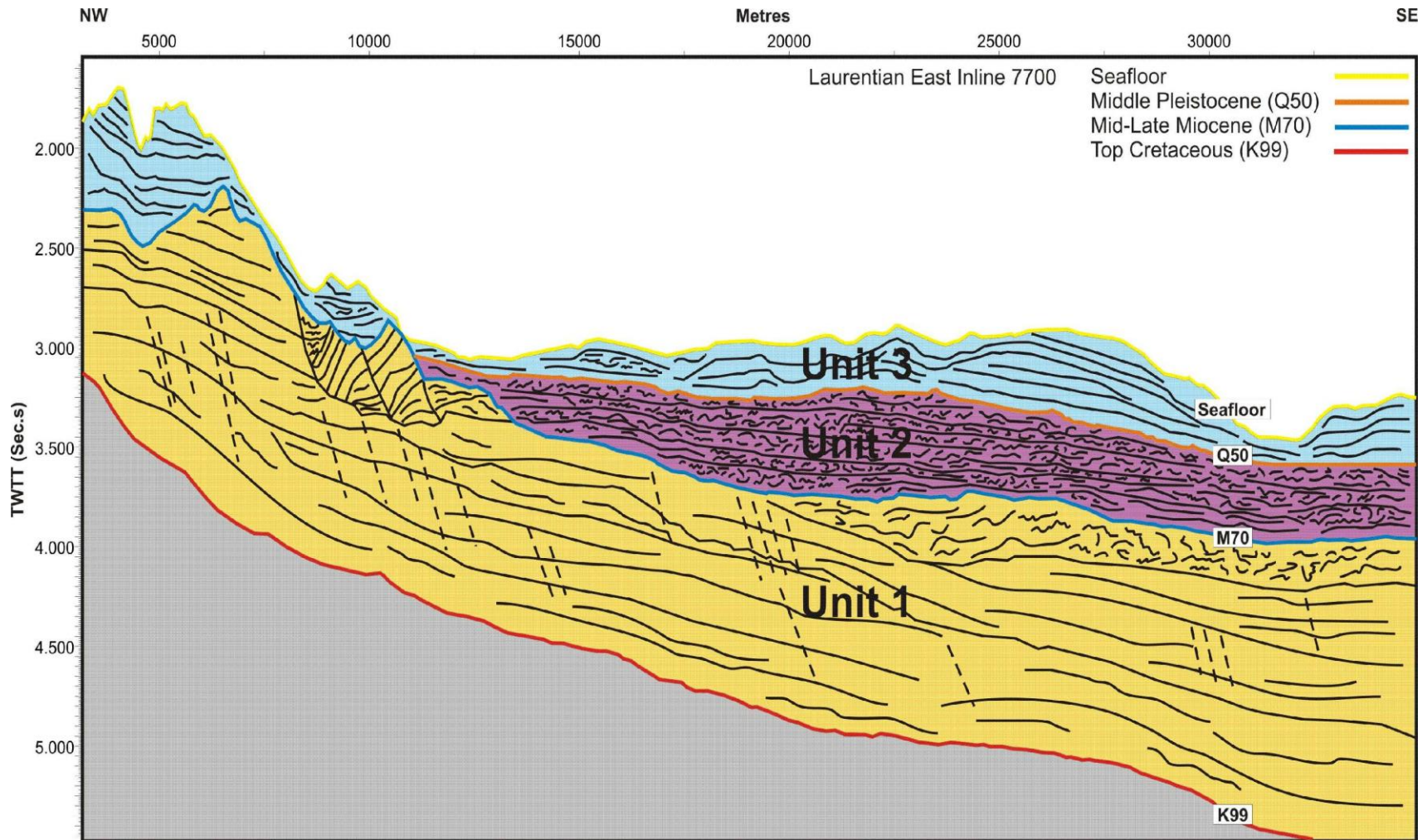


Figure 3.17: Line drawing of Inline 7700 showing the three seismic units defined in the Laurentian East 3D data set. The lower section of Unit 1 consists of parallel reflections that were offset by faults (dashed black lines). In the upper portion of Unit 1, reflections are rotated in the upper slope while further seaward reflections are chaotic in nature. Unit 2 consists mostly of stacked packages of chaotic reflections. Parallel reflections inter-bedded with thin chaotic reflection packages define Unit 3.

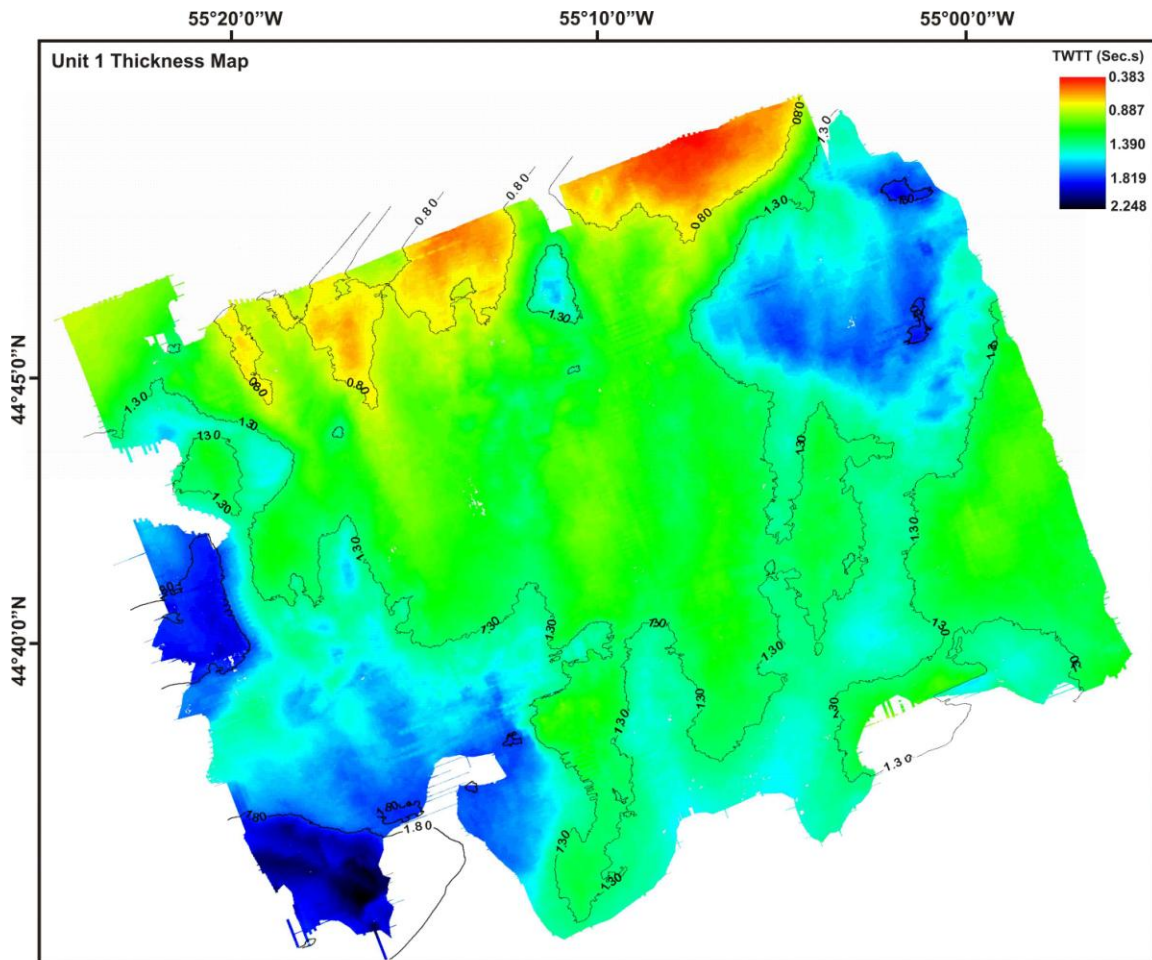


Figure 3.18: Thickness map for Unit 1 shows that the unit is of a uniform thickness as shown by the green. Blues in the northeast and southwest indicate thicker sedimentary sections.

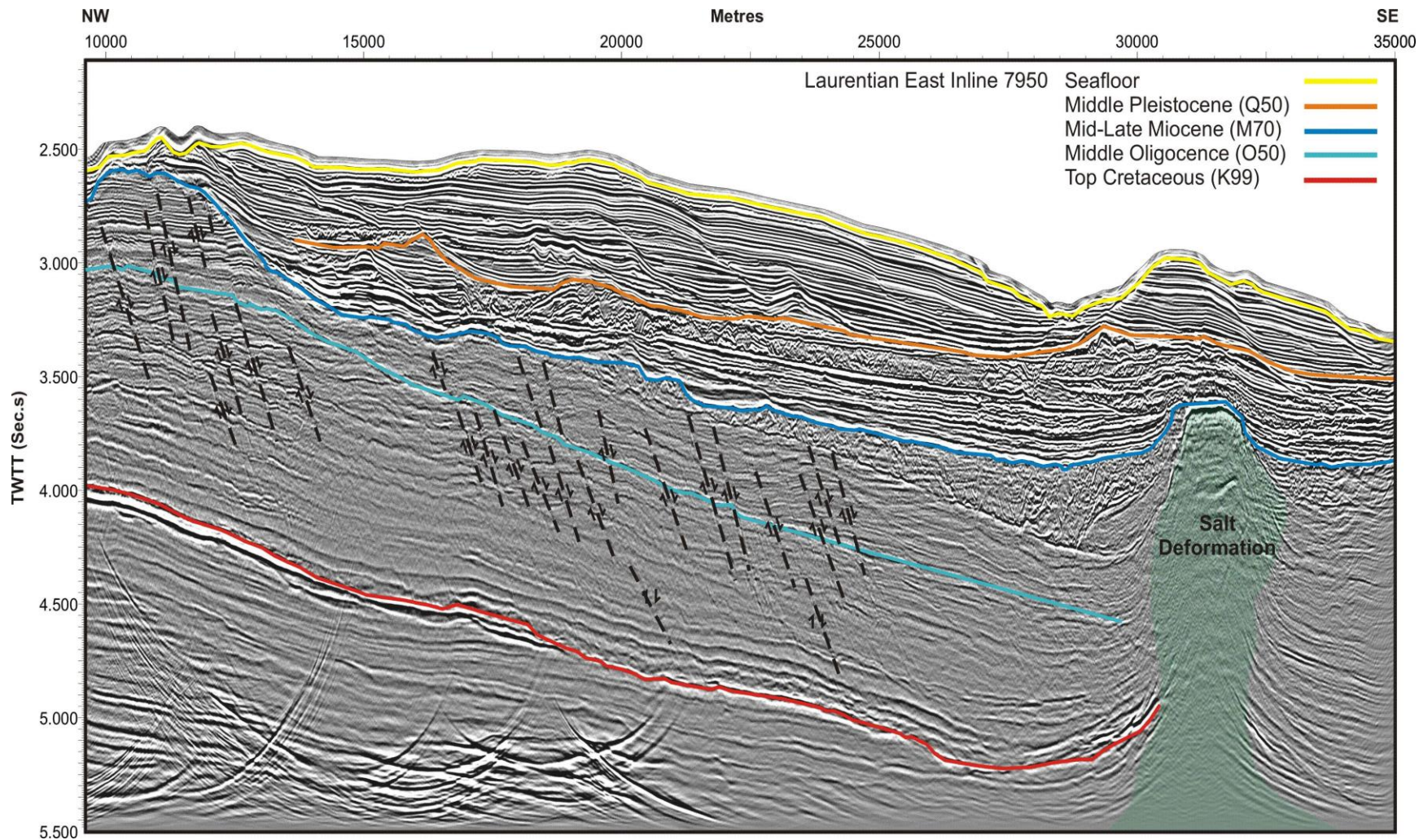


Figure 3.19: Inline 7950 from the Laurentian East 3D data set shows the deformation caused by Argo Salt diapirism in Units 1 and 2. The Argo Salt prevents correlation of some reflections within the data set. Faulting occurs through Unit 1 with faults terminating at the base of the thick chaotic package or at the M70 reflection.

contorted nature (Facies 4 and Facies 6). Moving up the unit towards **M70**, reflections in the lower slope alternate between reflection free and low to moderate amplitude, parallel continuous (Facies 1 and Facies 5). At the top of Unit 1, reflections become discontinuous and chaotic in nature (Facies 3 and Facies 6). These reflections have moderate amplitudes and are not laterally extensive. This package of discontinuous and chaotic reflections is thickest and most recognizable in the centre of the Laurentian East 3D data set, but it thins to the west and pinches out in the east. In the northeast corner of the data set, a small package of parallel reflections approximately 125 to 187 ms (~150 to 225 m based on a velocity of 2400 m/s) thick are rotated in comparison to proximal reflections (Fig. 3.20).

Unit 2 is the interval between the **M70** and the **Q50** reflections and has a thickness that varies between 71 and 238 ms (~75 to 250 m based on a 2100 m/s velocity), with the thickest section occurring in the centre of the data set (Fig. 3.21). At the base of Unit 2, there is a thin package of continuous and parallel reflections with moderate to high amplitudes (Facies 2). Above these parallel reflections, there is a section of alternating continuous reflection and chaotic reflection packages (Facies 3). Stacks of chaotic packages dominant the centre region of the study area but become less prevalent in the western and eastern regions and are replaced with sub-parallel to parallel reflections (Facies 2). Unit 2 is thickest from mid slope towards the abyssal plain, but it pinches out in the shelfward direction at the upper slope. Unit 2 is deformed by Argo Salt in the southern region of the study area, although deformation is not as severe as in Unit 1 (Fig. 3.19). In the St. Pierre Slope region of the study area, just above the **M70** reflection is a

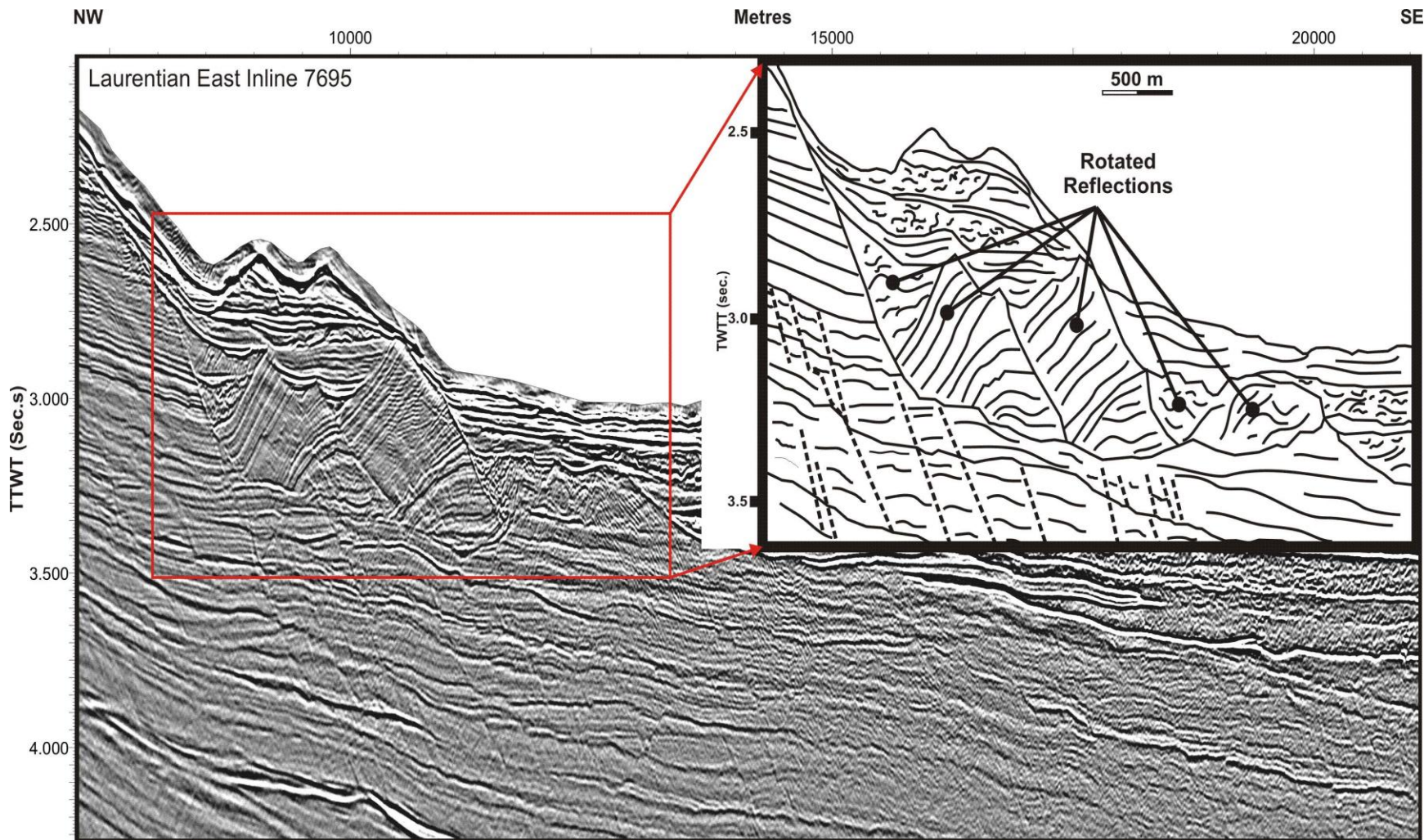


Figure 3.20: Inline7695 from the Laurentian East 3D data set shows 300 to 450 m thick rotated blocks of reflections that are located on the upper Newfoundland Slope. The inset in the top right corner is a line drawing representing the interpretation of the rotated reflections.

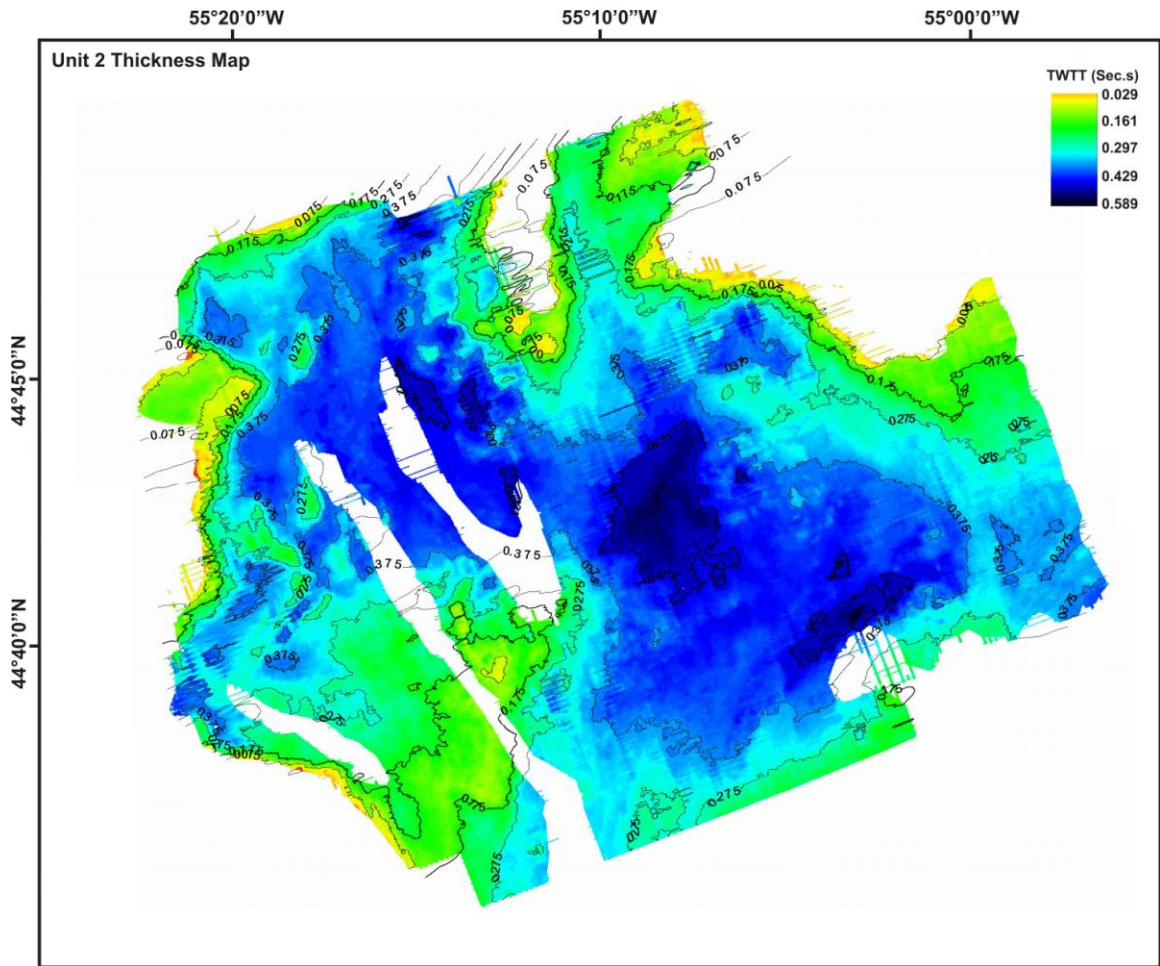


Figure 3.21: Thickness map for Unit 2 shows that the thickest section in this unit is about 450 m and runs from the northwest to the southeast (represented by the blue).

71 to 91 ms (~ 75 to 95 m based on a 2100 m/s velocity) thick facies of undulating and wavy reflections (Facies 4) that covers an area of approximately 1000 km².

The upper unit in the study area, Unit 3, is not present throughout the lateral extent of the data set. It is the interval between **Q50** and the seafloor pick and its thickness varies between 23 and 240 ms (~25 and 250 m based on a 2100 m/s velocity) (Fig. 3.22). It is thinnest through the centre of the study area where recent erosional processes have apparently removed it. Unit 3 consists of low and high amplitudes, parallel to mounded reflections (Facies 1 and Facies 2) with thin packages of chaotic reflections (Facies 3) through the section (Fig. 3.16 and 3.17). The inter-canyon ridges which are the bathymetric highs in the West Halibut, East Halibut, and Haddock Valley regions are confined to seismic Unit 3. Correlation of Unit 3 is more difficult in the western portion of the Laurentian East 3D data set compared to the central and eastern regions. Continuing east across the data set, Unit 3 thins moderately and identification of its base becomes difficult as result of inter-canyon ridges. Unit 3 is thickest at the mid slope but thins in the shelfward direction where it is not preserved in some areas.

3.4: Stratigraphic Framework

The stratigraphic framework for the southwestern Newfoundland margin was established through the integration of five stratigraphic markers into the Laurentian East 3D data set based on published data located on the neighbouring continental shelf and slope (Fig. 3.4). Well data, including age control, were correlated to seismic profiles with synthetic seismograms (Fig. 3.23). Well to seismic correlations are available in the Laurentian East

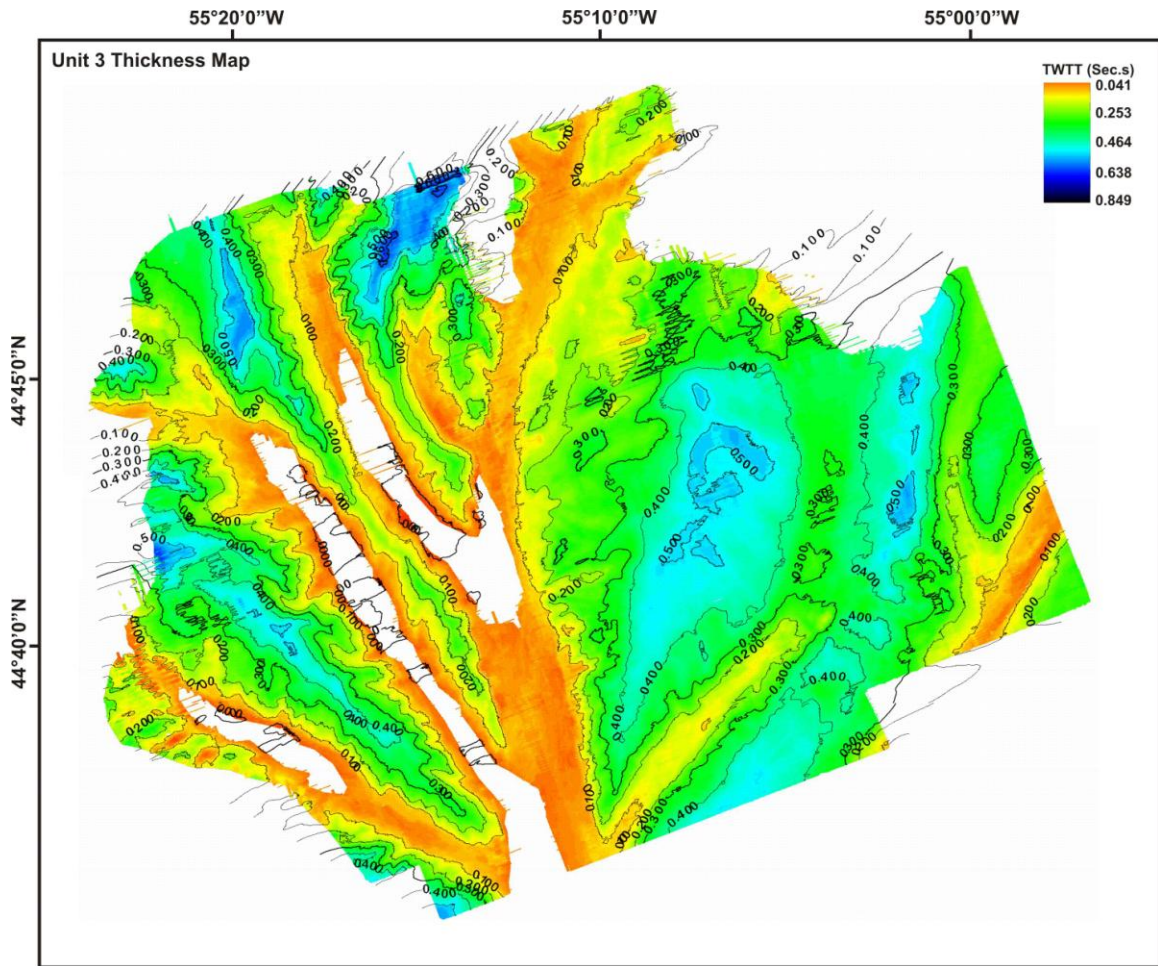


Figure 3.22: Unit 3 is relatively thin compared to Units 1 and 2. The thickest section for Unit 3 is found in the eastern region of the data. The unit is thinnest where presumed recent erosional processes removed material on the modern seafloor.

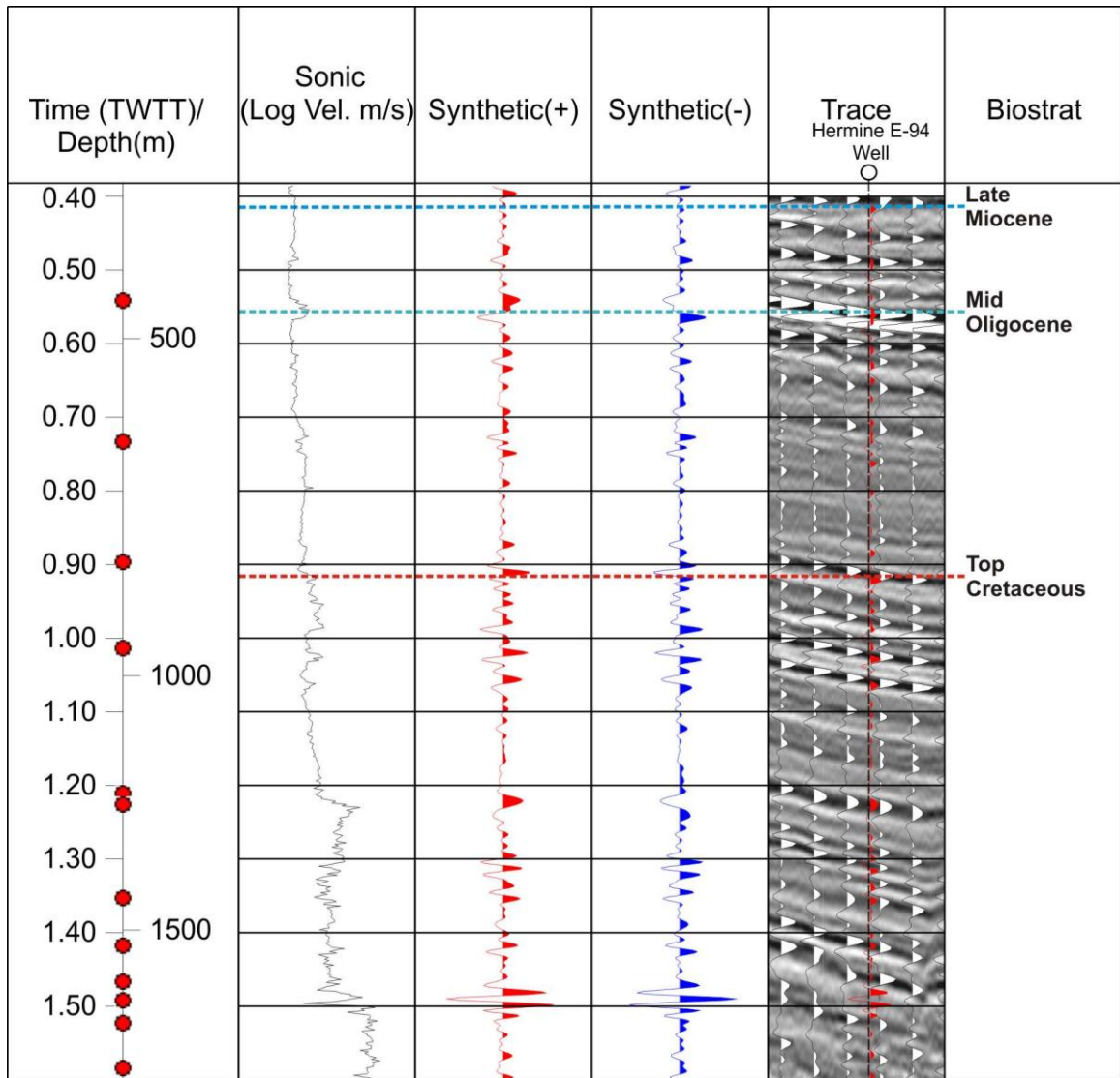


Figure 3.23: Age control diagram for Hermine E-94 well. Comparison of wiggle plot and seismic section to synthetic seismogram calculated from Sonic log.

3D volume using the Hermine E-94 and the STP 2D seismic survey. Correlating reflections from the southwestern Newfoundland continental shelf across the shelf break and to the continental slope is difficult because of erosional processes affecting the shelf to slope transition zone.

The five stratigraphic markers used to create the framework are **K99**, **O50**, **M70**, **Q50**, and the modern seafloor. The **K99** is a coeval marker for the top Cretaceous, **O50** represents the mid Oligocene unconformity, **M70** is a late Miocene marker, **Q50** is a middle Pleistocene marker and the seafloor which represents the present day morphology of the Halibut Valley region of the Newfoundland Slope. The top Cretaceous (**K99**) and mid Oligocene (**O50**) markers for the St. Pierre Slope were originally proposed by MacLean and Wade (1992) and confirmed by new biostratigraphy work presented in Piper et al. (2005). The M90 stratigraphic marker defined by the new biostratigraphy completed on the Hermine E-94 by Piper et al. (2005) represents a middle-late Miocene marker. When mapped in the Laurentian East 3D data set, M90 is located between two packages of chaotic reflections making it difficult to map laterally for any distance. **M70** was used to establish the stratigraphic framework as it was below the stack of chaotic reflections and correlated more easily across the data set.

The palynological analysis used to define the ages for the **K99**, **O50**, and **M70** markers are based on known stratigraphic ranges of dinoflagellates in European sections and other wells from the Grand Banks (Piper et al., 2005). The top Cretaceous (**K99**) strata from Santonian to Maastrichtian are recognized from ~ 920 m to ~ 1189 m by MacLean and

Wade (1992) and confirmed by Piper et al. (2005). Rupelian strata (early Oligocene) are recognized from ~ 470 m to ~ 545 m based on index species *Enneadocysta pectiniformis*, *Operculodinium divergens*, *Phthanoperidinium coreodites*, and *Wetzeliella coleothrypta*. Serravallian strata (late mid-Miocene) are sampled between ~ 441 m and ~ 463 m based on the diagnostic species *Cleistosphaeridium diversispinosum*, *Hystriochosphaeropsis obscura*, and *Unipontidinium aqueductus*. The late Miocene section extends from ~ 436 m to the highest available sample at ~341 m. The middle Pleistocene marker (**Q50**) was established on the Laurentian Fan by Piper and Normark (1989) and is based on the deepest, well-developed till tongues representing the onset of Pleistocene glaciations. Establishing this stratigraphic framework for the southwest Newfoundland margin allows for age determination of the three stratigraphic units and to relate their depositional processes with possible regional and/or global events.

Chapter Four: Discussion

4.1: Seismic Stratigraphic Units and Mass Transport Deposits

4.1.1: Interpretation of Seismic Units

In the study area, four key seismic reflection events are used to establish three Cenozoic units, where Unit 1 is the oldest and Unit 3 is the youngest. The base of Unit 1 is defined by the **K99** reflection event which is a coeval marker for the top Cretaceous (MacLean and Wade, 1992). Along the top Cretaceous paleo-shelf break, incisions that run northwest-southeast are interpreted to be canyon systems on the continental slope. The paleo-bathymetric highs between these canyon system represent inter-canyon ridges. These inter-canyon ridges have a dendritic morphology similar to the modern surface (Mosher and Piper, 2007) (Fig. 4.1). The canyon systems acted as conduits to transport sediment from the shelf break, bypassing the slope and depositing them further offshore similar to those mapped by Brake (2009) for the Oligocene and the modern canyons in this area (Jenner et al., 2006). In the southeast corner of the data set, mini basins are a result of diapirism from the underlying Argo Salt Formation (Fig. 4.2). In the western region of the study area, salt diapirism also affects sediments of the mid-slope as well as the **K99** horizon event, but no salt withdrawal mini basins appear to have developed as in the Gulf of Mexico (Peel et al., 1995; Hudec et al., 2009). Unit 1 is defined by sub-parallel to parallel reflections (Fig. 2.2) that likely represent background deposition or draping sediments that occur across the data set (Armitage et al., 2010). Seaward dipping faults occur across the study area through Unit 1 where they terminate at either the **Z** reflection event or the **M70** reflection event (Fig. 4.3). These faults are thought to weaken the sediment, making it more susceptible to failure and are believed to be created by

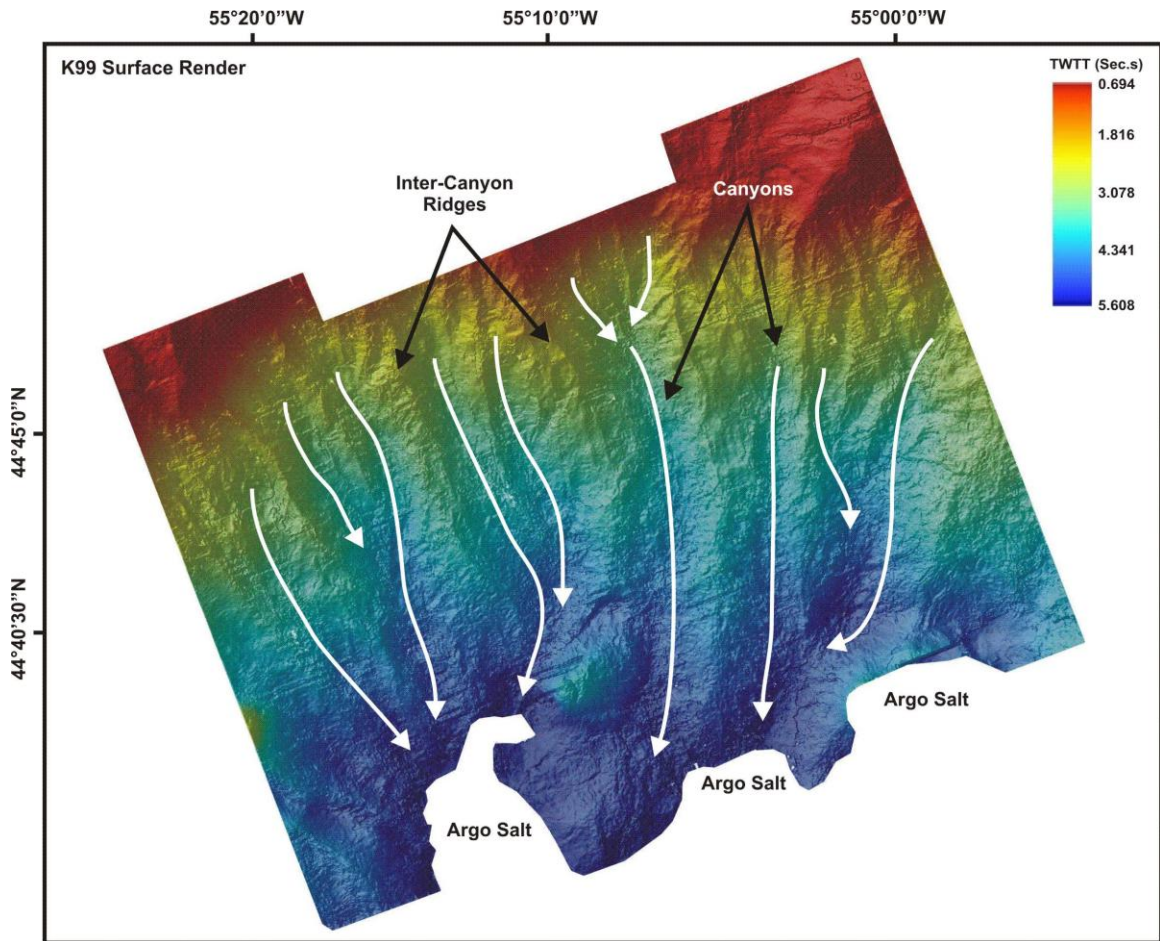


Figure 4.1: This rendering of the K99 horizon shows Late Cretaceous canyons (the areas of which are represented by white arrows) and inter-canyon ridges.

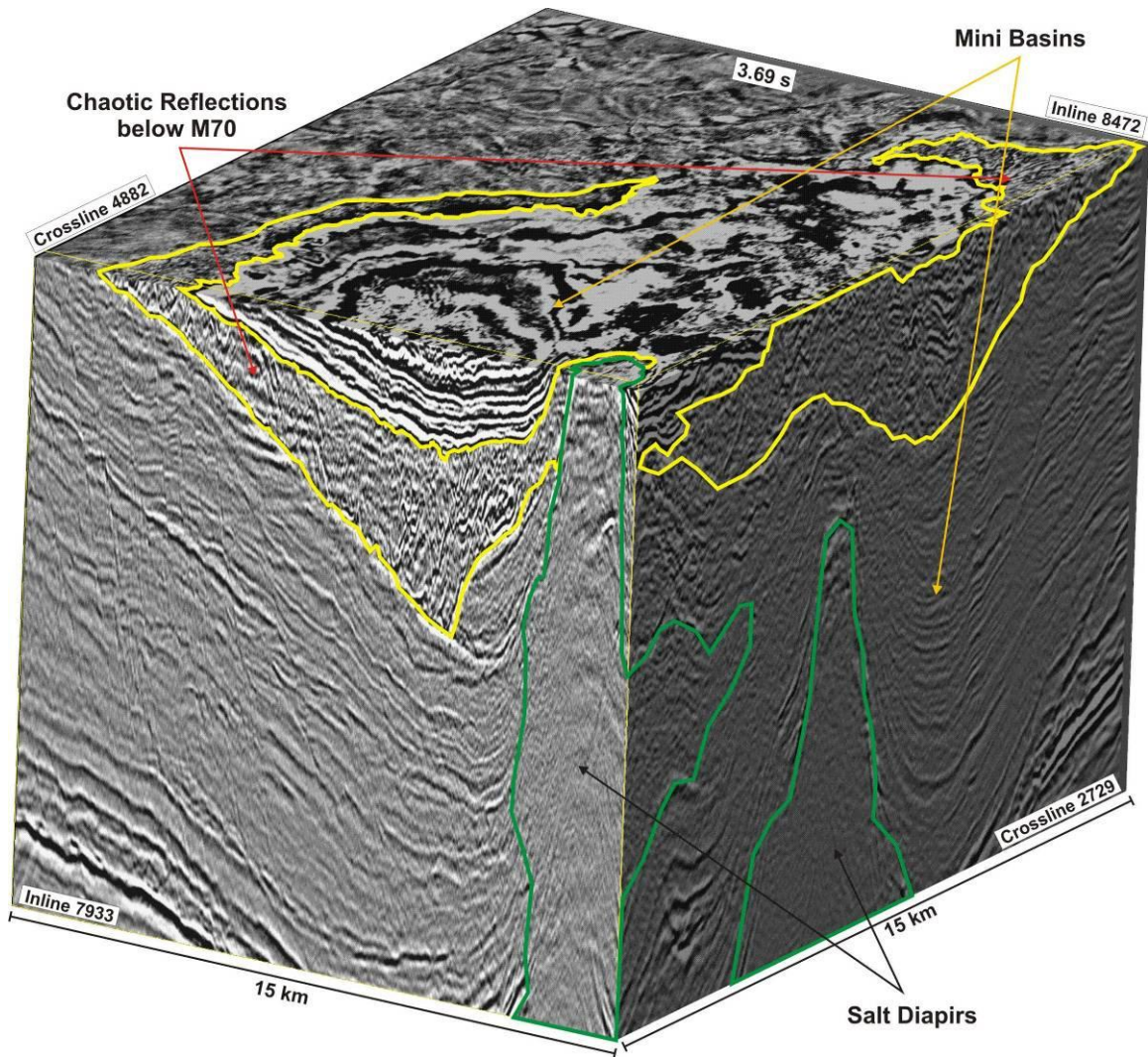


Figure 4.2: The Laurentian East amplitude volume shows formation of mini basins in response to diapirism of the Argo Salt Formation in the southeast corner of the study area. The yellow outlined MTD is late Miocene in age. The salt diapirs are outlined in green.

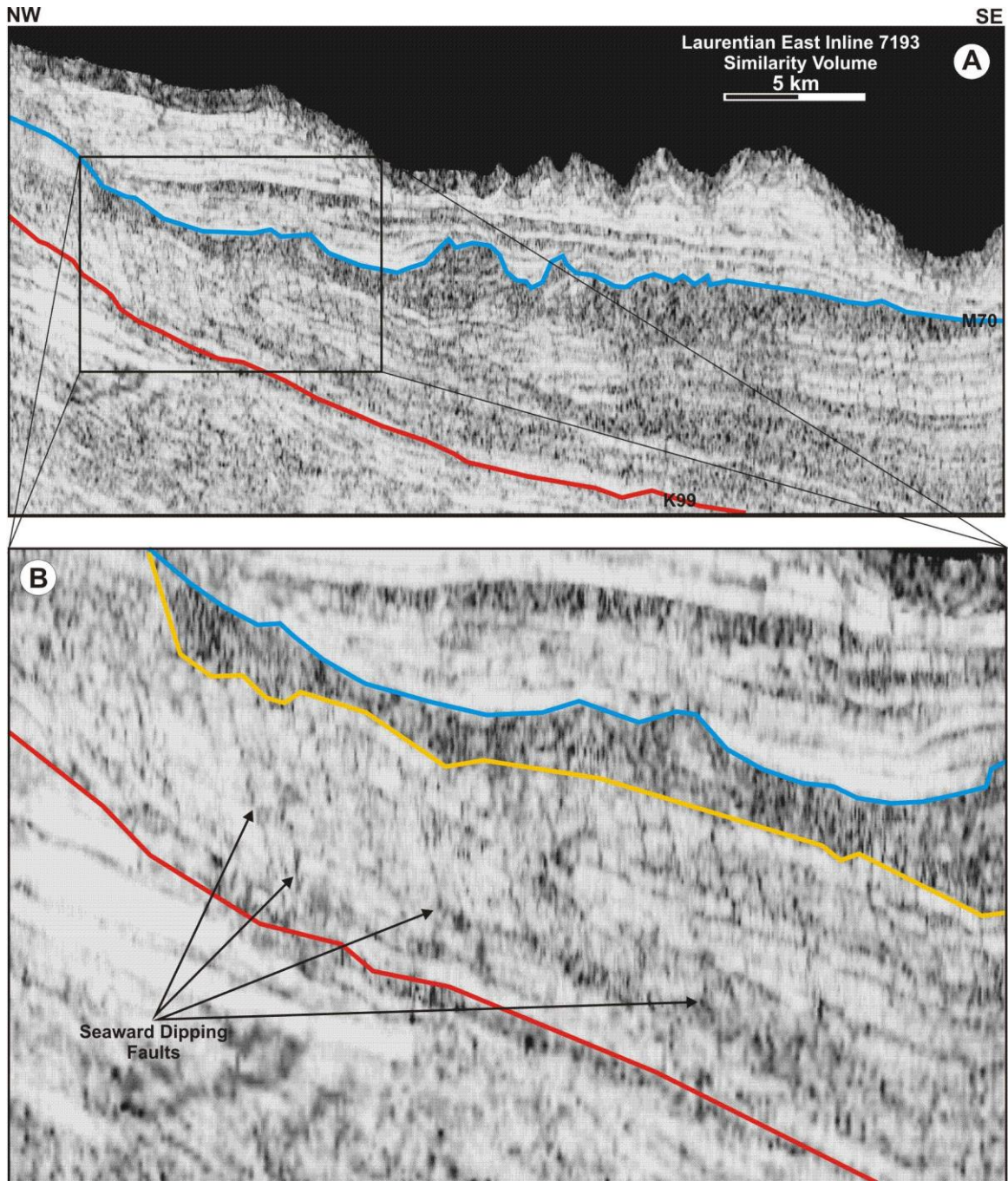


Figure 4.3: Seaward dipping faults present in Unit 1 are shown in a “similarity volume” of the Laurentian East data set. (A) Laurentian East Inline 7193 shows that the seaward dipping faults extend across the data set. (B) An enlargement from (A) represented by the black rectangle shows these faults extend from the red K99 reflection event and terminate at either the Z reflection event (yellow horizon) or the M70 event reflection.

loading and consequent extension developed during the deposition of the overlying strata similar to those in the Congo Basin (Gay et al., 2004) and North Sea Basin (Cartwright and Lonergan, 2003). Below the **Z** reflection event, wavy concordant reflections (Fig. 2.2 and Fig. 3.1) are believed to be sediment waves formed in response to contourite currents like those of the Faeroe-Shetland Channel (Knutz and Cartwright, 2003) and western Scotian margin (Campbell and Deptuck, in press) (Fig. 4.4). At the top of Unit 1, a thick package of chaotic reflections is interpreted as a mass transport deposit (MTD) where reflection event **Z** forms the erosional base of the MTD. This MTD represents a single failure event. The chaotic seismic facies is constant from its base to its top. Rotated slump and slide blocks in the upslope region of this MTD have comparable thicknesses suggesting that they were part of this single failure event. In the subsurface of the Halibut Channel, this MTD has an area of 900 km² and thicknesses as much as 500 ms (~600 m). Using an average thickness of 210 ms (~250 m), the volume for this MTD is estimated to be 225 km³. The **M70** reflection event defines the top of this large MTD. It also is a stratigraphic marker for the region and is approximately late Miocene in age based on stratigraphic ties with Piper et al. (2005) (Fig. 4.5). Paleo-topographic highs in the northeast corner of the data set and along the upper slope represent the paleo-shelf break during the mid-late Miocene. Incisions along the paleo-shelf break designate canyons which appear to converge towards the south. In the western section of the **M70** horizon, ridges running north-south represent the topography created by the blocky nature of the underlying large MTD.

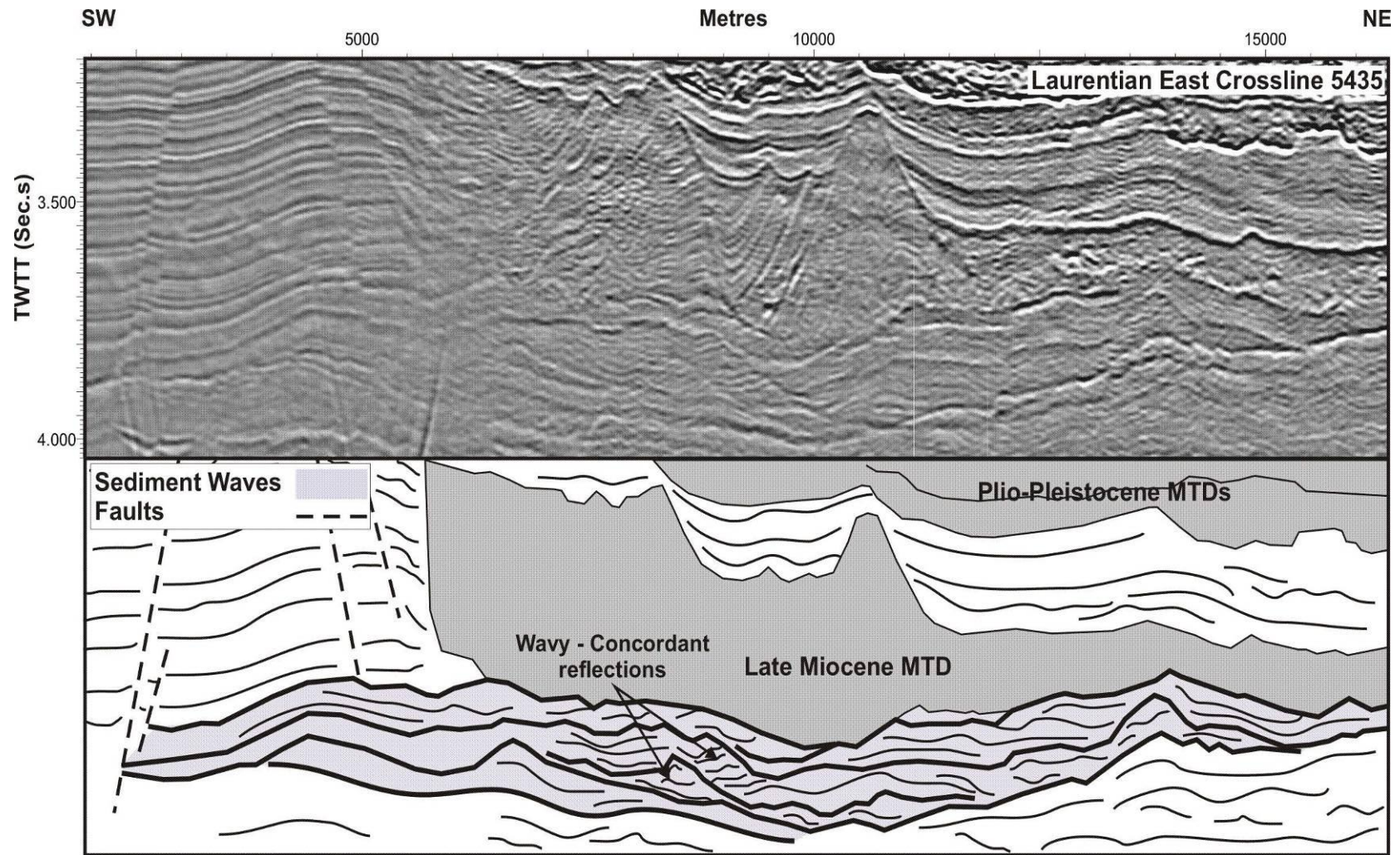


Figure 4.4: Wavy concordant reflections below the late Miocene MTD (represented by the purple) from the Laurentian East Crossline 5435 are interpreted to be sediment waves formed by bottom currents.

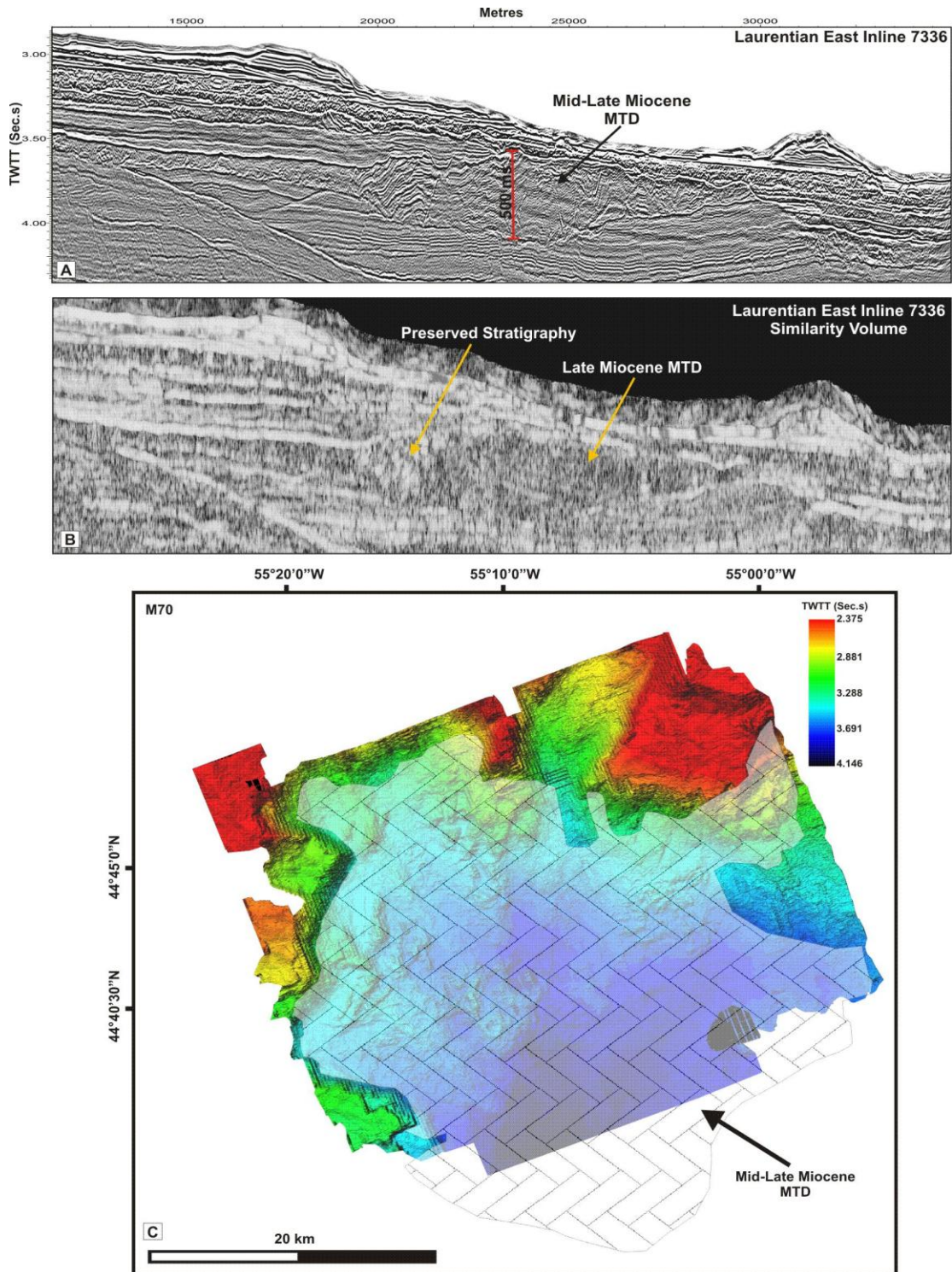


Figure 4.5: The late Miocene MTD: (A) In areas of the Laurentian East data set, the MTD has thickness up to 500 ms. (B) Shows the late Miocene MTD in the similarity volume as well as other small MTDs above it. MTDs darker and not continuous compared to the surrounding sediments which are interpreted as parallel and continuous bedding. (C) This MTD covers an estimated area of 900 km² as mapped in the Laurentian East and TGS-NOPEC data sets. It is represented as a translucent outline over the M70 surface render.

Seismic Unit 2 is characterized by a stack of chaotic reflection packages with thicknesses of up to 143 ms (~150 m). The base of Unit 2 is defined by the **M70** reflection event and the top is bounded by the **Q50** reflection event. The package of undulating reflections above **M70** on the St. Pierre Slope is interpreted as sediment waves (Fig. 4.6). A fault extends from the modern seafloor and soles out in this sediment wave package. Stacked packages of chaotic reflections are interpreted to be MTDs that are deposited on top of each other and they directly overlie the large, late Miocene MTD in some regions of the study area as a seismic unit (Fig. 4.7). This package of stacked MTDs could also be interpreted as a single, large scale MTD similar to the late Miocene failure in Unit 1. The presence of strong amplitude reflections between packages of chaotic reflections suggest individual events, particularly when some of the reflections appear to erode into lower depositional events. The preservation of parallel reflections packages between some of the chaotic units suggests periods of sediment deposition between events and further supports smaller, individual failures rather than one large failure. Nine MTDs are mapped in Unit 2 and have a range in sizes and scales as seen in Table 4.1. One MTD (#6) within Unit 2 has a thickness between 71 ms (~75 m) and 81 ms (~85 m), covers an area of 400 km² and has a volume of 35 km³. A second MTD (#9) from this unit has an approximate thickness of 143 ms (~150 m), covers an area of 375 km² and has a volume between 50 and 60 km³. The largest MTD in this unit (#8), has a thickness of 95 ms (~190 m), covers an area of over 400 km², and has a volume of > 60 km³. The MTDs in Unit 2 are likely larger than what is stated here as some extend outside of the Laurentian East 3D data set.

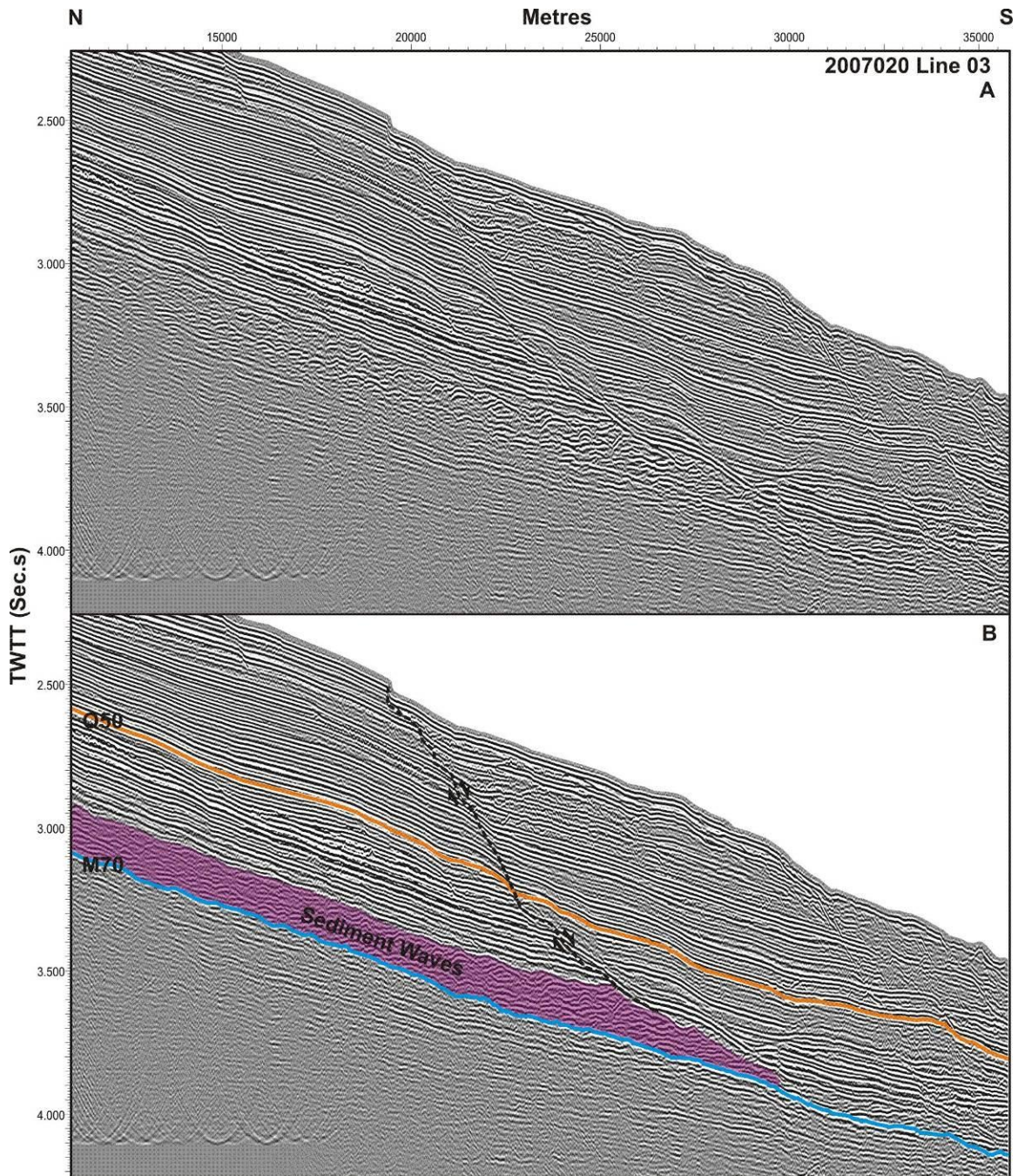


Figure 4.6: Sediment waves from the St. Pierre Slope. (A) An un-interpreted section of Line 03 from Cruise 2007020. (B) Undulating reflections above M70 are interpreted to be sediment waves (purple package). A fault extends from the seafloor and soles out in this package.

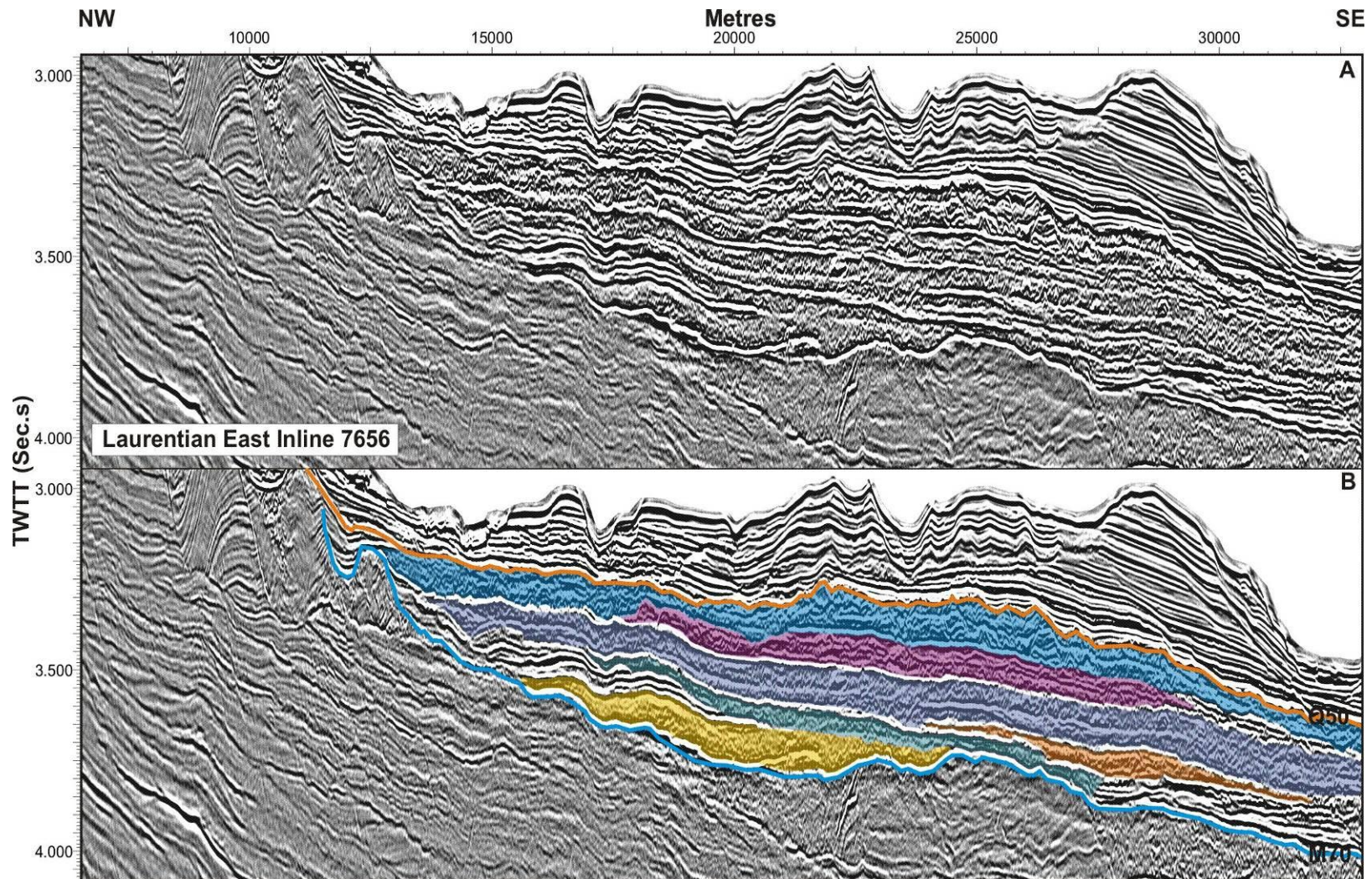


Figure 4.7: (A) represents an un-interpreted profile from Inline 7656 of the Laurentian East data set. (B) Stacks of recurring MTDs (coloured polygons) are interpreted between M70 (blue) and Q50 (orange) with volumes $\sim 60 \text{ km}^3$ and covering areas $\leq 400 \text{ km}^2$.

MTD	Thickness (Time - ms)	Thickness (km)	Area (km ²)	Volume (km ³)
2	55	0.11	30	3.3
3	50	0.1	58	5.8
4	45	0.09	40	3.6
5	45	0.09	79	7.1
6	60	0.12	397	48
7	45	0.09	72	6.5
8	95	0.19	317	60
9	70	0.14	403	57
10	55	0.11	30	3.3

Table 4.1: The dimensions of the nine MTDs mapped in Unit 2. Thicknesses in km are calculated using a velocity of 2000 m/s. The dimensions of the MTDs are likely larger as the MTDs typically extend outside of the coverage of the Laurentian East 3D volume. The numbering of the MTDs begins with 2 in order to correspond to Figure 4.28.

The MTDs mapped in Seismic Unit 1 and 2 represent a significant portion of the Cenozoic stratigraphy within the coverage of the Laurentian East 3D data set. The Cenozoic stratigraphy within the 3D data set has a volume of ~ 1560 km³ and of that volume, MTDs make up 425 km³. In total, the MTDs identified between the late Miocene and Middle Pleistocene represent 27 % of the sedimentary column since the top of the Cretaceous and up to 60 % of the sediment column since the Miocene. This indicates that mass transport processes were an important mechanism in the evolution of the southwestern Newfoundland margin during the Cenozoic and should be considered as a major component for sedimentation models of passive continental margins.

Mass transport processes in the late Miocene represent a change in sedimentation style from fine-grained, aggradational deposition for the majority of Unit 1 to the movement of massive amounts of sediment represented by the late Miocene MTD at the top of Unit 1 and the stacked MTDs in Unit 2. The **Q50** reflection event is the stratigraphic marker

between Unit 2 and Unit 3. It is Middle Pleistocene in age and signifies the onset of shelf-crossing glaciation that reached the St. Pierre Slope (Piper, et al., 2005). Incisions along the upper slope of the **Q50** horizon are interpreted to be canyon systems that cut the paleo-shelf and slope. The **Q50** horizon has similar characteristics as the erosional canyons of the modern seafloor. There is a canyon system in the east that runs northeast-southwest; central canyon systems that run north-south; a canyon system in the west that runs northwest-southeast; and a paleo-topographic high in the northeast (Fig. 4.8).

Unit 3 is the uppermost unit in the study area. Its base is defined by the **Q50** reflection event and its top is the modern seafloor. This unit consists of alternating high and low amplitude sub-parallel to parallel reflections that truncate and converge downslope to form wedge-shaped structures. High resolution reflection seismic data indicates that there are interspersed packages of chaotic reflections. The alternating high and low amplitude reflections may represent material deposited by turbidity currents and proglacial sediment plumes (Armitage et al., 2010). Small interspersed chaotic packages may represent local, small scale failures in the region. The wedge-shaped deposits are interpreted to be levees built by overbank deposits of turbidity currents directed along subaqueous channels. Deposits from turbidity currents and proglacial plumes as well as smaller-scaled sediment failures (e.g. channel and canyon wall collapse) represent another dramatic change in sedimentation style on the margin where aggradation and progradation control the evolution of the margin. Modern inter-canyon ridges create the majority of relief on the slope and are the remaining remnants of sediment from Unit 3. The canyons between these ridges formed through the erosional flows and/or local failure events.

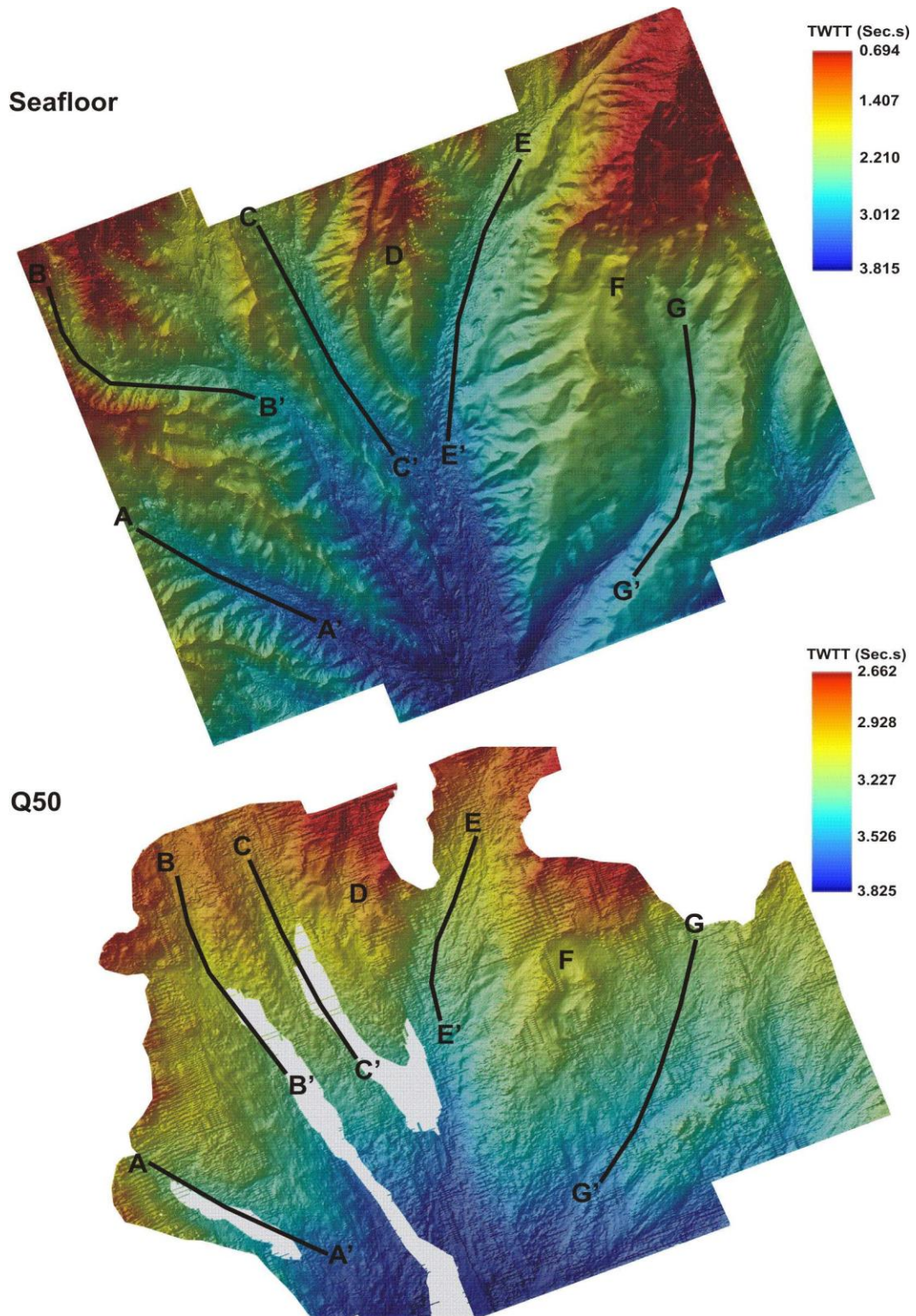


Figure 4.8: The Q50 and Seafloor rendered surfaces have canyon systems located in similar positions as denoted by canyon incisions (A, B, C, E, and G) and topographic highs (D and F). This observation suggests that the process responsible for the Q50 surface recurs through the evolution of the margin.

4.1.2: Comparison to the Scotian and NE Newfoundland margin

This comparison will provide insight into the timing and scale of mass sediment failure along Canada's eastern margin during the Cenozoic (Fig. 4.9). Published case studies to east of this study completed by MacDonald (2006), Brake (2009) and Deptuck (2003) to the west, are used to compare similar sedimentary processes across the Scotian and Newfoundland margins.

4.1.2.1 – Central Scotian margin

The Central Scotian margin is 650 km west of the study area where MacDonald (2006) studied a relatively complete Cenozoic section of the Scotian margin. The study focused on the influences of sealevel change, paleo-channel incision and overbank deposition, and salt tectonics on the stratigraphy of that region. MacDonald (2006) divided the Cenozoic section of his study area into five sequences correlated to biostratigraphic control in wells. Age control was established with two wells on the shelf and two wells on the slope (Shubenacadie H-100, Eagle D-21, Glenelg N-49, and Newburn H-23). MacDonald's Sequence Unit 1 through to Sequence Unit 3 represents the same time interval as Unit 1 on the southwestern Newfoundland margin. Sequence Unit 4 and part of Sequence Unit 5 correlate to Unit 2, and the remainder of Sequence Unit 5 is equivalent to Unit 3. Thickness maps are not available for the study of the central Scotian margin (MacDonald, 2006), but based on seismic sections, Sequence Unit 1 through 3 has approximately the same thickness (~1500 m) as Unit 1 (~1700 m) found on the southwestern Newfoundland margin. Sequence Unit 4 (~500 m) and part of Sequence Unit 5 (~625 m) is the equivalent to Unit 2 (~500 m) and appears to be thicker on the

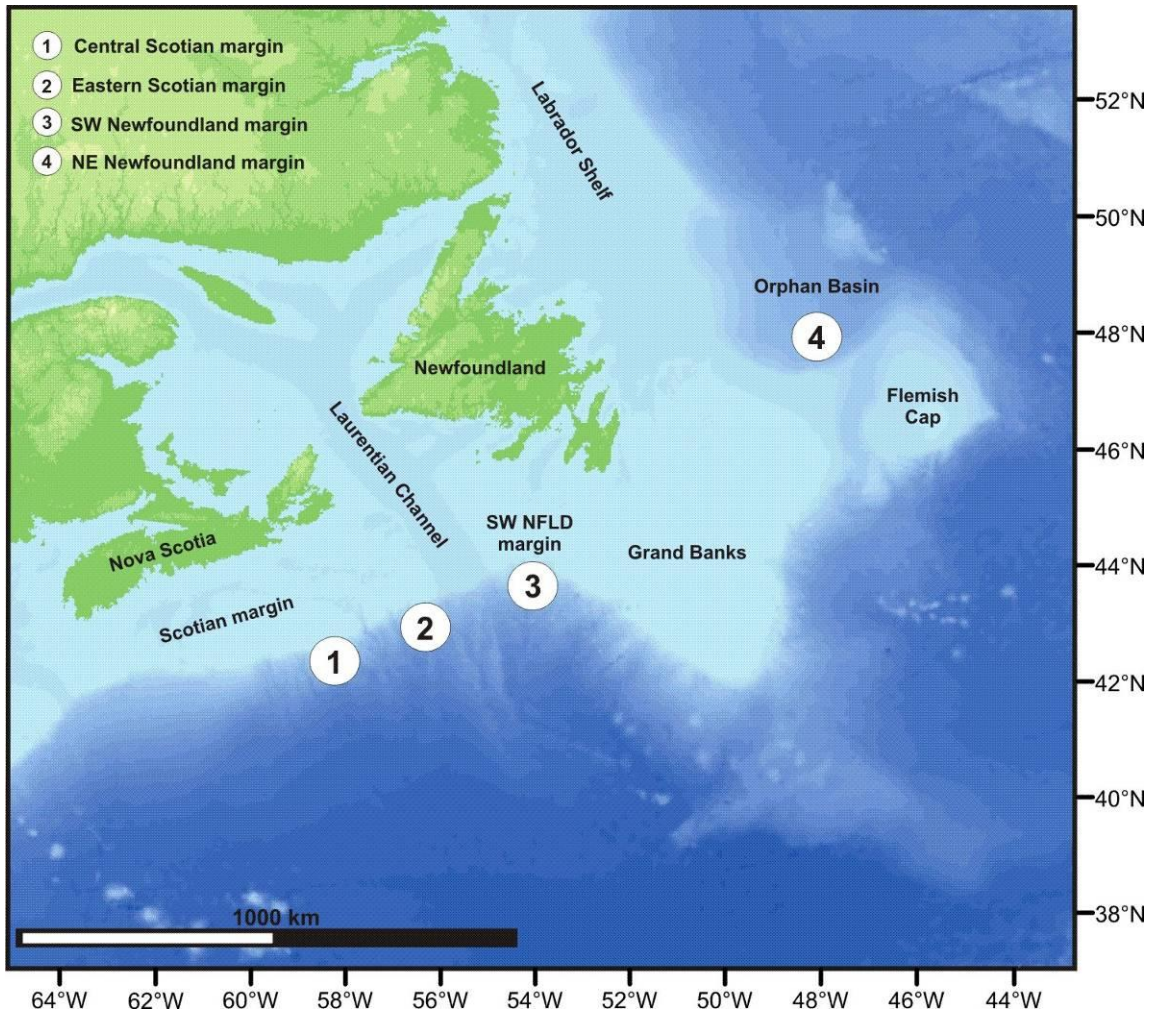
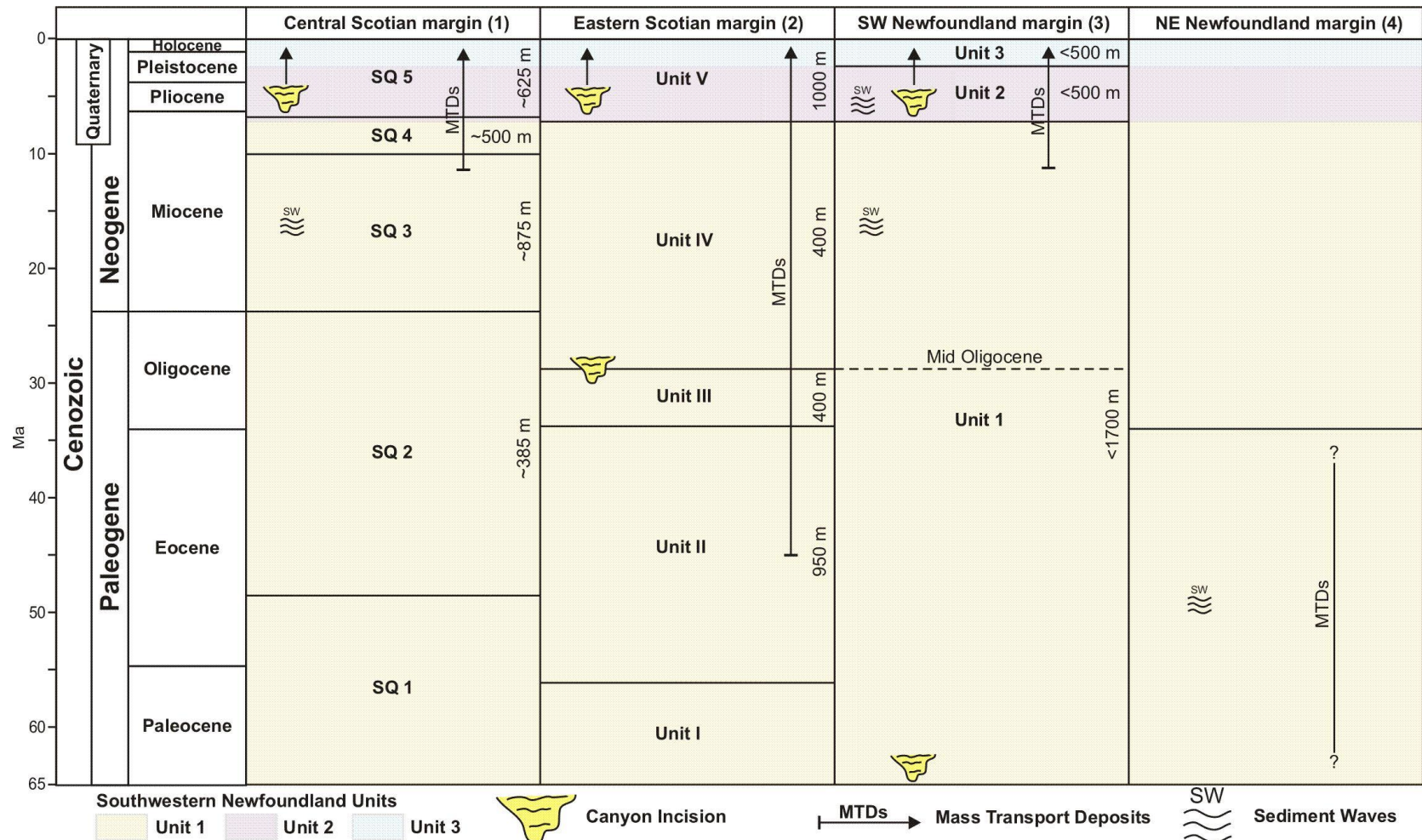


Figure 4.9: Location map of the studies used for comparison with the southwestern Newfoundland margin: 1 – MacDonald (2005), 2 – Brake (2009), 3 – this study, and 4 – Deptuck (2003).

central Scotian margin compared to southwestern Newfoundland. There is no Quaternary marker mapped on the central Scotian margin for MacDonald's study area and therefore it is difficult to compare the thickness for Seismic Unit 3. However, based on the location of Early Pliocene (P60) and Late Pliocene (P70) markers, the central Scotian margin has a thinner Quaternary section compared to the southwest Newfoundland margin (Fig. 4.10).

Similar sedimentation styles occurred on both the central Scotian and southwestern Newfoundland margins at approximately the same time. Sediment failure began around the Late Miocene and continued to the Early Pliocene on the central Scotian margin (Campbell et al., 2004 and MacDonald, 2006). Sediment failure began in the mid to Late Miocene on the southwestern Newfoundland margin but the scale of failures varied. The central Scotian margin had smaller MTDs that stacked on one another, whereas on the Newfoundland margin a significantly large MTD occurred that was followed by stacked MTDs that were larger than those on the central Scotian margin. These small failures continued through the Miocene and Pliocene until the style of sedimentation and scale of sediment failure changed during the Middle Pleistocene. Beginning in the late Pliocene continuing through the Quaternary, considerably smaller MTDs persisted through the evolution of the central Scotian margin and are similar to those seen on the southwestern Newfoundland margin during the same time period. Sedimentary bedforms interpreted to be sediment waves are identified on the central (MacDonald, 2006) and southwestern Scotian margin (Campbell and Deptuck, in press) as well as the southwestern Newfoundland margin. These sediment waves formed during the middle Miocene and are



Sources: (1) MacDonald, 2006 (2) Brake, 2009 (3) This Study (4) Deptuck, 2003

Figure 4.10: Comparison chart to show how different areas of the Canadian's eastern margin are related in terms of estimated sediment thickness and sedimentary processes. The yellow, purple, and blue represent Units 1 to 3 on the southwestern Newfoundland margin. Time scale is modified from the International Stratigraphic Chart proposed by the International Commission on Stratigraphy (Gradstein et al., 2004).

of similar scale on both margins. Channel development occurs on the central Scotian margin during the Quaternary as a result of glaciation, and the same features are seen on the southwestern Newfoundland margin. Although there is some discrepancy in unit thicknesses between the two regions, sedimentary processes are very similar in both style (MTDs and sediment waves) and timing.

4.1.2.2 – Eastern Scotian margin

The eastern Scotian Slope lies 240 km west of the southwestern Newfoundland margin where Brake (2009) studied work on shelf to slope sedimentation processes with respect to the development of an Oligocene canyon system. Brake (2009) divided the Cenozoic section into five units and correlated them to two wells (Sachem D-76 and Tantallon M-41). Brake's Unit I through IV represents the equivalent amount of time as Unit 1 of the southwestern Newfoundland margin. Part of Unit IV and V represent Unit 2 while the majority of Brake's Unit V represents Unit 3 on the southwestern Newfoundland margin. Thickness maps created for the eastern Scotian margin allow comparison of equivalent units from both areas. The equivalent of Unit 1 on the eastern Scotian margin has a similar thickness, between 1000 to 1700 m as the Newfoundland margin. Comparable thicknesses for equivalent Unit 2 (150 to 500 m) and Unit 3 (50 to 500 m) are seen on the eastern Scotian margin (Fig. 4.10).

Sedimentation styles are similar for both the eastern Scotian margin and the southwestern Newfoundland margin during the Cenozoic. Stacked and similarly scaled MTDs are observed on both margins but there is evidence that sediment failure began during the

Eocene on the eastern Scotian margin (Campbell et al., 2004) compared to the Late Miocene on the southwestern Newfoundland margin. Sediment failure continued on both margins throughout Plio-Pleistocene but generally deposits became smaller in scale during these times. Major canyon incision occurred during the Oligocene and was followed by relatively continuous sedimentation throughout the Quaternary on the eastern Scotian margin. Although the Quaternary section of the eastern Scotian margin is thinner compared to the southwestern Newfoundland margin, both margins endured canyon incision during this time. Overall, both margins experienced similar sedimentary processes (sediment failures and canyon incision) during similar times, and sediment failure significantly influenced the construction of the margins.

4.1.2.3 – Northeast Newfoundland margin

Northeast of the southwestern Newfoundland margin, Deptuck (2003) studied the post-rift geology of Jeanne d'Arc Basin focusing on the architecture and evolution of early Paleogene submarine fans. Although Deptuck (2003) focused on the Paleogene section, comparisons with the southwestern Newfoundland margin are still made to assess the relative importance of slope sedimentation processes along northeast Newfoundland margin. The Jeanne d'Arc Basin formed a depression bounded by basement highs during the Late Cretaceous and Middle Eocene. Prograding clastics, submarine fans, pelagic drape and sediment transport by ocean currents were the major fill mechanisms in the Jeanne d'Arc Basin (Deptuck, 2003), and identified mass transport deposits within the fill of the Jeanne d'Arc that are between the size of the large MTD and the recurring MTDs apparent on the southwestern Newfoundland margin, but are older in age (Fig. 4.10).

4.1.2.4 – Analysis

Cenozoic evolution of the eastern Canadian margin was influenced by many sedimentary processes and these processes seem to be coeval along the margin, with some geographic and temporal variation. MTDs became more abundant in the Eocene on the western and eastern Scotian margin but were rare on the central Scotian and southwestern Newfoundland margins. Miocene and Plio-Pleistocene sections show recurring failures across both margins suggesting that factors influencing the location of these failures are widespread. Formation of sediment waves on both margins during the middle Miocene suggest that bottom currents affected both margins in a similar manner. Sediment failure continued after the Middle Pleistocene on the Scotian and southwestern Newfoundland margin but became smaller in scale. Quaternary sections in both regions have similar channels with levee development, implying that glacier processes affected the evolution of the entire eastern Canadian margin. The northeast Newfoundland margin has comparable sized MTDs preserved in the Jeanne d'Arc Basin on the southwest Newfoundland margin, although older, suggesting sediment mass failures are a fundamental aspect of continental slopes.

Evidence for large MTDs, similar to the late Miocene failure on the southwestern Newfoundland margin exists on the Scotian margin. On the western Scotian Slope, a Pliocene large-scale failure was identified (Shimeld et al., 2003; Mosher et al., 2009). The slump component of this failure deposit is similar in magnitude ($>100 \text{ km}^3$) to the large Miocene MTD on the southwestern Newfoundland. Both failures have similar characteristics, with rotated and folded reflections in their upslope components,

transitioning to a debris flow further downslope. The occurrence of large-scaled sediment failures on adjacent margins further suggests the importance of sediment mass failures in the construction of Canada's east coast margin.

4.1.3: Identifying Components of Mass Transport Deposits

Mass transport deposits are identified in seismic profiles by their chaotic seismic reflection pattern (Fig. 4.11). In these chaotic packages there are structures that can be interpreted and used to interpret the failure process and flow dynamics. These indicators represent particular components of a failure and provide insight into its initiation, evolution and termination. Recent papers (e.g. Frey-Martinez et al., 2006; Bull et al., 2009) have divided mass transport deposits into three domains (headwall domain, translational domain, and the toe domain) (Fig. 4.12). Within these three domains are associated structures and components. The headwall domain is the upslope, extensional region of the mass transport deposit, characterized by three associated structures: headwall scarps, extensional ridges, and blocks. The translational domain lies between the upslope and downslope limits, where intense deformation can occur. Associated structures, or kinematic indicators for this domain are related to the lateral margins, basal shear surface, internal body structures (translated and outrunner blocks and slump folds), and the top surface of mass transport deposits. The toe domain is the downslope region of the mass transport deposit including the termination, or "toe" of the failure. The toe components of these failures typically have a convex, downslope morphology with associated pressure ridges and thrust and fold systems (Bull et al., 2009). Based on the toe domain, Frey-Martinez et al. (2006) further divided failures into "frontally confined"

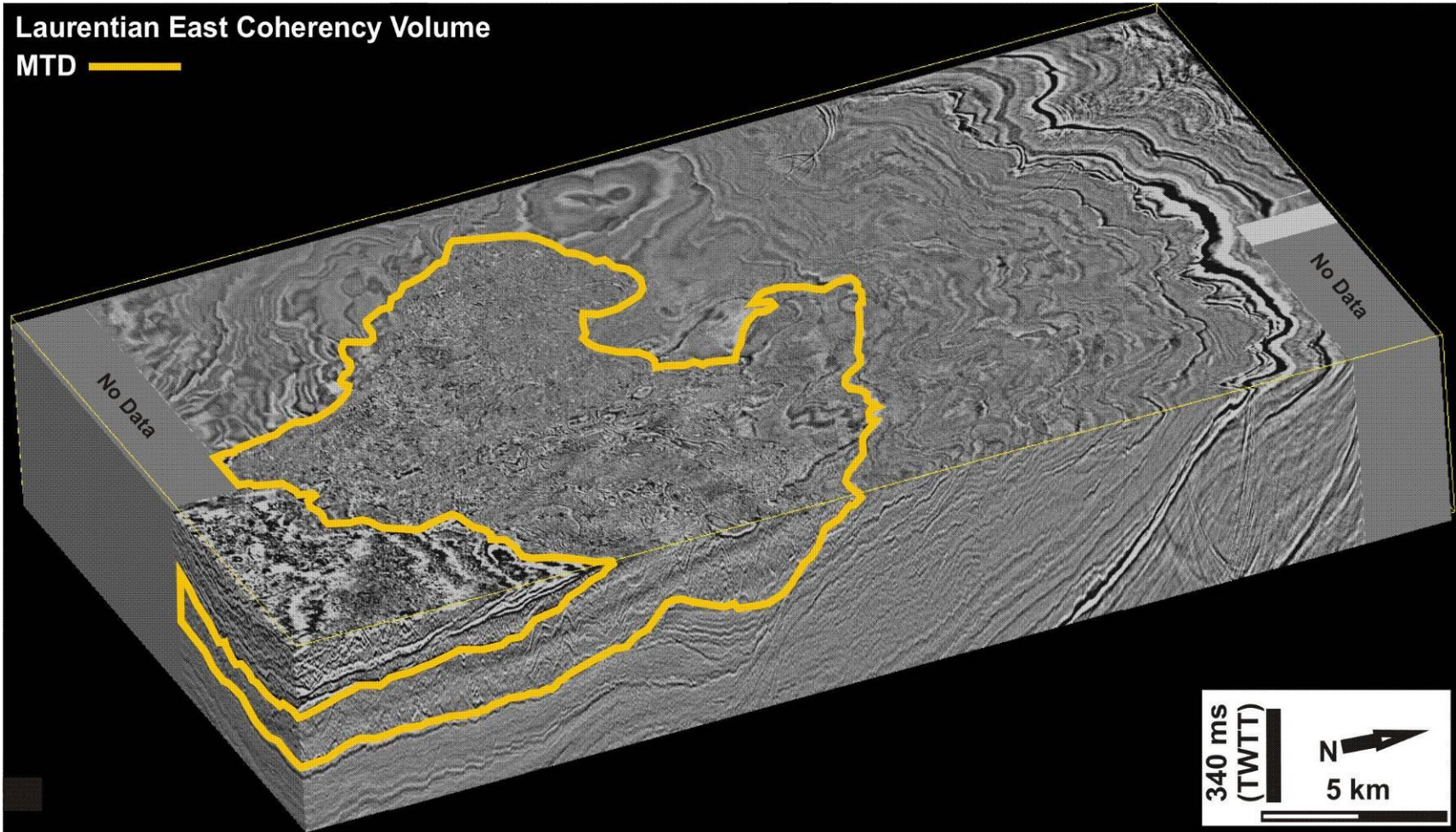


Figure 4.11: Time slice of Coherency volume of the Laurentian East data set showing the incoherent and chaotic nature of the late Miocene MTD. The MTD is represented by the orange polygon where the incoherent reflections as seen in both cross section and plan views.

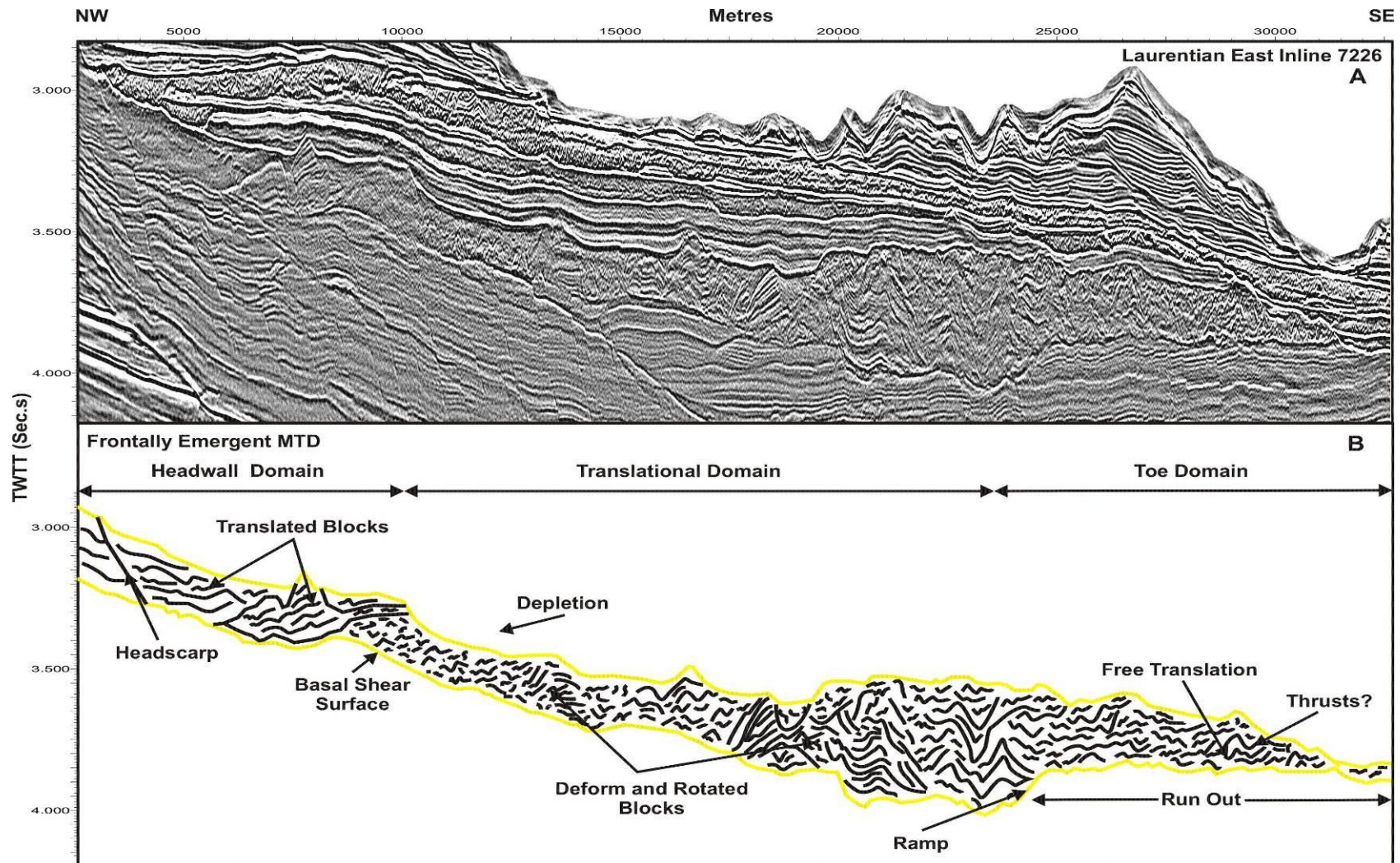


Figure 4.12: MTDs are broken into three domains: headwall, translational, and toe domains (Frey-Martinez et al., 2006; and Bull et al., 2009). (A) An un-interpreted section from Laurentian East Inline 7226. (B) The line drawing of the mid-late Miocene MTD shows different domains and components of a MTD as well as an example of frontally emergent MTD.

or “frontally emergent” submarine failures. A “frontally confined” failure refers to the buttressing of failed sediment against a frontal ramp preventing the sediment from leaving the original basal shear surface. “Frontally emergent” failures are characterized by the movement of the failed sediment from the basal shear surface to the seafloor via the frontal ramp which allows the failed sediment to translate freely over the undeformed seafloor possibly for considerable distances (Fig. 4.12) (Frey-Martinez et al., 2006).

4.1.4: Styles of Mass Transport Deposits

There are different styles of mass transport processes on the continental margins of the World’s oceans (e.g. Mosher et al., 2010). During the Cenozoic, four styles of mass transport processes with distinctive deposits dominate the evolution of southwestern Newfoundland margin at specific times. Debris flows, slides, and rotated slumps are significant processes that influenced the morphology of the seafloor during the Late Miocene (upper section of Unit 1). During the Pliocene and Pleistocene (Unit 2) mass transport processes were a combination of debris flows and slides, where components of both are identified in single deposits. After the mid Pleistocene, smaller-scaled debris flows and turbidity currents were the main styles of mass transport processes that contributed to the construction of the margin.

4.1.5: Case Study of the late Miocene MTD

The late Miocene MTD of this study provides an excellent example to demonstrate the components of submarine landslides and to define the three domains of a MTD. Thinning of the MTD to both the NW and NE as seen in inline and crossline profiles indicates that

the direction of travel for this MTD is north - south (Fig. 4.13). A base surface render of the MTD (Fig. 4.14) represents the basal shear surface of the failure where several features are identified. This surface will also be used to show the location of seismic profiles which intersect the features of interest, discussed below. Figure 4.12 shows seismic inline 7226 from the Laurentian East data set with a line drawing illustrating the head, translational, and toe domains of the MTD. It shows evidence of how this failure transitions from a blockier failure in the head domain, into the start of a debris flow in the translation domain, and finally a debris flow in the toe domain. In the headwall domain of the late Miocene MTD, the headwall scarp is identified along sections of the head of the failure while in other areas it has been eroded. Rotated and deformed slump blocks are preserved extremely well in the western and eastern edges of the deposit as well as in the upper central slope. Preserved blocks also are present in the seaward extent of the translational domain (Fig. 4.15 and 4.16). In the central upper slope of the deposit, the slump blocks rotated up to a slightly higher stratigraphy before translating into a debris flow further downslope. There is a zone between the blocks and the debris flow where the deposit is not preserved and may be a result of bypass or it has been removed by subsequent failures (Fig. 4.15). In the surface rendering of the top of the late Miocene MTD, the upper extent of the deformed blocks creates a rugose topography (Fig. 4.17). Preservation of deformed blocks within the failure creates a blocky texture in the translational domain (Fig. 4.18). The black outlines seen in Figure 4.17 represent specific regions where the “corners” of these blocks create an irregular surface. The majority of these preserved blocks are located in the downslope vicinity of paleo-topographic highs indicating that the blocks may have been locally sourced. In the mid-slope section of the

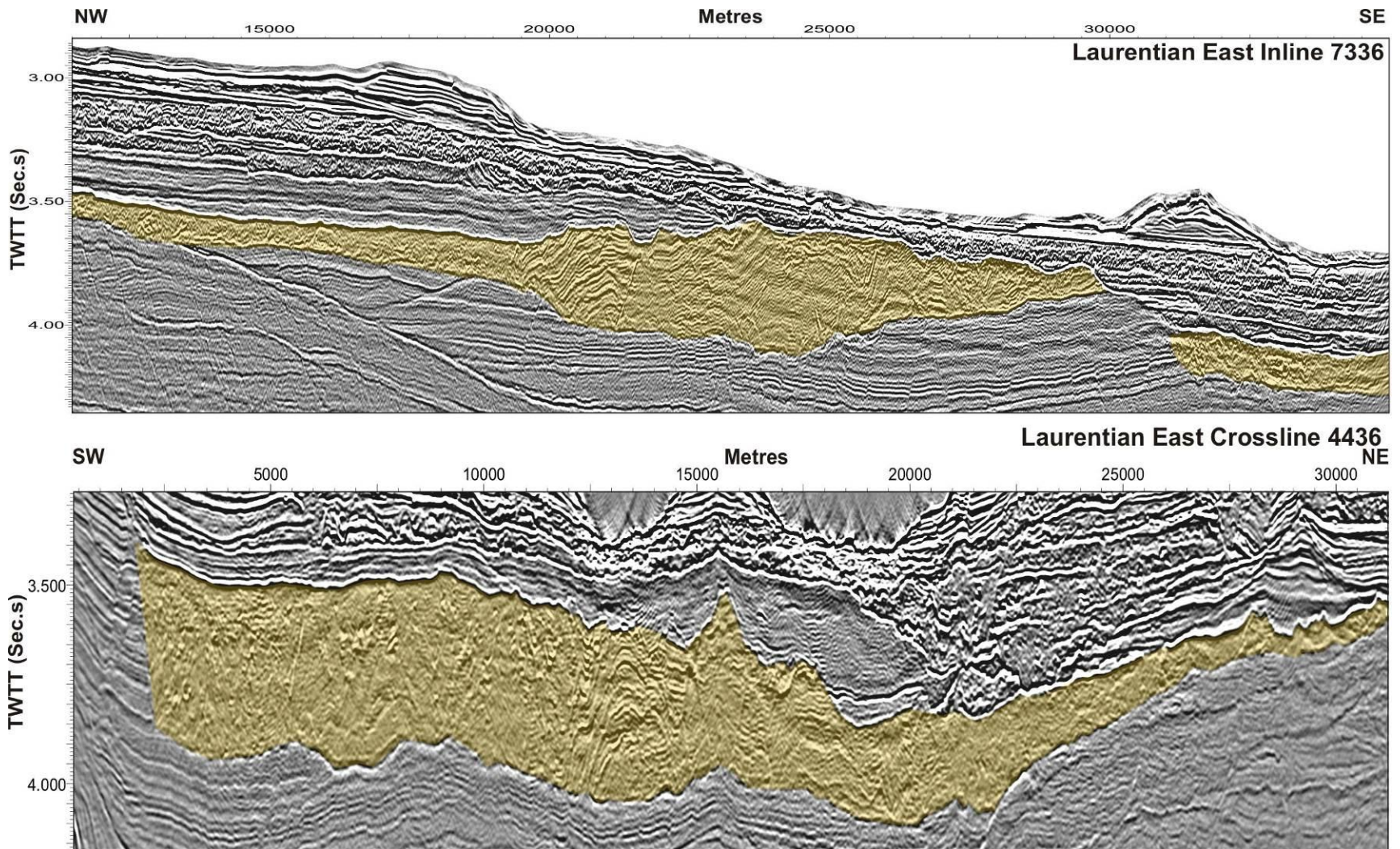


Figure 4.13: Inline and crossline profiles of the late Miocene MTD showing the N to S direction of travel.

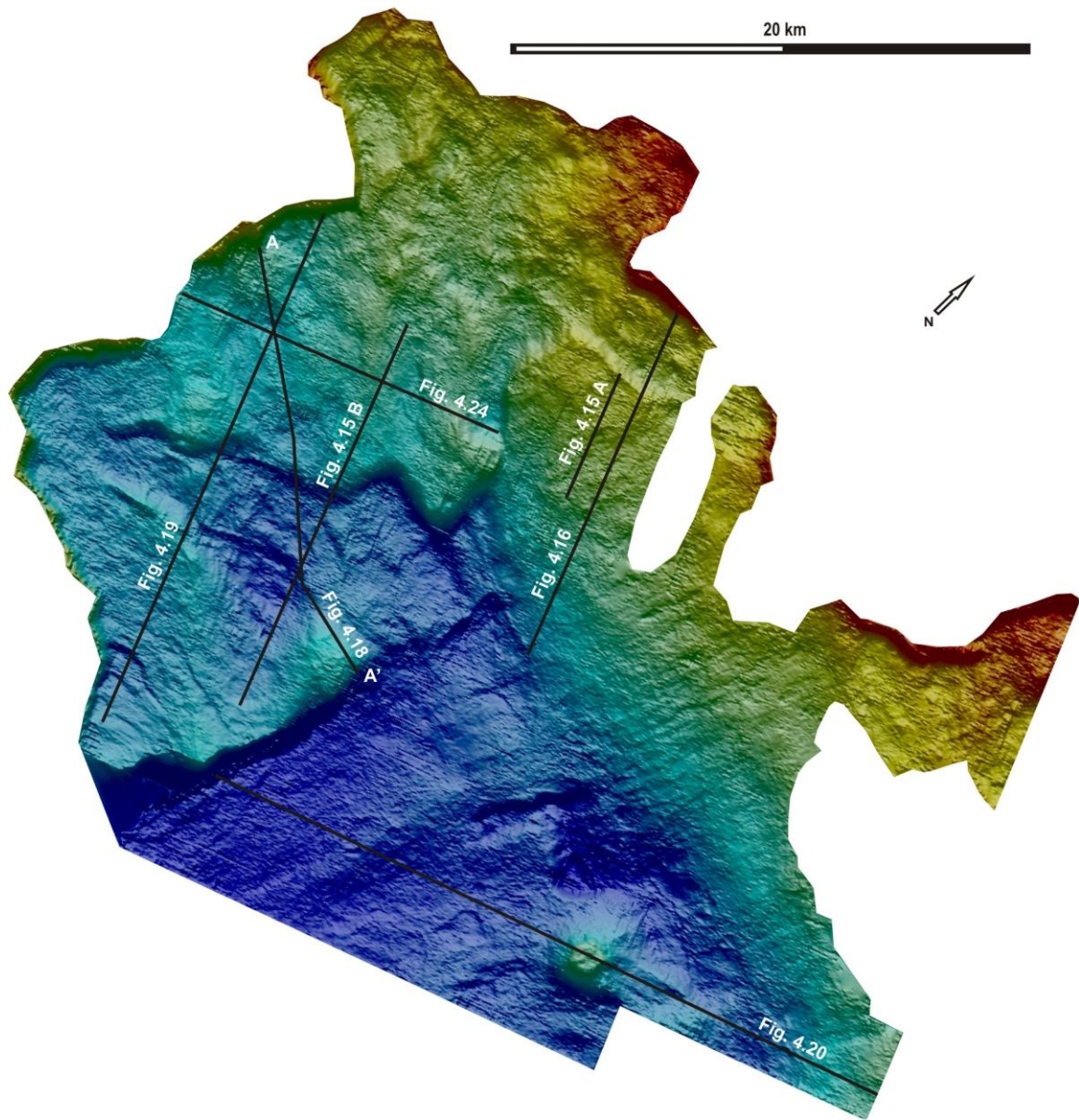


Figure 4.14: The basal surface of the late Miocene MTD showing. Locations of the seismic profiles (black lines) in figures are shown.

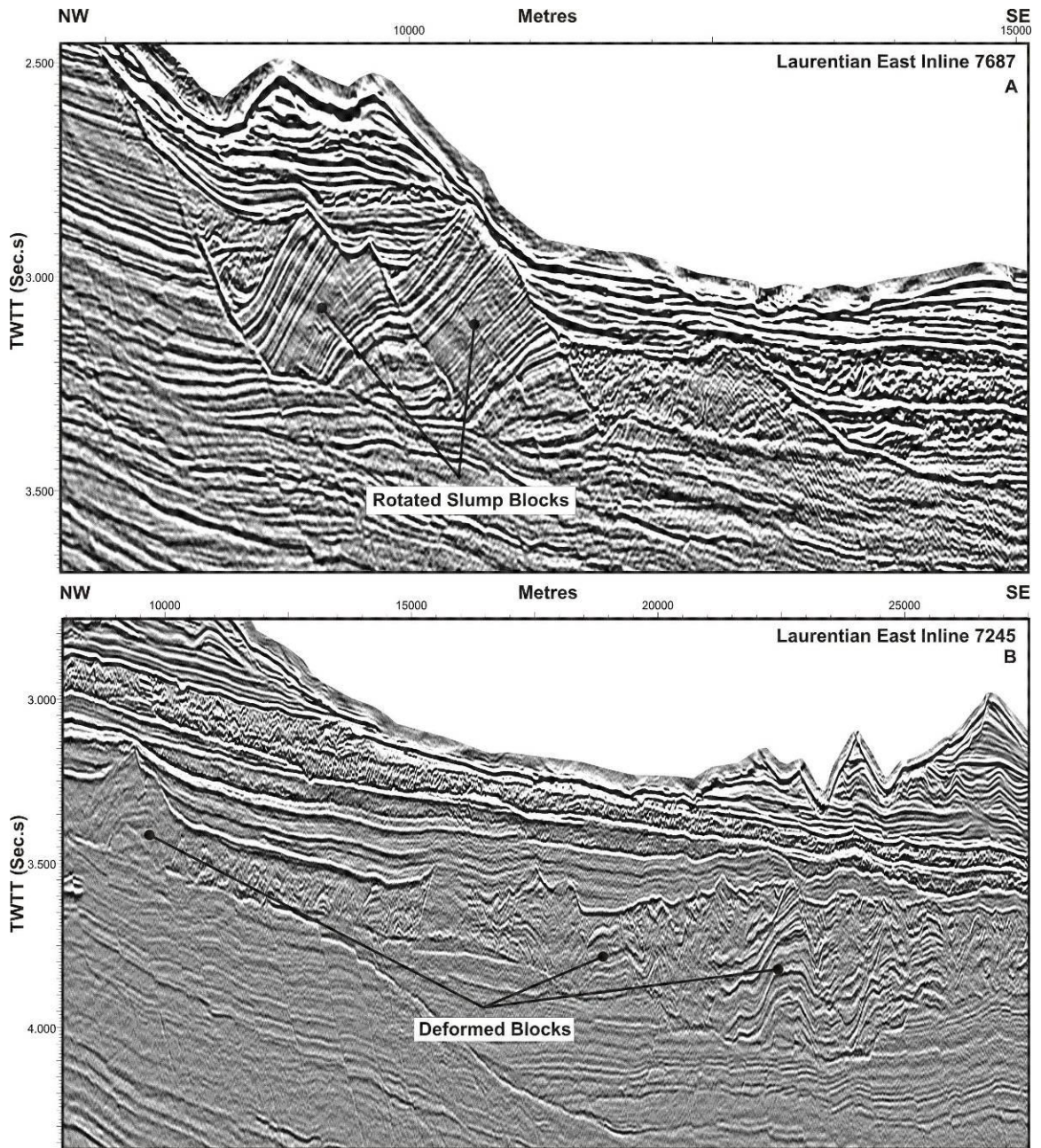


Figure 4.15: (A) Examples of rotated blocks in Laurentian East Inline 7687. (B) Deformed blocks which moved from the headwall domain into the translational domain are preserved in the failure deposit.

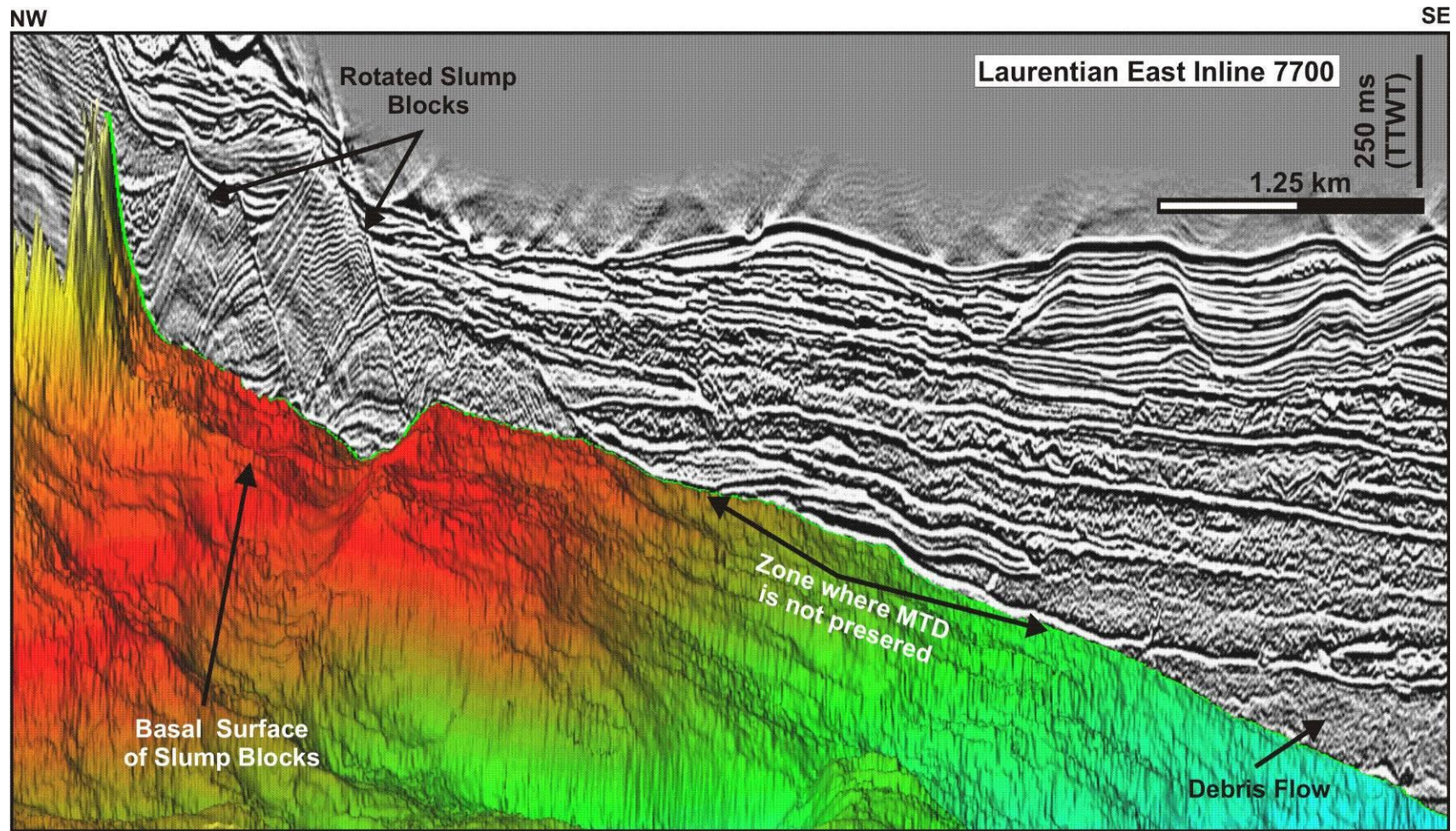


Figure 4.16: Rotated slump blocks from the upper central slope of the late Miocene MTD.. A section between blocks and the debris flow where the deposit is not preserved is represented by either a zone of bypass, or the failure was removed by subsequent failures.

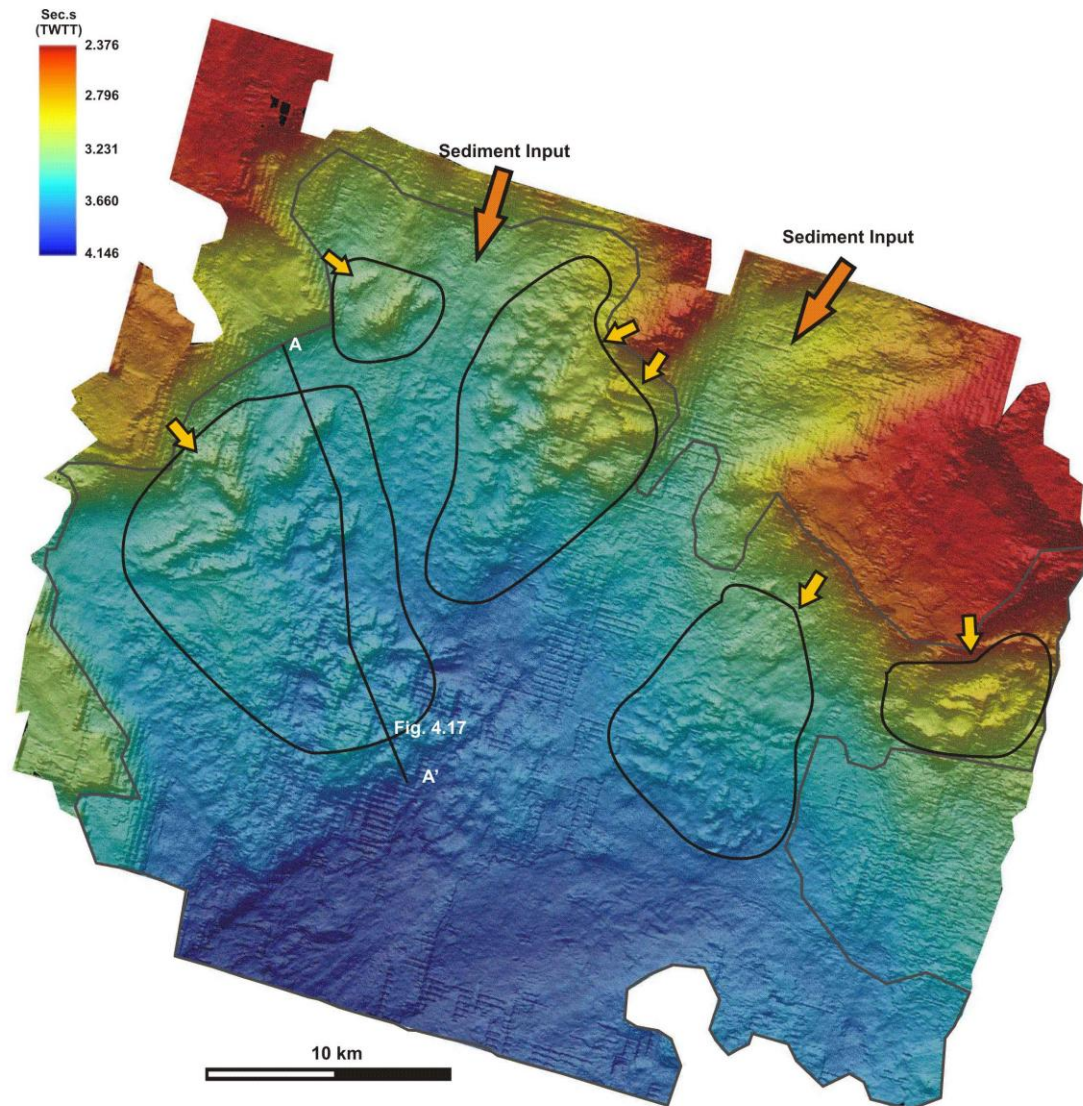


Figure 4.17: The top of the Late Miocene MTD has a rugose topography created by slumping. The black outlines represent specific regions where expression of these block are most prominent. Outside the black polygons, the deposit is represented by a debris flow style of failure. The yellow arrows indicate the source and transport direction of the rotated and deformed blocks. The larger orange arrows show the location of two Miocene-aged channels.

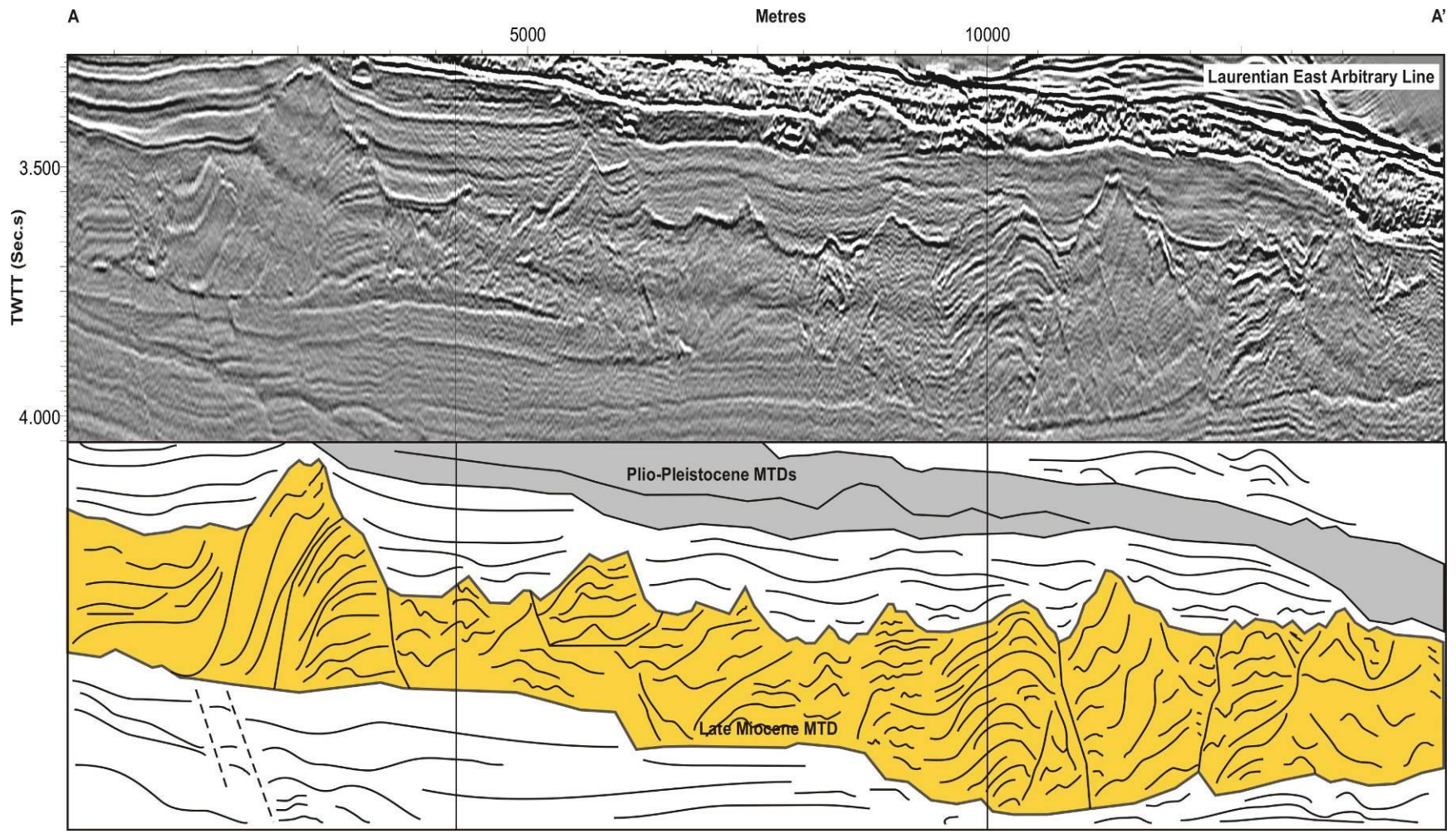


Figure 4.18: The blocky nature of the late Miocene MTD is shown in this arbitrary seismic profile from the Laurentian East 3D volume.

failure, a large gouge is seen in the basal surface of the MTD (Fig. 4.14 and Fig. 4.19). The size and depth of the gouge indicates that this mass transport flow was highly erosive in nature (Fig. 4.13). Diapirism of the Argo Salt Formation penetrates the late Miocene MTD in the eastern lower slope creating a structural high with sediment onlap and draping on the crest. A ramp system landward of the salt is over steepened by salt movement and created a trench feature at the base of the MTD (Fig. 4.20). The basal shear surface for the late Miocene MTD is identified in the three domains of the failure. The translational domain typically represents the longest section of a failure and the basal shear surface is prevalent in this domain.

The late Miocene MTD is not the only significant submarine mass failure to occur on the southwestern Newfoundland margin. The historic 1929 Grand Banks Landslide occurred on the St. Pierre Slope, west of the late Miocene MTD, and has a similar volume (140 - 185 km³) (Piper and Aksu, 1987). The major difference between the two is the style of failure. The late Miocene MTD is classified as a blocky debris flow that affected a thick (≤ 500 m) stratigraphic section of the margin, whereas the 1929 event is identified as a turbidity current that affected a relatively thin (≤ 3 m) stratigraphic section but a larger surface area ($\sim 160,000$ km²) (Piper and Aksu, 1987). These two submarine landslides occurred in the same region and have similar volumes but represent opposite end members of sediment mass failures. This suggests that any style of failure can occur on a margin at anytime and that the factors responsible for sediment mass failures also play a role in the style of the failure.

SE

NW

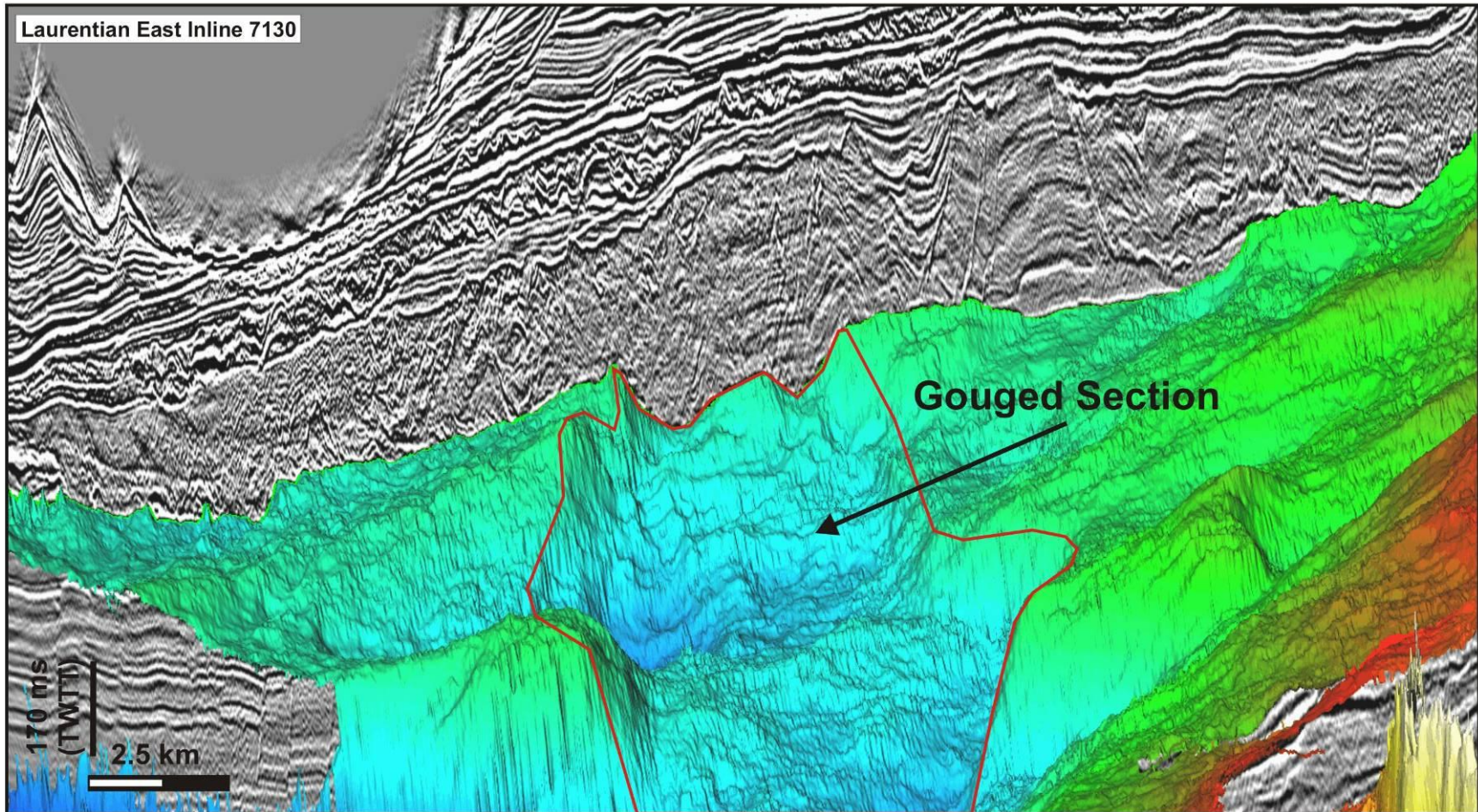


Figure 4.19: The large gouge seen in the base of late Miocene MTD on Laurentian East Inline 7130. The gouge deeply cuts the underlying stratigraphy indicating it was highly erosive in nature.

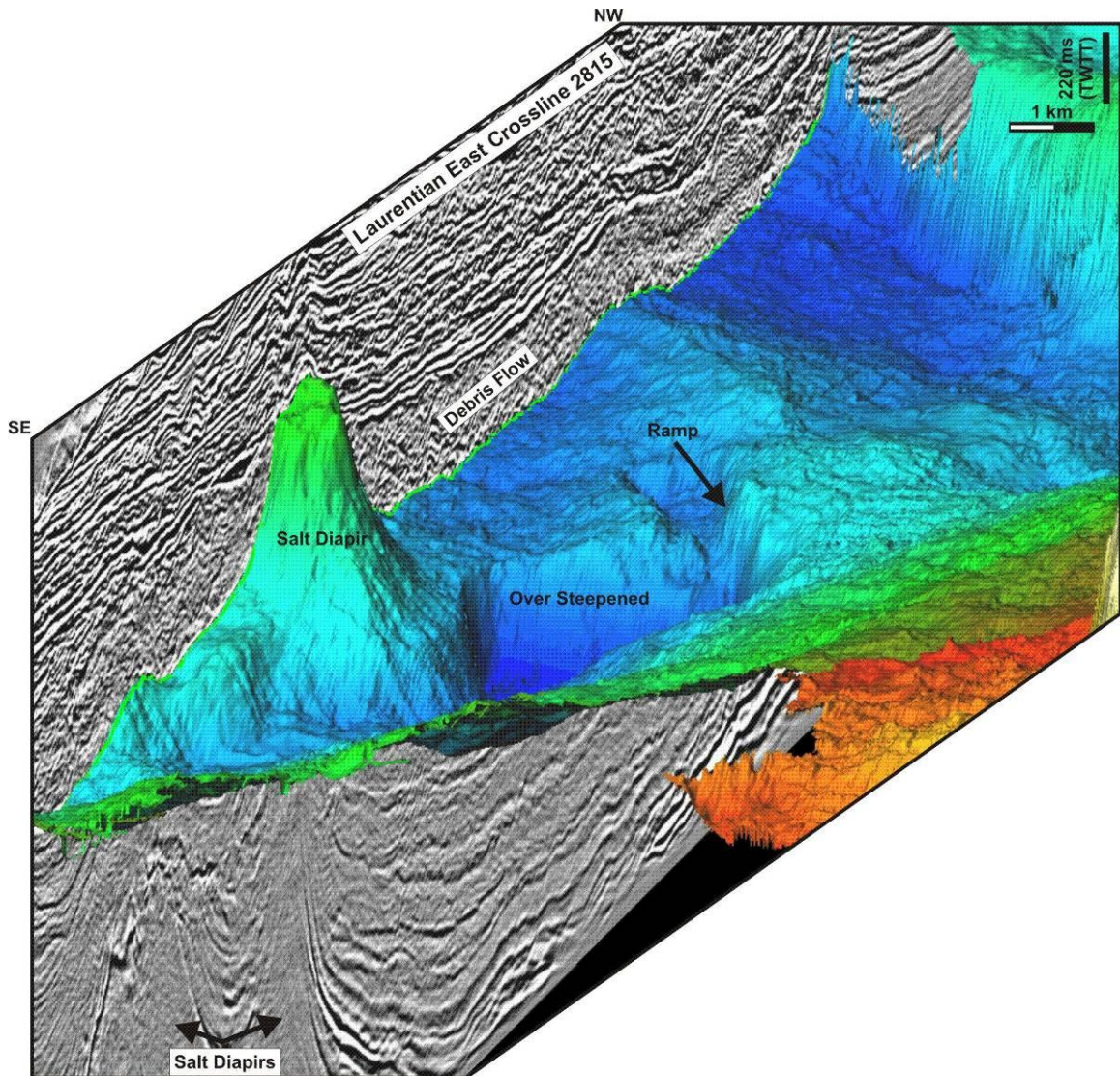


Figure 4.20: The late Miocene MTD is penetrated by syndepositional salt tectonics, evident in Crossline 2815 from the Laurentian East data set. A ramp landward of the salt diapirs is over steepened as a result of the salt movement. From this profile at the lower slope, the MTD has travelled some distance and the failure can be described as a debris flow.

4.2: Factors Influencing Mass Transport Deposit Location

Near surface sediments (top 25 m) of Scotian Slope are stable under static conditions (Mosher et al., 1994; Mosher et al., 2010). On the St. Pierre Slope, a geotechnical study by Marsters (1986) showed that sediments were over-consolidated but noted there was a high percentage of silt in the samples, leading to poor consolidation test quality in many instances. If sediments from the St. Pierre Slope are comparable to those from the Scotian Slope and are therefore stable, it is expected an external factor is required to either increase the stress acting on seafloor sediments (Lee et al., 2002), reduce the strength of the sediment (increase pore pressure), or there is a combination of the two, that triggers a slope failure.

The Canadian east coast margin is susceptible to a higher frequency of seismicity than expected, demonstrated by historic earthquake data (Basham et al., 1983; Adams, 1986; and Adams and Atkinson, 2003), perhaps as a result of latent tectonic structures in the region, such as the Cobequid-Chedabucto fault system. The 1929 Grand Banks landslide was clearly activated by a M7.2 earthquake in the study area (Bent, 1995). Other failures documented from eastern Canada are presumed to have been triggered by earthquakes (Piper et al., 1999; and Locat et al., 2003). The study area lies in the Laurentian Slope Seismic Zone (LSP), a 15000 km² area that surrounds the 1929 M7.2 event as well as four subsequent M5.0 earthquakes (Basham et al., 1983). An estimated 50 % of recorded earthquakes that occur on the eastern Canadian margin are located in the LSP but the majority of those are likely after shocks related to the 1929 event (Basham et al., 1983). The seismicity document on the eastern Canadian margin can be described by one of two

models: the random seismicity model (random distribution) or plate boundary zone model (focused distribution) (Mazzotti, 2007; and Basham et al., 1986). When sediment is subjected to strong seismic motions, pore pressure of the sediment will increase and its shear strength will be reduced. This can result in the liquefaction of unconsolidated sediments (silts and clays) and/or the failure/fracturing of consolidated sediments (Wright and Rathje, 2003; Biscontin et al., 2004). Based on the increased levels of seismicity in the study area and the examples of seismically triggered sediment failures in the region, it is concluded that mass transport processes since the Miocene were likely initiated by ground accelerations triggered by earthquakes. The distribution of sediment mass failures across the Scotian margin (Mulder and Moran, 1995; Piper and McCall, 2003; Campbell et al., 2004; and Mosher et al., 2010) and southwestern Newfoundland margin (this study) also suggests that random seismicity model or random distribution model may best describe occurrence of seismic events on the eastern Canadian margin.

Statically stable sediments require an external factor, in this case ground accelerations associated with earthquakes, to trigger a slope failure but typically these sediments require pre-conditioning factors that are responsible for weakening the sedimentary column and preparing the sediment for failure. Without these pre-conditioning factors, failures on the southwestern Newfoundland margin would probably require larger magnitude seismic events in order to initiate them. Pre-conditioning factors include: structural faults, sedimentary bedforms, contourite currents, salt tectonics, high sedimentation rates, and over-steepened bedding.

There are two different scales of failure that occur on the southwestern Newfoundland margin and it is these pre-conditioning factors that are believed to be responsible for those differences. During the Miocene to the early Pleistocene (representing Units 1 and 2), MTDs are regionally extensive and are linked to seaward dipping faults (~10°) between the top of a Cretaceous unconformity (**K99**) and the late Miocene (**M70**). In plan view of the similarity volume, these faults are polygonal in shape and occur more frequently in the mid-slope of the Laurentian East data set (Fig. 4.21). Where the late Miocene MTD is present, it cuts these faults; otherwise the faults extend to the **M70** reflection event.

Another pre-conditioning factor for the late Miocene MTD is the presence of sedimentary bedforms interpreted as sediment waves (Fig. 4.22). These sediment waves have an estimated crest-to-crest amplitude of 5 km and a wave height of 62 ms (~45 m). The preserved portion of these sediment waves suggests they are asymmetrical and formed by westward flowing deepwater currents. Similar aged and scaled bedforms are identified on the Scotian Slope by Campbell and Deptuck (in press). During the late Miocene, intensification of a strong deep thermohaline bottom-water current was documented on the New Jersey margin (Mountain et al., 1994). Bottom water circulation further north is supported by evidence preserved in the sediment record from the Labrador Rise (Piper, 2005). The presence of sediment waves in the region indicates the movement of sediments in deep water which may lead to erosion of the lower slope. Removing sediments from the lower slope, reduces the support for middle and upper slope sediments, and sets up a situation prone to failure in the region. In seismic crosslines and

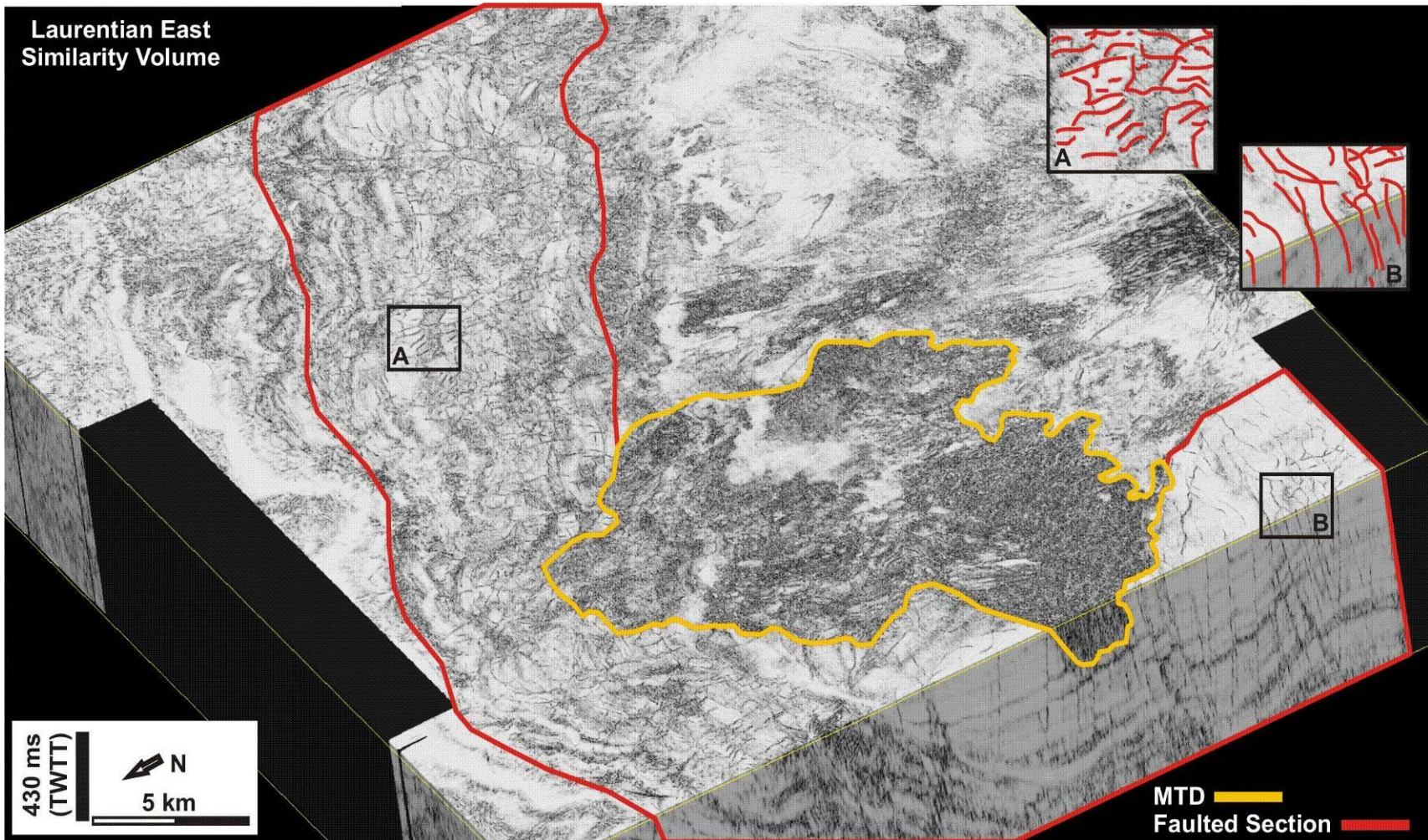


Figure 4.21: The similarity volume of the Laurentian East data set show the seaward dipping faults in both in plan view and in cross section. These faults are typically found mid slope and are Miocene in age. Inset A is a detailed plan view of the faults and shows their polygon shape. Inset B shows the relationship of these faults going from the cross section to the plan view. Faults extend to the M70 horizon event or are cut by the late Miocene MTD shown here as the orange polygon.

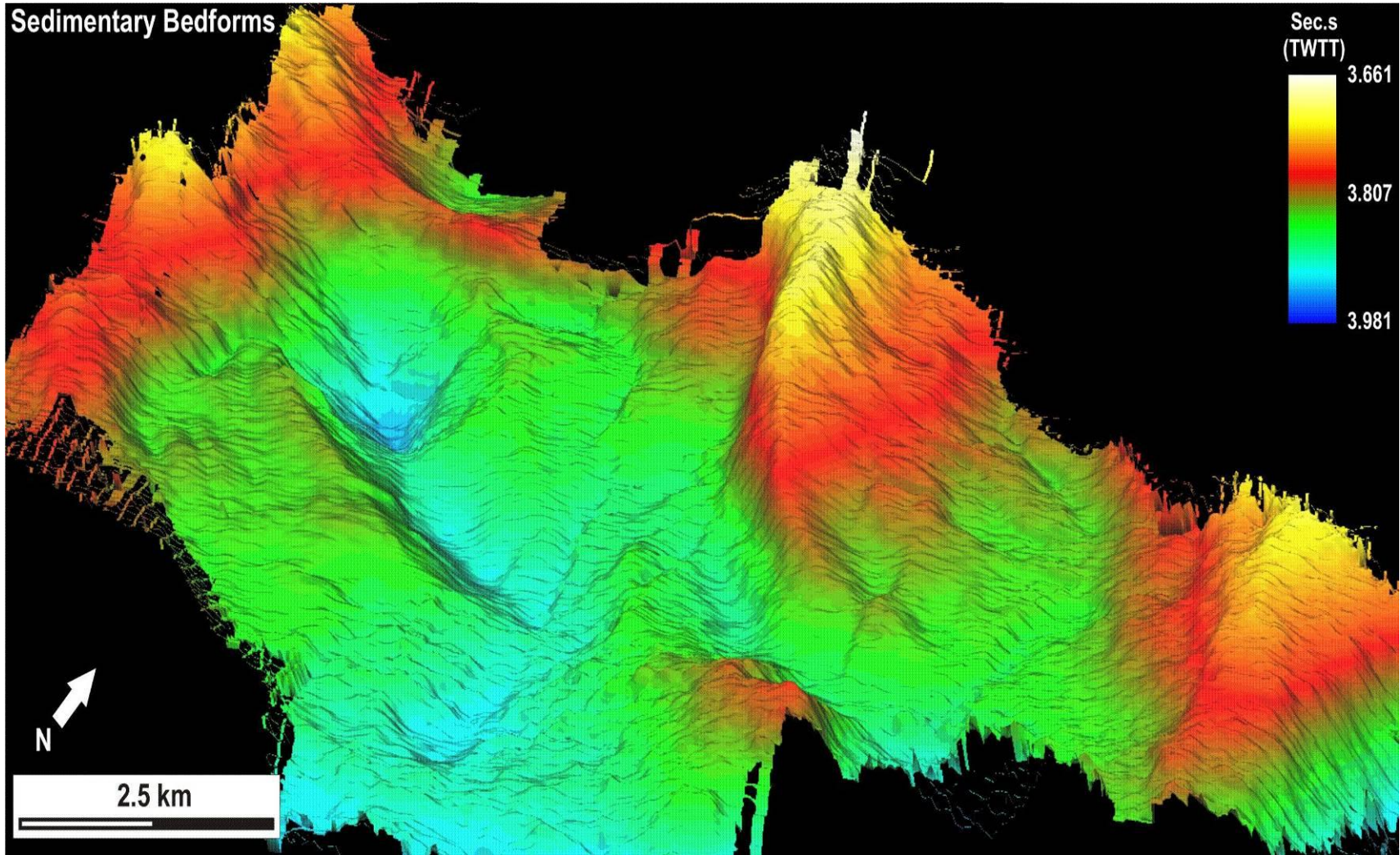


Figure 4.22: Sedimentary bedforms identified at the base of the late Miocene MTD are interpreted to be sediment waves. The sediment waves are only mapped in a small area as they have been eroded in the upper slope by the overlying late Miocene MTD.

the surface render for the basal shear surface of the late Miocene MTD, these sedimentary bedforms influence the morphology in the western, upper slope portion of the deposit. It appears that rotated blocks preserved in the western margin of the deposit occur on the flank, or in the trough of these sediment waves (Fig. 4.23). These bedforms are mapped in a small region as they are eroded in the upper slope by the overlying late Miocene MTD. This fact suggests these bedforms influenced the location, and to some degree, the style of this MTD.

During the Miocene to the Early Pleistocene, there is a strong possibility that sedimentary sections became oversteepened in response to ongoing salt tectonics of the Argo Formation. The development of salt diapirs creates vertical movement within the sedimentary column where uplift occurs over diapirs and subsidence between the diapirs (McAdoo et al., 2000). The vertical movement caused by the salt movement plays a role by increasing the slope angle, directing fluid flow and sediment transport, and removing downslope support. Salt tectonic features in the greater Laurentian Channel region are documented by Shimeld (2004) and Cribb (2009). The topographic highs created as result of ongoing salt tectonics also influenced sediment transport on the slope by focusing sediment deposition into bathymetric lows. These lows are a result of salt evacuation or failure scars from previous slope failures that created accommodation space for sediment to pond and accumulate. Increased levels of sediment deposition within these lows can create potential sections of under-consolidated sediment which have a higher susceptibility of failure. This process of filling bathymetric lows within a relatively short

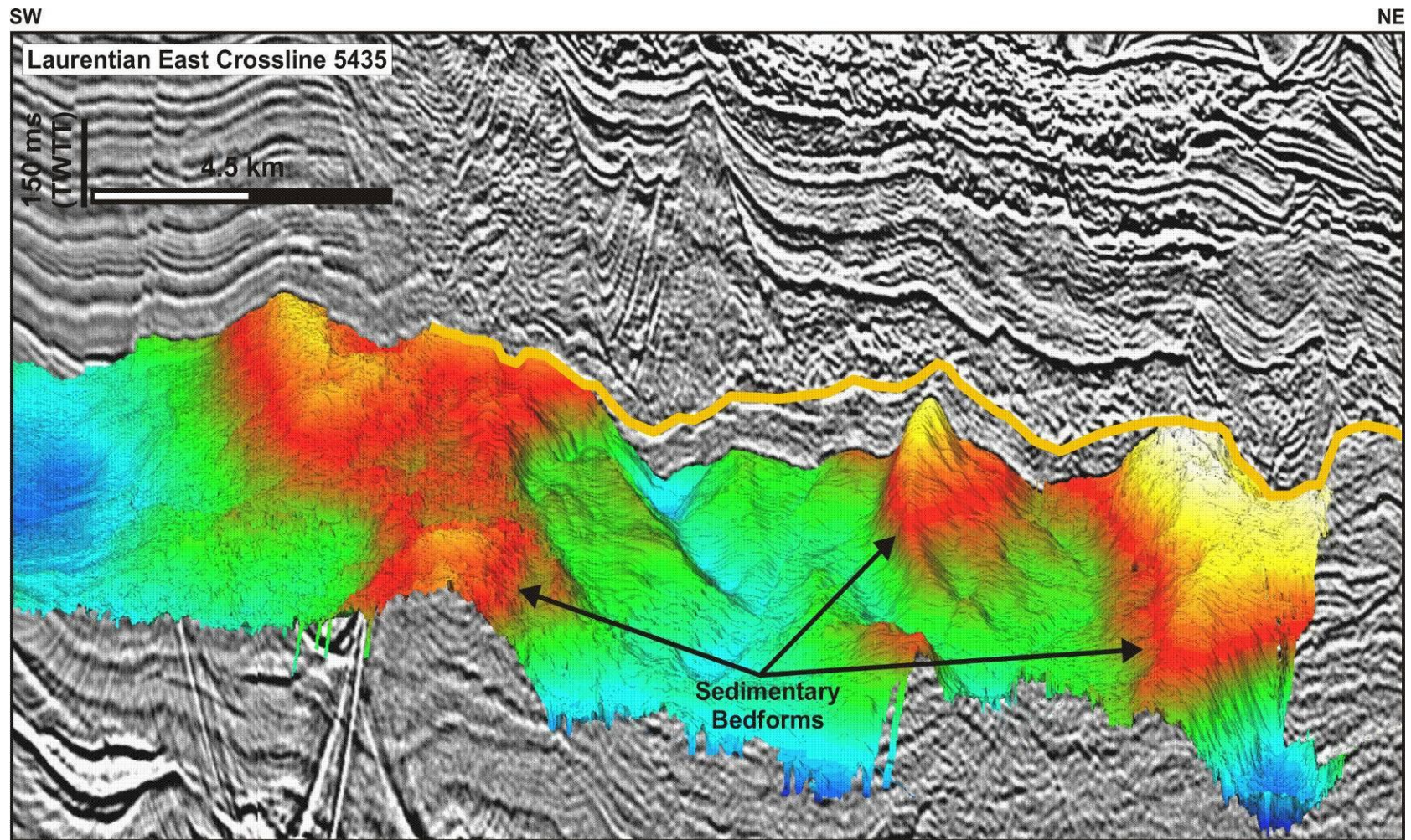


Figure 4.23: The sediment waves have influenced the morphology of the late Miocene MTD as seen in crossline 5435 from the Laurentian East data set. Rotated blocks located in the western edge of the deposit occur on the flank or in the trough of the sediment waves.

time could be one explanation for the occurrence of stacked MTDs (Masson et al., 2006) within Unit 2.

Failures that occurred since the Middle Pleistocene (representing Unit 3) are smaller in scale compared to those of the late Miocene to Pleistocene (Unit 1 and 2). They occur more frequently, likely in response to high sedimentation rates during the Pleistocene interglacial cycles and seismicity, which is typically more frequent during isostatic rebound in early phases of post-glacial episodes (Bryn et al., 2003). During periods of rapid sedimentation, there are typically mixed lithologies. Interglacial periods are marked by hemipelagic, fine-grained sedimentation (Mosher et al., 2004). Loading of interbedded sediments may trap pore waters within certain layers causing overpressure zones to develop. The pore water begins to support the overburden pressure and reduces the effective stress. This creates a weak layer until the fluid pressures become greater than the confining pressure and failure can occur (Sultan et al., 2004; Owen et al., 2007). In addition, seismicity likely is more frequent during isostatic rebound. Several glacial advances and retreats and sea level changes during the Pleistocene and Holocene, may have resulted in the formation of a number of potential weak layers within the sedimentary column of the southwestern Newfoundland margin.

Younger failures in the upper section of Unit 3 may have been pre-conditioned to failure by stratigraphic trapping, with bedding angles of between 4° and 6° in inter-canyon ridges. Mosher et al. (1994) and Mosher et al. (2010) show that slope angles on the Scotian margin $\geq 7^\circ$, with sediment thicknesses greater than 20 m are unstable. Although

the bedding angles preserved in inter-canyon ridges are lower with respect to the unstable regime identified by Mosher et al. (1994), the angles are steep enough to increase the susceptibility of failure in the inter-canyon ridges. This could be a possible factor influencing the smaller failures in the youngest section.

Changes in sealevel may have also contributed to the sediment mass failures identified on the southwestern Newfoundland slope. Variations in global sea level are typically related to the growth and decay of continental ice sheets which produce rapid eustatic changes (Miller et al., 2005). Sea level low stands are related to the growth of glacial ice sheets which can extend to the outer shelf during glacial maximums. During glacial low stands, the continental shelf can become partially exposed to erosion by rivers as well as gravitational processes. Ice sheet thickness can reduce the shear strength of near surface sediments to the point that failure initiation occurs as shown by Mulder and Morgan (1995) for Verrill Canyon on the Scotian margin. There are many eustatic sealevel curves in the literature that look at different magnitudes of sea level change over varying time intervals (e.g. Kominz, 1984; Haq et al., 1987; Fairbanks, 1989; Miller et al., 1996; Zachos et al., 2001; and Miller et al., 2005). The sea level curves generally show that sea level begins to fall during the middle or late Miocene and continued to do so until the Holocene (Fig. 4.24). The lowest sea level low stand over the past 100,000 years occurred during the late Wisconsinan at about 18 ka, where sea level was ~ 120 m lower than present in the Atlantic Ocean (Fairbanks, 1989). The present southwestern Newfoundland shelf and shelf break lie in water depths of between 50 and 250 m. During the last glacial low stand, regions of the modern shelf were sub aerially exposed and the

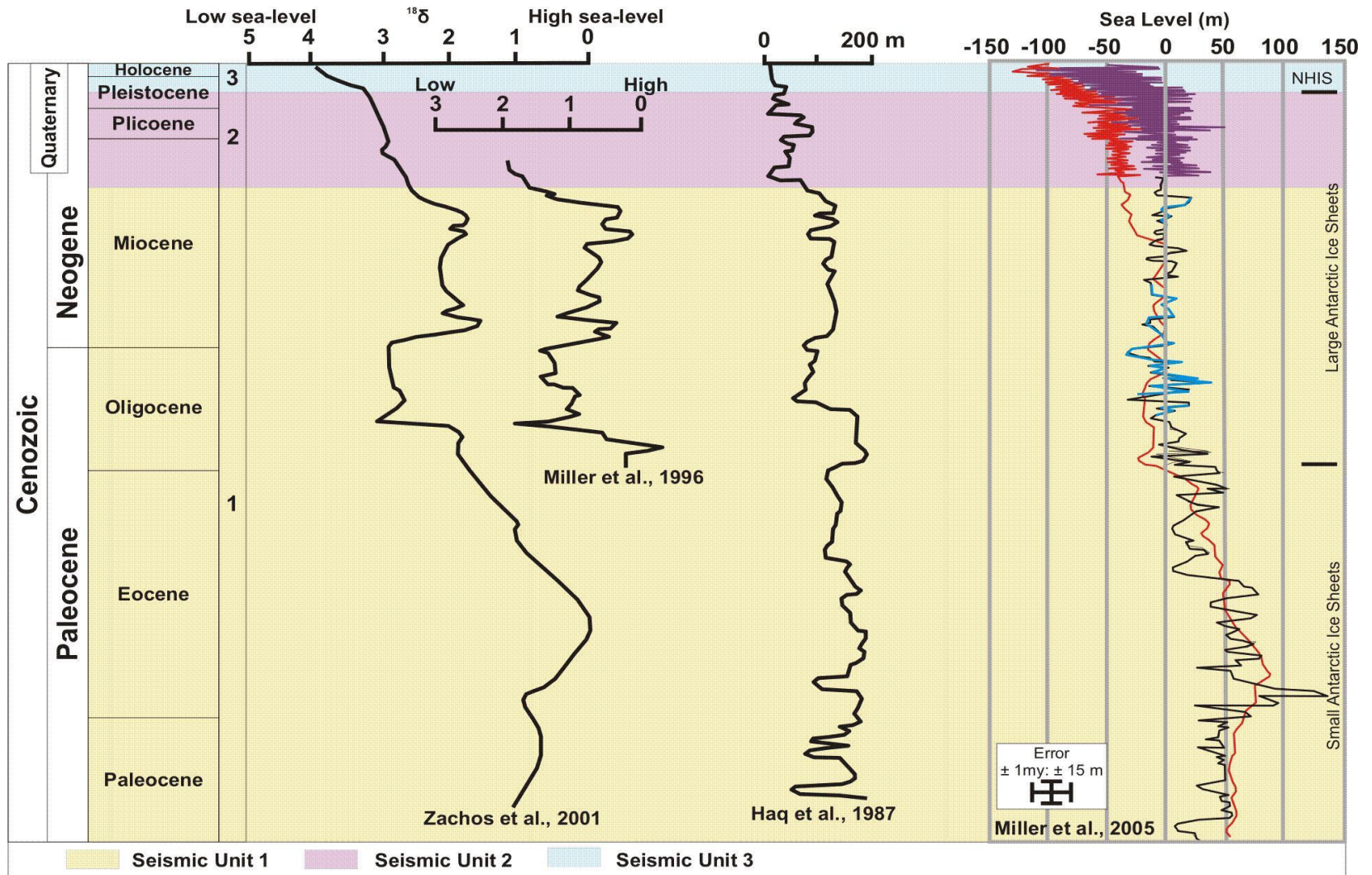


Figure 4.24: Comparison of global sealevel of Zachos et al., 2001; Miller et al., 1996; Haq et al., 1987; and Miller et al., 2005 (image modified from MacDonald, 2006).

modern shelf break occurred at 100 to 150 m water depth. Sealevel lowering since the Miocene is another factor that may have influenced the initiation of sediment failures on the southwestern Newfoundland margin by exposing the continental shelf to erosional processes and/or reducing the shear strength of near surface sediments.

In regions where slope gradients are low ($\leq 5^\circ$), such as the St. Pierre and Whale slopes, the occurrence of submarine failure is relatively rare, but those failures that occur on an open continental slope are typically some of the largest, such as the Storegga slide (Haflidason et al., 2004). These large failures are the result of accumulation of thick packages of fine grained sediment that occur at high latitudes during glaciations. On these open continental margins with gentle slope gradients ($1-2^\circ$), the transition from shelf edge to abyssal plain can be a five kilometre drop that occurs over several hundred kilometres. This low gradient slope extending over long distances allows for the accumulation of parallel bedded sediments over large areas (Masson et al., 2006). Although this sediment accumulation will not lead to a failure, if conditions responsible for slope failure do occur then a large area would be affected simultaneously. Another factor that could contribute to the building of thick, nearly homogenous sediments on these low gradient slopes is the low triggering periodicity. Higher triggering periods would prevent accumulation of fine grained sediments and may explain why there is an absence of large MTDs on tectonically active margins (Owen et al., 2007) as well as during glaciated times.

Mass transport deposits from the southwestern Newfoundland margin occur at a variety of scales throughout the late Cenozoic. Sediment from the margin is statically stable until ground accelerations, due to earthquakes, trigger mass sediment failures; where these deposits are observed in the sedimentary record. MTDs are regionally extensive and much thicker through the Miocene and Pliocene but become smaller and more frequent from the Pleistocene to Recent. Thus, it is believed that the pre-conditioning factors and possibly the recurrence rate of seismic events control the size of mass transport processes on the southwestern Newfoundland margin.

4.3: Classification of MTDs

Identifying MTDs based on observed structures and features from the southwestern Newfoundland margin provides information about the failure process, the triggering mechanisms, and pre-conditioning factors of those failures. The oldest and largest of the MTDs is at the top of Unit 1. This late Miocene age MTD is a frontally emergent landside based on how the deposit is able to freely translate in the toe domain and thin down slope. The deposit is laterally confined in west (Fig. 4.25) but because the failure was able to freely translate down slope as well as to the east, it is classified as being frontally emergent. In terms of scales and dimensions as well as pre-conditioning factors, this 900 km² MTD fits into the slope attached category of submarine landslides. Including the style of failure, this MTD is classified as a frontally-emergent, slope attached blocky debris flow (Table 4.2).

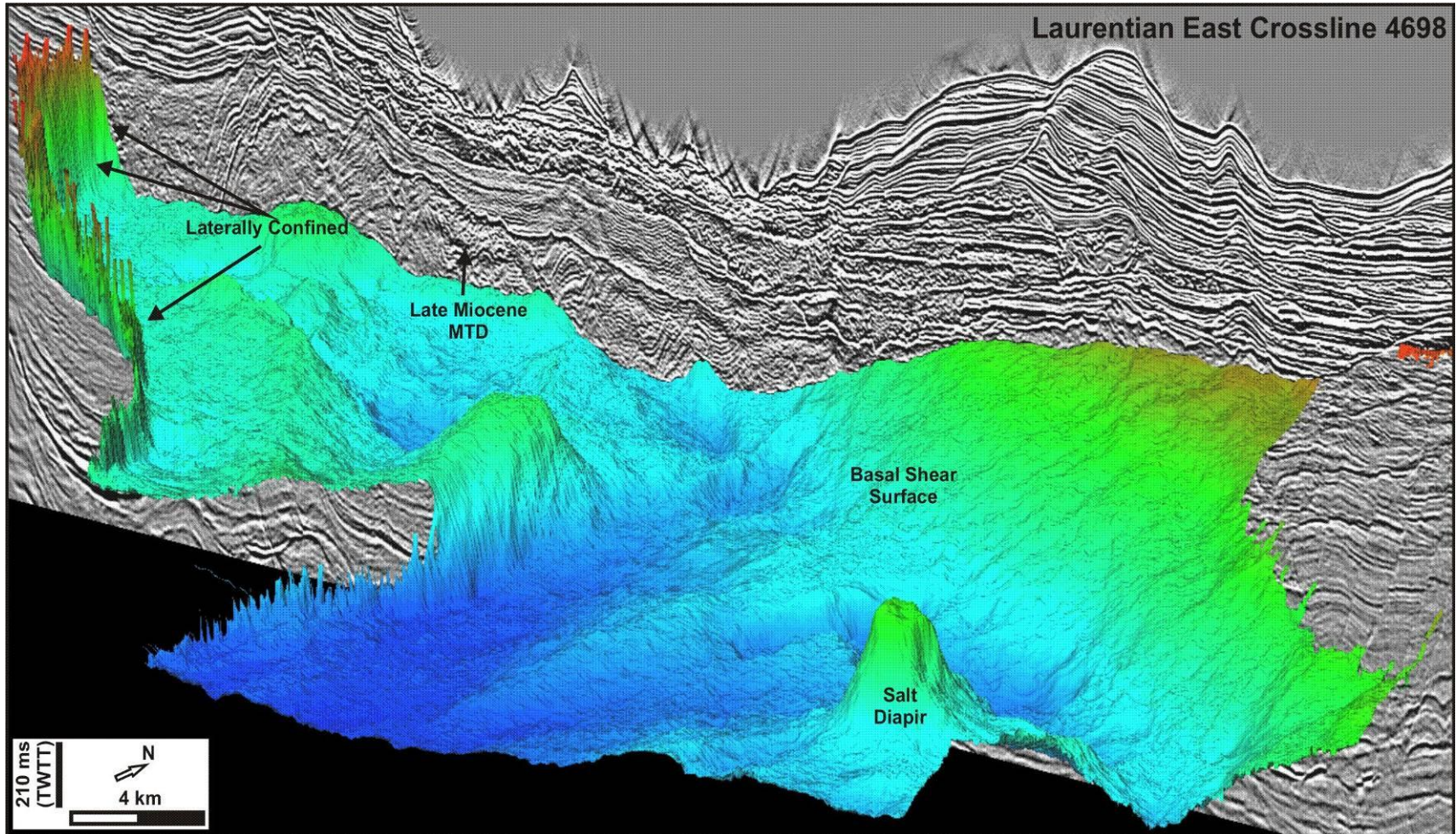


Figure 4.25: The late Miocene MTD is classified as a frontally emergent MTD but it is also laterally confined at the western edge of the deposit as seen in crossline 4698 and the surface render from the Laurentian East data set.

The stack of MTDs within Unit 2 (Fig. 4.26) are a similar type of failure and are classified by the components preserved in individual failures. These failures were able to freely translate over the undeformed slope and thin out in their lateral extents. Although it is difficult to distinguish between the toe domains of upper MTDs in this unit, based on the lower MTDs these failures are frontally emergent landslides. These MTDs cover areas up to 400 km² which could make them slope attached failures but due to the fact there are two channel or canyon systems upslope of these MTDs, suggests these are shelf-attached submarine landslides. These MTDs are classified as frontally emergent, shelf attached debris flows (Table 4.2).

The MTDs present in Unit 3 represent a small percentage (<5%) of the sedimentary column between **Q50** and the seafloor. These MTDs are very thin (15 to 25 m) in comparison to those found in Units 1 and 2 and cover less than 1km². Based on their seismic profiles, these failures are frontally emergent as they thin seaward. Due to their small areas, they would be considered detached submarine landslides. The MTDs found in this Unit are classified as frontally emergent, detached debris flows (Table 4.2).

Unit	Thickness (km)	Area (km ²)	Volume (km ³)	Classification
Unit 1	≤ 0.6	900	225	Frontally emergent, slope attached, blocky debris flow
Unit 2	0.09-0.19	30-403	3.3-60	Frontally emergent, shelf attached debris flows
Unit 3	0.015-0.025	≤ 1		Frontally emergent, detached debris flows

Table 4.2: Classification of MTDs identified in the study area on the southwestern Newfoundland slope (modified from Mulder and Cochonat, 1996; Frey-Martinez et al., 2006; and Moscardelli and Woods, 2008).

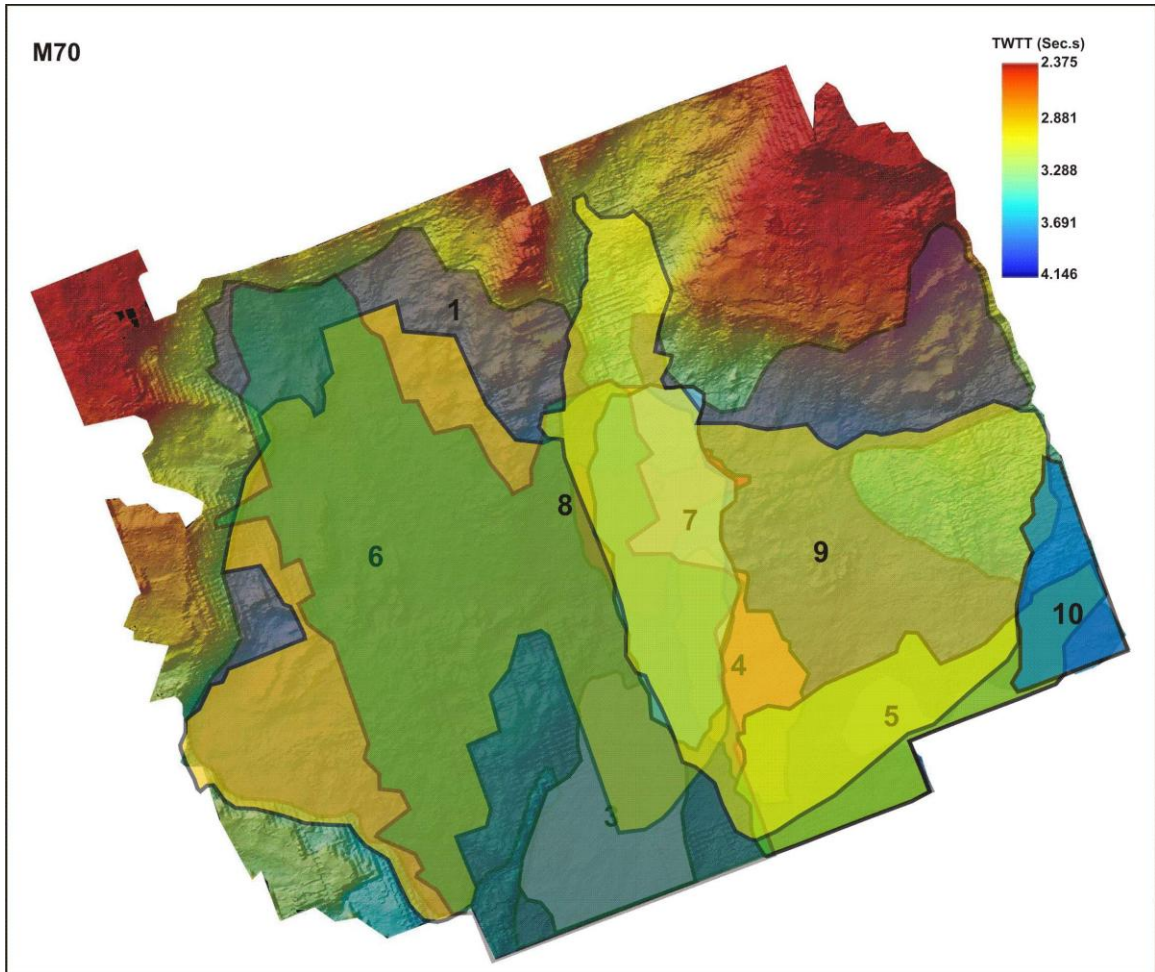


Figure 4.26: After the late Miocene (~M70), MTDs became smaller but their frequency increased. Between M70 and Q50, at least nine other MTDs are mapped (1 represents the top of the late Miocene MTD) with areas between 30 and 400 Km². Plio-Pleistocene MTDs are represented by the numbers 2-10 and different coloured polygons which overlay the M70 surface render.

The MTDs seen on the southwestern Newfoundland margin are interpreted to be a debris flow style of failure based on their chaotic seismic facies and laterally extensive deposits; however, these deposits preserve other styles of failures (slump blocks and slides) as well. There is a stratigraphic variation in the style of failures seen on the southwestern Newfoundland margin. Failures containing preserved blocks within a debris flow matrix from the late Miocene became more chaotic debris flows in the Plio-Pleistocene and finally thinner debris flows inter-fingered with possible turbidite deposits in the Late Pleistocene.

4.4: Channels

Channels systems of various scales occur throughout the evolution of the margin. In the Pleistocene to Holocene sections, these are typically preserved in “relatively” undisturbed strata. They appear, for example as high amplitude reflections which erode into the top of a Lower Pleistocene MTD (e.g. Fig. 4.27). An amplitude map for the top of this MTD, identified sinuous channels on the northwest and southeast sections of the failure (Fig. 4.28). This channel development suggests that between the failure events of Unit 2 (Late Miocene to Middle Pleistocene), sediment from the shelf may have bypassed the upper and middle slope as it was transported through these channels to the lower slope. Channels were only easily identifiable in the top MTD from Unit 2, perhaps because the channels systems in the lower MTDs were eroded by subsequent failures. This erosion could be one of the factors responsible for Unit 2 having relatively little thickness of sediment preserved compared to the amount of time between the **M70** and **Q50** horizon events.

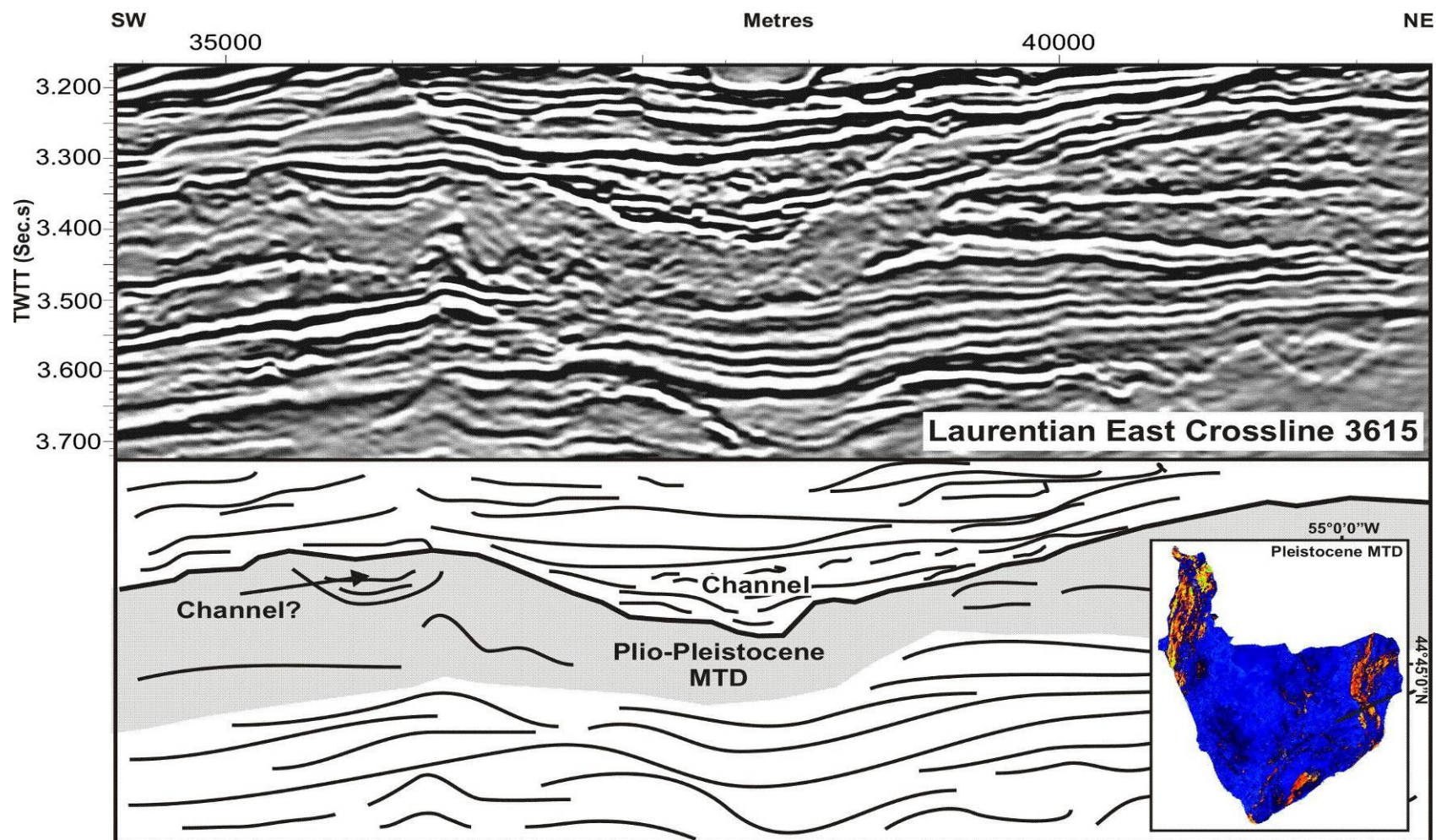


Figure 4.27: A broad v-shaped erosional feature seen in the top of a Plio-Pleistocene MTD with high amplitudes is interpreted to be a channel. Other high amplitude, concave reflections at the top of the same MTD are also interpreted to be channels. The presence of these channels suggests that sediment was bypassed the top of these MTDs and deposited further downslope.

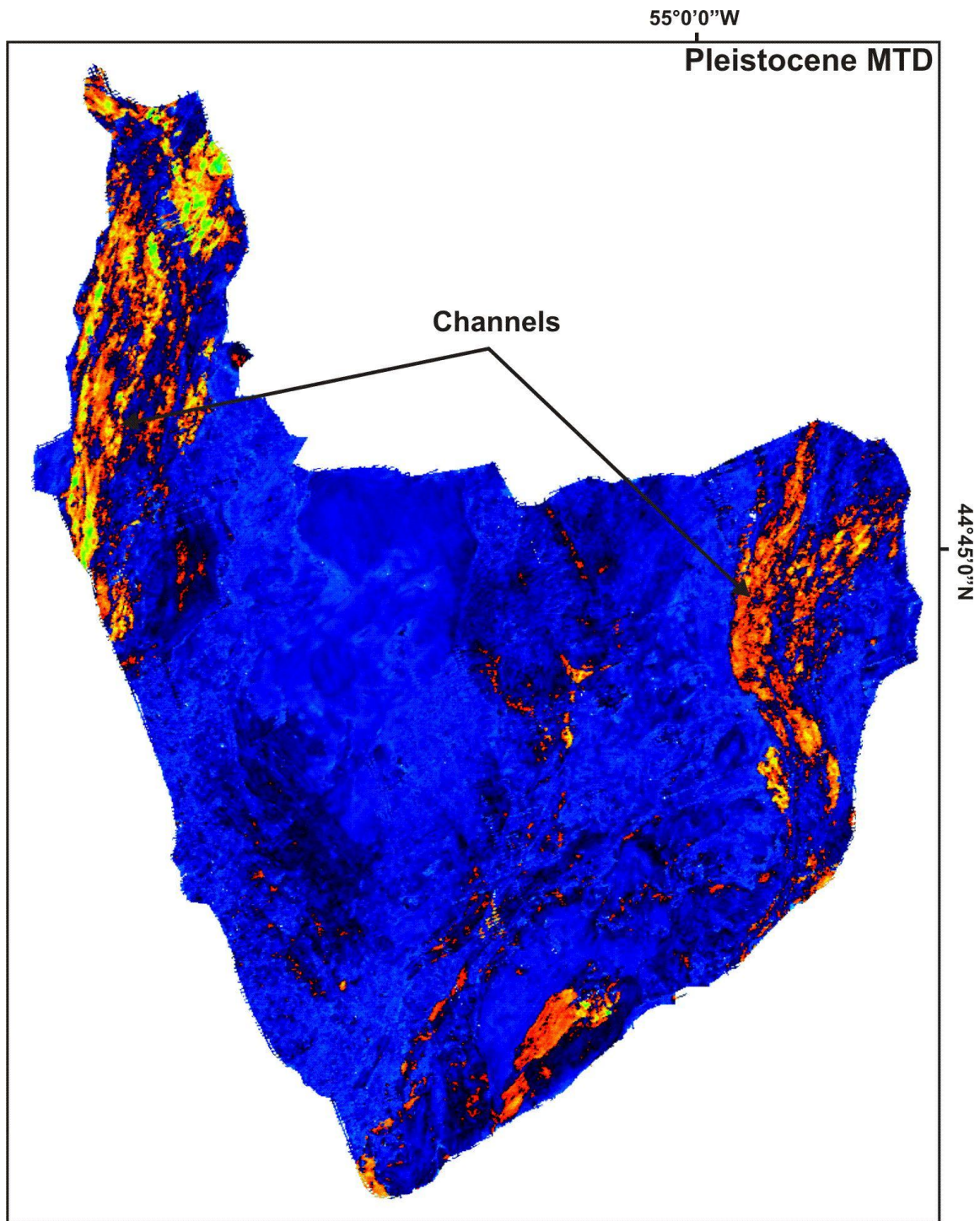


Figure 4.27: Amplitude map of the top of a Plio-Pleistocene MTD. The high amplitudes (yellow-orange-red) indicate sediment infill of sinuous channels that run north south. Sediment from the shelf bypassed the upper and middle slope as it was transported through these channels to the lower slope.

4.5: Impacts of Mass Transport Processes

Mass sediment failure on continental margins has many implications on the evolution of a margin; it can also have a tragic affect on the infrastructure of coastal communities and human activities that occur along these margins. The geohazard potential of these events became of particular interest to scientists as they try to understand why these failures occur and where they are going to occur. This information then becomes of interest to governments who are trying to promote their offshore resources, to industry who are trying to develop potential offshore resources, and to the communities who might be affected by the possible consequences, such as a tsunami created by a submarine landslide.

4.5.1: Hydrocarbon Exploration and Production Impacts

As the demand for hydrocarbons increases and exploration for these resources extends across the continental shelf into deeper water of continental slopes, the presence of MTDs further complicates an already difficult activity. In terms of exploration and production, MTDs have several issues: 1) their lithologic variability and associated range in sediment geotechnical properties create engineering constraints; 2) the potential of overpressures associated with these types of deposits; and 3) the recurrence of mass transport processes and slope stability of a region.

MTDs are typically composed of mixed lithologies, which make it difficult to predict how they will react when encountered during drilling of a well. Sand packages within these deposits can trap shallow gas and create the potential for a blowout during the

drilling of a well (Shipp and Gibson, 2009). If MTDs are more mud-dominated, then they may act as top and lateral seals for stratigraphic traps as suggested by Moscardelli et al., (2006) for offshore Trinidad and Venezuela. Also, if mud-dominated MTDs are located within reservoirs unit, they may act as baffles and further complicate the hydrocarbon recovery process and discovery of a field.

Thick successions of sediment dominated by MTDs can have interfingering, high density turbidite deposits and are typically overlooked as exploration targets. When this type of deposit is associated with salt diapirs, as seen in the Gulf of Mexico, sandy packages can be trapped and covered by MTDs, possibly creating a stack of target reservoir intervals (Adams and Schlager, 2000). Thick packages of MTDs with possible interbedded turbidites could be found in the “mini-basins” that form on the landward side of salt diapirs, as seen in the eastern lower slope of the southwestern Newfoundland margin (Fig. 4.2). MTDs can erode and limit the extension of turbiditic rich strata, reducing the potential size of reservoirs but they can also create significant accommodation space which typically will fill with sand rich sediments (Moscardelli et al., 2006; Armitage et al., 2010).

In areas where rapid sedimentation rates allow for the accumulation of thick packages of unconsolidated sediment, such as on glaciated margins (Peizhen et al., 2001) the potential to create fluid overpressures is possible (McAdoo et al., 2000). When these unconsolidated sediment packages are covered by MTDs, overpressures may build at the

base of the MTD. If these overpressures are unknown during the drilling of a well, then a blow out may occur which may have serious consequences.

In terms of exploration potential, MTDs appear to play a role in the re-distribution of sediments after their deposition. The presence of channels at the top of a MTD coupled with a thin preserved unit suggests that potential reservoir sediments may be transported further down slope by these channels than previously assumed. This suggests that exploration activities need to be pushed to deeper waters in areas with historic recurring sediment failures in order to investigate the potential of the lower slope.

Most MTDs consist of muddy deposits, but sandy MTDs are also common. It is estimated that at least 10% of MTDs are sand rich (> 20%) deposits making them potential reservoir units. Sand-dominated MTDs are typically thinner in scale compared to mud-dominated MTDs and they exhibit different reservoir geometries when compared to ponded turbidite deposits (Olson and Damuth, 2010). These sandy MTDs were encountered as producing targets in over 25 hydrocarbon fields world wide. In the Gulf of Mexico, sandy MTDs are identified in late Quaternary intraslope basins. This has important implications with respect to hydrocarbon exploration as these modern analogues imply that sandier MTDs may be present in deeper sections of the basin (Olson and Damuth, 2010). There is a possibility of sandy MTDs on the southwestern Newfoundland margin but without ground truthing, it is impossible to confirm.

If there is a concern of seafloor instability, avoiding areas with steep slopes generally reduces the risk imposed by seafloor instability. The rugose topography created by the remnants of a shallow MTD can create abrupt variations in the topography of the seafloor. This seafloor morphology can create difficulties for the hydrocarbon recovery operations and the positioning of subsurface infrastructure. Pipelines and telecommunications cables in a region with rugose topography should be re-routed through smooth topography.

4.5.2: Societal Impacts

The processes that occur 200 km offshore on continental margins are largely unknown to the majority of the population that inhabit coastal areas. They are unaware of the possible consequences of large scale events such as submarine landslides. The most important consequence of which coastal communities need to be aware is the possible formation of a tsunami due to a submarine landslide. Coastal communities of Atlantic Canada need to be particularly aware of this fact as the southwestern Newfoundland margin has a history of submarine landslides. The earthquake of November 18th, 1929 on the upper St. Pierre slope resulted in sediment slumping and a turbidity current that broke submarine cables for up to 13 hours after the earthquake. An estimated 150 to 200 km³ of sediment was transported to the Sohm Abyssal Plain with the turbidity current reaching velocities of 19 m/s (~68 km/h) with a duration of between 4 and 11 hours (Piper and Aksu, 1987). The initiation of this submarine landslide resulted in a tsunami which was the most catastrophic tsunami in Canadian history and claimed the lives of 27 people from the Burin Peninsula of Newfoundland (Doxsee, 1948; Heezen and Ewing, 1952). The

tsunami was observed along the Atlantic coast of North America with the maximum waves occurring on the coast of the Burin Inlet (Fig. 2). Tsunami heights ranged between 3 and 13 m on the southwestern Newfoundland coast where associated run-up distances were in the order of 1 km (Ruffman, 1997; Tuttle et al., 2004; Fine et al., 2005).

Chapter Five: Conclusions

The Cenozoic evolution of the southwestern Newfoundland margin documents periods of slope erosion linked to channel development and mass transport processes. A composite seismic stratigraphic framework derived from the Laurentian East 3D seismic volume and adjacent 2D seismic reflection data was completed for the southwestern Newfoundland slope. Five key seismic reflection events are recognized across the study area in the 3D and 2D data. These seismic reflection events are age-constrained for the last 65 Ma through biostratigraphic ties to industry wells on the adjacent shelf. The reflection events are top Cretaceous (**K99**), middle Oligocene (**O50**), late Miocene (**M70**), Middle Pleistocene (**Q50**) in age. Regional mapping within the southwestern Newfoundland slope reveals nine mass transport deposits (MTDs) that occur between the top Cretaceous and Middle Pleistocene. These MTDs are regionally extensive events that cover areas up to 900 km² and have volumes up to 225 km³. MTDs are identified by their incoherent and chaotic seismic character and are represented by failures which include rotated and deformed slump blocks, slides and debris flows.

During the Upper Cretaceous and early Paleocene, the upper slope of the southwestern Newfoundland margin experienced canyon incision (Fig. 4.1), likely in response to sealevel lowering (Miller et al., 2005). A significant shift in sedimentation style occurred on the margin during the Miocene where more constant, predictive sedimentation rates associated with sealevel fluctuations, were replaced with large scale, regionally extensive sediment failures. It was during late Miocene and Middle Pleistocene when high

sedimentation rates associated with periods of sealevel lowering deposited large amounts of sediments on the upper and middle slope (Fig. 1.4 and 4.2.4). In the late Miocene and early Pliocene, bottom water currents affected the southwestern Newfoundland slope which reworked bottom sediments and deposited seismic scale bedforms. Regionally extensive sediment failures became less frequent during the Lower-Middle Pleistocene as sedimentation styles changed once again on the margin in association with decreasing global sealevel. The onset of shelf-crossing glaciation began in the Middle-Upper Pleistocene and resulted in the deposition of 200 m of proglacial sediment on the continental margin. This stratigraphic section is represented by a mixed combination of turbidite deposits and thin, localized MTDs. Finally, the southwestern Newfoundland margin was incised by glacial melt waters which created the canyonized slope and dendritic ridges of the modern seafloor.

A significant proportion of the Cenozoic stratigraphy on the southwestern Newfoundland margin is composed of mass transport deposits, indicating that these processes are important mechanisms in the construction and evolution of the margin. Nine MTDs are identified between the top of a Cretaceous unconformity and the Middle Pleistocene section of the margin. MTDs represents between 30 - 40 % of the entire section and up to 60 % of the mid Miocene to recent section. Late Miocene MTDs are larger than Plio-Pleistocene MTDs, but the latter appear to be more frequent. Above the Middle Pleistocene marker, thin localized failures alternate with turbidite deposits and represent an additional 5 % of the sedimentary column. The preserved MTDs between **M70** and **Q50** correspond to a relatively thin section of stratigraphy for the 7 Ma it represents. The

presence of channel systems on the uppermost MTD suggests that between failures, sediment bypassed the mid slope via these channels and was deposited further downslope. This is an explanation for the minimal amount of sediment preserved during this time. The process of sediment mass failure on continental margins can represent a significant proportion of the sedimentary column and therefore should to be considered as a major component of sedimentation models for passive continental margins.

The southwestern Newfoundland margin has a history of large scale submarine landslides with one occurring during the late Miocene and the more recent 1929 Grand Banks Landslide. Both are of a similar size, moving $\sim 200 \text{ km}^3$ of sediment but are two different styles of failure. The late Miocene MTD is classified as a blocky debris flow and the 1929 failure is identified as a turbidity current, each representing opposite end members of sediment mass failure. This indicates that the conditions responsible for these distinctively different failures can occur on one margin and suggests that any style of failure is possible depending on the trigger mechanisms and pre-conditioning factors.

Triggering mechanisms responsible for submarine landslides are hard to pinpoint for a particular margin, let alone a particular failure. Historic earthquake data from the greater Laurentian Fan region demonstrate that the region is susceptible to increased levels of seismicity. The 1929 Grand Banks Landslide was clearly activated by a M7.2 earthquake that occurred in the area. Submarine landslides in the region were initiated by ground accelerations due to earthquakes. However, pre-conditioning factors are required to prepare the sediment for failure in the region and it is believed that these factors are

responsible for the areal and volumetric differences of MTDs on the southwestern Newfoundland margin. The preservation of MTDs across the Scotian and southwestern Newfoundland margin suggests that the distribution of seismicity across the eastern Canadian margin may be best described by the random seismicity model (random distribution) suggested by Basham et al. (1983) and Mazzotti (2007).

Mass transport deposits on the southwestern Newfoundland slope are serious geohazards for hydrocarbon exploration with the potential of blowouts associated with increased overpressure and trapped gas. Submarine landslides are a significant threat to coastal communities and could result in the initiation of a tsunami. The southwestern Newfoundland coast experienced a historic tsunami in 1929 (initiated by the Grand Banks Landslide) which devastated the Burin Peninsula. Today the effects of tsunamis could be far greater with increased population density and infrastructure amongst the coastal communities of Atlantic Canada.

Potential hydrocarbon exploration on the southwestern Newfoundland margin could use the preserved turbidite deposits as an analogue for deeper reservoir targets in the basin. These turbidite deposits are found interbedded within stacked MTDs and are typically preserved in “minibasins” associated with salt withdrawal. These deposits may be small but they could occur as several stacked reservoir targets. Another consideration is that some of the Cenozoic MTDs from the margin may be sand-rich deposits. This would suggest the possibility of sandier MTDs in the deeper basin which may have reservoir potential but this will remain unknown until the interval is sampled. One other potential

location for reservoir type sediments would be in deeper water on the lower slope. Evidence of channels on the top of Plio-Pleistocene MTDs suggests that sediment bypassed the middle slope through channels between failure events and was deposited further downslope.

In summary, mass transport processes on the southwestern Newfoundland margin are significant mechanisms for transporting large amounts of sediments (up to 225 km³) in the slope environment. These processes have greatly influenced the construction and the evolution of the margin since the Miocene and can represent as much as 60 % of the sedimentary column since the Cenozoic. Their initiation is linked to the increased levels of seismicity in the region where pre-conditioning factors such as, seaward dipping faults, sealevel lowering, high sedimentation rates, bottom currents, and over-steepening of sediments control the size of the failure. Finally, mass transport processes and their deposits can create implications for the development of offshore resources as well as impose a possible risk to the population of Atlantic Canada.

References

Adams, E. W., and Schlager, W., 2000. Basic Types of Submarine Slope Curvature. *Journal of Sedimentary Research*, **70**, no. 4, pp. 814-828.

Adams, J.A., 1986. Changing assessment of the seismic hazard along the southeastern Canadian margin. In: *Proc. Third Canadian Conference on Marine Geotechnical Engineering*, Vol. 1, pp. 42-53. St John's, Newfoundland.

Adams, J., and Atkinson, G. M., 2003. Development of seismic hazard maps for the 2005 National Building Code of Canada. *Can. J. Civil Eng.*, **30**, pp.255–271.

Armitage, D.A., Piper, D.J.W., McGee, D.T., and Morris, W.R., 2010. Turbidite deposition on the glacially influenced, canyon-dominated Southwest Grand Banks Slope, Canada. *Sedimentology*, pp. 1-22.

Basham, P.W., Adams, J., and Anglin, F.M., 1983. Earthquake source models for estimating seismic risk on the eastern Canadian continental margin. In: *Proc. Fourth Canadian Conference on Earthquake Engineering*, pp. 495-547. Vancouver, Canada.

Bent, A.L., 1995. A Complex Double-Couple Source Mechanism for the M7.2 1929 Grand Banks Earthquake. *Bulletin of Seismological Society of America*, **85**, No. 4, pp. 1003-1020.

Biscontin, G., Pestana, J. M., and Nadim, F., 2004. Seismic triggering of submarine slides in soft cohesive soil deposits. *Marine Geology*, **203**, pp. 341–354.

Brake, V.I., 2009. Evolution of an Oligocene Canyon System on the Eastern Scotian margin. Unpublished M.Sc. thesis, Dalhousie University, 126p.

Brown, A.R., 1999. Interpretation of three-dimensional seismic data, 5th edition. AAPG Memoir 42, Tulsa, Ok. pp.514

Brown, A.R., 2003. Interpretation of three dimensional seismic data. AAPG Memoir 42, SEG Investigations in Geophysics, No. 9: pp. 20-42.

Bryn, P., Solheim, A., Berg, K., Lien, R., Forsberg, C. F., Haflidason, H., Ottesen, D., and Rise, L., 2003. The Storegga slide complex: repeated large scale landsliding in response to climatic cyclicity. In, J. Locat and J. Mienert (Eds.), *Submarine mass movements and their consequences*, pp. 215–222. Dordrecht, Netherlands: Kluwer Academic Publishers.

Bull, S., Cartwright, J., and Huuse, M., 2009. A review of kinematic indicators from mass-transport complexes using 3D seismic data. *Marine and Petroleum Geology*, **26**, pp. 1132-1151.

Campbell, D.C., and Deptuck, M.E., In Press. Alternating bottom current dominated and gravity flow dominated deposition in a lower slope an rise setting – Insights from the seismic geomorphology of the western Scotian margin, Eastern Canada. SEPM Special Publication.

Campbell, D.C., Shimeld, J.W., Mosher, D.C., and Piper D.J.W., 2004. Relationships between sediment mass-failure modes and magnitudes in the evolution of the Scotian Slope, offshore Nova Scotia. Offshore Technology Conference Paper 16743, May, 2004 Houston, TX.

Cartwright, J.A., and Lonergan, L., 2003. Volumetric contraction during the compaction of mudrocks: a mechanism for the development of regional-scale polygonal fault systems. *Basin Research*, **8**, pp. 183-193.

Catuneanu, O., 2002. Sequence stratigraphy of clastic systems: concepts, merits, and pitfalls. *Journal of African Earth Sciences*, **35**, Issue 1, pp. 1-43.

Chopra, S., and Marfurt, K.j. (Ed.s). Seismic attribute for prospect identification and reservoir characterization. SEG, Tulsa, OK., pp. 464, 2007.

Claerbout, J.F. Fundamentals of geophysical data processing: with applications to petroleum prospecting. Palo Alto, California. Blackwell Scientific Publications. 1976.

Claerbout, J.F. Fundamentals of geophysical data processing: with applications to petroleum prospecting. Palo Alto, California. Blackwell Scientific Publications. 1985.

Cribb, J., 2009. The tectono-stratigraphic evolution and salt tectonic of the Laurentian sub-basin and it's deepwater extension, offshore NS. Unpublished M.Sc. thesis, Dalhousie University.

Deptuck, M.E., 2003. Post-rift geology of the Jeanne D'Arc Basin, with a focus on the architecture and evolution of early Paleogene submarine fans, and insights from modern deep-water systems. Unpublished Ph.D. thesis, Dalhousie University, pp. 369.

Dott, R.H., 1963. Dynamics of subaqueous gravity depositional processes. *AAPG Bulletin*, **47**, pp. 104-128.

Doxsee, W.W., 1948. The Grand Banks earthquake of November 18, 1929. *Publications Dominion Observatory, Canada* **7**, pp. 323-336.

Drake, C.L., and Burk, C.A. 1974. Geological significance of continental margins. In, C.A Burk and C.L. Drake (Eds.), *The Geology of Continental Margins*: New York, Springer-Verlag, pp. 3-10.

Fairbanks, R. F., 1989. A 17,000-year glacio-eustatic sea level record: influence of glacial melting rates on the Younger Dryas event and deep-ocean circulation. *Nature*, **342**, pp. 637-642.

Farre, J.A., McGregor, B.A., Ryan, W.B.F., and Robb, J.M., 1983. Breaching the shelfbreak; Passage from youthful to mature phase in submarine canyon evolution. In, D.J. Stanley and G.T. Moore (Eds.), *The shelfbreak: Critical interface on continental margins*, Society of Economic Paleontologists and Mineralogists Special Publication No. 33, pp. 25-39.

Fine, I.V., Rabinovich, A.B., Bornhold, B.D., Thomson, R.E., and Kulikov, E.A., 2005. The Grand Banks landslide-generated tsunami of November 18, 1929: preliminary analysis and numerical modeling. *Marine Geology*, **215**, pp. 45-57.

Frey Martinez, J., Cartwright, J., and James, D., 2006. Frontally confined versus frontally emergent submarine landslides: a 3D seismic characterisation. *Marine and Petroleum Geology*, **23**, pp. 585–604.

Garziglia, S., Migeon, S., Ducassou, E., Loncke, L., and Mascle, J., 2008. Mass-transport deposits on the Rosetta province (NW Nile deep-sea turbidite system, Egyptian margin): Characteristics, distribution, and potential causal processes. *Marine Geology*, **250**, pp. 180-198.

Gay, A., Lopez, M., Cochonat, P., and Sermondadaz, G., 2004. Polygonal faults-furrows system related to early stages of compaction – upper Miocene to recent sediments of the Lower Congo Basin. *Basin Research*, **16**, pp. 101-116.

Gradstein, F.M., Ogg, J.G., and Smith, A.G., 2004. *A Geologic Time Scale*. Cambridge University Press.

Haflidason, H., Sejrup, H.P., Nygard, A., Mienert, J., Bryn, P., Lien, R., Forsberg, C.F., Berg, K., and Masson, D., 2004. The Storegga Slide: architecture, geometry and slide development. *Marine Geology*, **213**, pp. 201-234.

Haq, B.U., Hardenbol, J. and Vail, P.R., 1987. Chronology of Fluctuating Sea Levels Since the Triassic. *Science*, **235**, pp.1156-1167.

Heezen, B.C., and Ewing, M., 1952. Turbidity currents and submarine slumps and the 1929 Grand Banks earthquake. *American Journal of Science*, **250**, pp. 849-873.

Hudec, M.R., Jackson, M.P.A., and Schultz-Ela, D.D., 2009. The paradox of minibasin subsidence into salt: Clues to the evolution of crustal basins. *GSA Bulletin*, **121**, pp. 201-221.

Hughes, T.J., 1998. *Ice Sheets*. Oxford University Press, Oxford, pp.343.

Imbo, Y., De Batist, M., Canals, M., Prieto, M.J., and Baraza, J., 2003. The Gebra Slide: a submarine slide on the Trinity Peninsula Margin, Antarctica. *Marine Geology*, **193**, pp. 235-252.

Jansa, L.F., and Wade, J.A., 1975a. Paleogeography and sedimentation in the Mesozoic and Cenozoic, southeastern Canada. In, C.J. Yorath, E.R. Parker, and D.J. Glass (Eds.), *Canada's Continental Margins and Offshore Petroleum Exploration*. Canadian Society of Petroleum Geologists, Memoir 4, pp. 79-102.

Jansa, L.F., and Wade, J.A., 1975b. Geology of the continental margin off Nova Scotia and Newfoundland. In, W.J.M. van der Linden and J.A. Wade (Eds.), *Offshore Geology of Eastern Canada, Volume 2, Regional Geology*. Geological Survey of Canada, Paper 74-30, **2**, pp. 51-106.

Jenner, K.A., Piper, D.J.W., Campbell, D.C., and Mosher, D.C., 2007. Lithofacies and origin of late Quaternary mass transport deposits in submarine canyons, central Scotian Slope, Canada. *Sedimentology*, **54**, pp. 19-38.

Khain, V.E., and Polyakova, I.D., 2004. Oil and Gas Potential of Deep- and Ultradeep-Water Zones of Continental Margins. *Lithology and Minerals Resources*, **39**, pp. 530-540.

Keen, C.E., Loncarevic, B.D., Reid, I., Woodside, J., Haworth, R.T., and Williams, H., 1990b. Tectonic and geophysical overview. In, M.J. Keen and G.L. Williams (Eds.), *Geology of the Continental Margin of Eastern Canada*. Geological Survey of Canada, *Geology of Canada*, no. 2, pp. 31-35.

Kidston, A., Brown, D., Alheim, B., and Smith, B., 2002. Hydrocarbon Potential of the Deep-Water Scotian Slope. Canada Nova Scotia Offshore Petroleum Board, Halifax, Nova Scotia, pp. 1-111

Kidston, A., Smith, B., Brown, D., Makrides, C., and Alheim, B., 2007. Nova Scotia Deepwater post-drill analysis 1982-2004. Canada Nova Scotia Offshore Petroleum Board, Halifax, Nova Scotia, pp. 1-181.

King, L.H., and Fader, G.B.J., 1986. Wisconsinan glaciation of the Atlantic continental shelf of southeast Canada. *Geological Survey of Canada, Bulletin* 363, 72.

King, L.H., and Fader, G.B.J., 1990. Late Wisconsinan ice sheet margins of the Laurentian Channel. Abstract, The Geological Society of America, Northeastern Section, 25th Annual Meeting, March 1990.

Knutz, P.C., and Cartwright, J., 2003. Seismic stratigraphy of the West Shetland Drift: Implications for later Neogene paleocirculation in the Faeroe-Shetland gateway. *Paleoceanography*, **18**, pp. 1-17.

Kominz, M. A., 1984. Oceanic ridge volumes and sea level change, An error analysis. In, J. Schlee (Eds.), *Interregional unconformities and hydrocarbon accumulation*. American Association of Petroleum Geologists, Memoir 36, pp. 109-127.

Ledger-Piercey, S., and Piper, D.J.W., 2005. Quaternary geology and seabed geohazards of the continental margin offshore Haddock Channel off southeast Newfoundland. Atlantic Geoscience Society, Annual Meeting 2005, Saint John, Program and Abstracts, pp. 28.

Lee HJ, Locat J, Desgagnes P, Parsons JD, McAdoo BG, Orange DL, Puig P, Wong FL, Dartnell P, and Boulanger E, 2007. Submarine mass movements on continental margins. In, C.A. Nittrouer, J.A. Austin, M.E. Field, J.H. Kravitz, J.P.M. Syvitski, and P.L. Wiberg (Eds.), *Continental Margin Sedimentation*. Special Publication Number 37 of International Association of Sedimentologists, pp. 213-274.

Locat, J., Martin, F., Levesque, C., Locat, P., Leroueil, S., Konrad, J.-M., Urgeles, R., Canals, M. and Duchesne, M. J., 2003. Submarine mass movements in the upper Saguenay Fjord (Quebec, Canada) triggered by an earthquake. In, J. Locat and J. Mienert (Eds.), *Submarine mass movements and their consequences*, pp. 509–519. Dordrecht, Netherlands: Kluwer Academic Publishers.

Louden, K., 2002. Tectonic Evolution of the East Coast of Canada. *CSEG Recorder*, pp. 37-48.

MacDonald, A.W., 2006. Cenozoic seismic stratigraphy of the central Nova Scotian continental margin: The interplay of erosion, deposition and salt tectonics. Unpublished M.Sc. thesis, Saint Mary's University, 152p.

MacLean, B.C., and Wade, J.A., 1992. Petroleum geology of the continental margin south of the islands of St Pierre and Miquelon, offshore eastern Canada. *Bulletin of Canadian Petroleum Geology*, **40**, pp. 222–253.

Marsters, J.C., 1986. Geotechnical analysis of sediments from the eastern Canadian Continental Slope, south of St. Pierre Ban. M.Eng. thesis, Technical University, Nova Scotia.

Masson, D.G., Canals, M., Alonso, B., Urgeles, R., and Huhnerbach, S., 1998. The Canary Debris Flow: source area morphology and failure mechanisms. *Sedimentology*, **45**, pp. 411-432.

Masson, D.G., Harbitz, C.B., Wynn, R. B., Pedersen, G., Lovholt, F., 2006. Submarine landslides: processes, triggers and hazard prediction. *Philosophical Transactions of The Royal Society A*, **364**, pp. 2009-2039.

Mazzotti, S., 2007. Geodynamic models for earthquake studies in intraplate North America. *The Geological Society of America Special Paper*, **425**, pp. 17-33.

- McAdoo, B., Pratson, G., Orange, L.F., 2000. Submarine Landslide Geomorphology, U.S. Continental Slope. *Marine Geology*, **169**, pp. 103-136.
- McIver, N.L., 1972. Mesozoic and Cenozoic stratigraphy of the Nova Scotia Shelf. *Canadian Journal of Earth Sciences*, **9**, pp. 54-70.
- Miller, K.G., Liu, C., and Feigenson, M., 1996. Oligocene to middle Miocene Sr-isotope stratigraphy of the New Jersey continental slope. *Proceedings of the Ocean Drilling Program, Scientific Results*. v. 150, pp. 97-114.
- Miller, K.G., Mountain, G.S., Browning, J.V., Kominz, M.A., Sugarman, P.J., Christie-Blick, N., Katz, M.E., and Wright, J.D., 1998. Cenozoic global sea level, sequences, and the New Jersey transect: Results from coastal plain and continental slope drilling. *Reviews of Geophysics*, **36**, pp. 569-601.
- Miller, K.G., Kominz, M.A., Browning, J.V., Wright, J.D., Mountain, G.S., Katz, M.E., Sugarman, P.J., Cramer, B.S., Christie-Blick, N and Pekar, S.F., 2005. The Phanerozoic record of global sea-level change. *Science*, **310**, pp. 1293-1298.
- Mitchum, R.M., Vail, P.R. and Sangree, J.B., 1977a. Seismic stratigraphy and global changes of sea level; Part 2, The depositional sequence as a basic unit for stratigraphic analysis. In, C.E. Payton (Eds.), *Seismic stratigraphy; applications to hydrocarbon exploration*. AAPG Memoir 26, Tulsa, Ok, pp. 53-62.
- Mitchum, R.M., Vail, P.R., and Sangree, J.B., 1977b. Seismic stratigraphy and global changes of sea level; Part 6, Stratigraphic interpretation of seismic reflection patterns and depositional sequences. In, C.E. Payton (Eds.), *Seismic stratigraphy; applications to hydrocarbon exploration*. AAPG Memoir 26, Tulsa, Ok, pp.117-133.
- Mitchum, R.M., 1977. Seismic stratigraphy and global changes of sea level; Part 11, Glossary of terms used in seismic stratigraphy. AAPG Memoir no. 26, Tulsa, OK, pp. 205-212.
- Moscardelli, L., and Wood, L., 2008. New classification system for mass transport complexes in offshore Trinidad. *Basin Research*, **20**, pp. 73–98.
- Moscardelli, L., Wood, L. and Mann, P. 2006. Mass-transport complexes and associated processes in the offshore area of Trinidad and Venezuela. *AAPG Bulletin*, **90** (7), pp.1059-1088.
- Mosher, D.C., Moran, K., and Hiscott, R.N., 1994. Late Quaternary sediment, sediment mass-flow processes and slope stability on the Scotian Slope. *Sedimentology*, **41**, pp. 1039–1061.

- Mosher D.C., Piper D.J.W., Campbell D.C., and Jenner K.A., 2004. Near surface geology and sediment-failure geohazards of the central Scotian Slope. AAPG Bulletin 88, pp. 705-723.
- Mosher, D., Bigg, S., and LaPierre, A., 2006. 3D seismic versus multibeam sonar seafloor surface renderings for geohazard assessment: Case examples from the central Scotian Slope. The Leading Edge, pp. 1484-1494.
- Mosher, D.C., and Piper, D.J.W., 2007. Analysis of Multibeam Seafloor Imagery of the Laurentian Fan and the 1929 Grand Banks Landslide Area. In, V. Lykousis, D. Sakellariou, and J. Locat (Eds.), Submarine Mass Movements and Their Consequences: 3rd International Symposium.. Springer Netherlands, pp. 77-88.
- Mosher, D.C., and West, M.T.N., 2007. CCGS Hudson 2007-020 Expedition Report, Argentina to Halifax, June 19 to July 3, 2007: Laurentian Fan and eastern Scotian Slope. Geological Survey of Canada, Open File 5668.
- Mosher, D.C., Xu, Z., and Shimeld, J., 2009. The Pliocene Shelburne Mass Movement and Consequent Tsunami, Western Scotian Slope. In, D.C. Mosher, R.C. Shipp, L. Moscardelli, J.D. Chaytor, C.D.P Baxter, H.J. Lee, R. Urgeles (Eds.), Submarine Mass Movements and Their Consequences: 4th International Symposium. Springer Netherlands, pp. 765-776.
- Mosher, D.C., Shipp, R.C., Moscardelli, L., Chaytor, J.D., Baxter, C.D.P, Lee, H.J., and Urgeles, R. (Eds.). Submarine Mass Movements and Their Consequences: 4th International Symposium, Springer, Netherlands, pp. 783, 2009.
- Mosher, D.C., MacKillop, K., Latour, V., Fenton, G., and Mitchelmore, P., 2010. Regional Slope Stability Assessment: Challenges in Spatial and Stratigraphic Geologic and Geotechnical Data Integration. Geological Survey of Canada Open File 6646.
- Mountain, G.S., 1987. Cenozoic margin construction and destruction offshore New Jersey. In, C. Ross and D. Haman (Eds.), Timing and depositional history of eustatic sequences: constraints on seismic stratigraphy. Cushman Foundation for Foraminiferal Research, Special Publication, **24**, pp. 57-83.
- Mountain, G.S., Miller, K.G., and Blum, P., 1994. Proc. ODP, Initial Reports 150. College Station, TX (Ocean Drilling Program), 885 pp.
- Mountain, G.S., Damuth, J.E., McHugh, C.M., Lorenzo, J.M., and Fulthorpe, C.S., 1996. Origin, re-burial and significance of mid-Miocene canyon, New Jersey continental slope. In, G.S. Mountain, K.G. Miller, P. Blum, C.W. Poag and D.C. Twichell (Eds.), Proceedings of the Ocean Drilling Program, Scientific Results, 150: College Station, Texas, Ocean Drilling Program, pp. 283-292.

- Mulder, T., and Moran, K., 1995. Relationship among submarine instabilities, sea level variations and the presence of an ice sheet on the continental shelf: An example from the Verrill Canyon area, Scotian Shelf. *Paleoceanography*, **10**, pp. 137–154.
- Mulder, R. and Cochonat, P., 1996. Classification of offshore mass movements. *Journal of Sedimentary Research*, **66**, pp. 43-57.
- Myers, R.A., and Piper, D.J.W., 1988. Seismic stratigraphy of late Cenozoic sediments in the northern Labrador Sea: a history of bottom circulation and glaciation. *Canadian Journal of Earth Sciences*, **22**, pp. 2059-2074.
- Nardin, T.R., Hein, E.J., Gorsline, D.S., and Edwards, B.D., 1979. A review of mass movement processes, sediment and acoustic characteristics, and contrasts in slope and base of slope systems versus canyon-fan-basin floor systems. In, L.J. Doyle and O.H. Pilkey (Eds.), *Geology of continental slopes*. Society of Economic Paleontologists and Mineralogists Special Publication 27, pp. 61-73.
- Olson, H.C., and Damuth, J.E., 2009. Character, Distribution and Timing of Latest Complexes on the Magdalena Deepwater Fan. In, D.C. Mosher, R.C. Shipp, L. Moscardelli, J.D. Chaytor, C.D.P Baxter, H.J. Lee, R. Urgeles (Eds.), *Submarine Mass Movements and Their Consequences: 4th International Symposium*. Springer Netherlands, pp. 607-617.
- Owen, M., Day, S., and Maslin, M., 2007. Late Pleistocene submarine mass movements: occurrences and causes. *Quaternary Science Reviews*, **26**, pp. 958-978.
- Peel, F.J., Travis, C.J., and Hossack, J.R., 1995. Genetic structural provinces and salt tectonics of the Cenozoic offshore U.S., Gulf of Mexico: a preliminary analysis. In, M.P.A. and S. Nelson (Eds.), *Salt Tectonics a global perspective*. AAPG Memoir 65, pp. 153-175.
- Peizhen, Z., Molnar, P., and Downs, W.R., 2001. Increased sedimentation rates and grain size 2-4 Myr ago due to the influence of climate change on erosion rates. *Nature*, **410**, pp. 891-897.
- Piper, D.J.W., 2005. Late Cenozoic evolution of the continental margin of eastern Canada. *Norwegian Journal of Geology*, **85**, pp. 231-244.
- Piper, D.J.W., and Aksu, A.E., 1987. The Source and Origin of the 1929 Grand Banks Turbidity Current Inferred from Sediment Budgets. *Geo-Marine Letters*, **7**, pp. 117-182.
- Piper, D. J. W., Cochonat, P., and Morrison, M. L., 1999. The sequence of events around the epicentre of the 1929 Grand Banks earthquake: Initiation of the debris flows and turbidity current inferred from side-scan sonar. *Sedimentology*, **46**, pp. 79– 97.

Piper, D.J.W., and McCall, C., 2003. A synthesis of the distribution of submarine mass movements on the eastern Canadian margin. In, J. Locat and J. Mienert (Eds.), *Submarine mass movements and their consequences*. Kluwer, Dordrecht, pp. 291-298.

Piper, D.J.W., and Gould, K., 2004. Late Quaternary geological history of the continental slope, South Whale Basin, and implications for hydrocarbon development. Geological Survey of Canada, Current Research. 2004-D01, pp. 9.

Piper, D.J.W., Macdonald, A.W.A., Ingram, S., Williams, G.L., and McCall, C., 2005. Late Cenozoic architecture of the St. Pierre Slope. *Canadian Journal of Earth Sciences*, **42**, pp. 1987-2000.

Piper, D.J.W., and Normark, W.R., 1982. Acoustic interpretation of Quaternary sedimentation and erosion on the channelled upper Laurentian Fan, Atlantic margin of Canada. *Canadian Journal of Earth Sciences*, **19**, pp. 1974-1984.

Piper, D.J.W., and Normark, W.R., 1989. Late Cenozoic sea-level changes and the onset of glaciation: impact on continental slope progradation off eastern Canada. *Marine and Petroleum Geology*, **6**, pp. 336-348.

Piper, D.J.W., Stow, D.A., and Normark, W.R., 1984. The Laurentian Fan: Sohm Abyssal Plain. *Geo-Marine Letters*, **3**, pp. 141-146.

Posamentier, H.W., and Allen, G.P. 1999. Fundamental concepts of sequence stratigraphy. In, R.W. Dalrymple (Eds). *Siliclastic sequence stratigraphy - concepts and applications*. SEPM special publications, Tulsa OK. pp. 9-51.

Praston, L.F., Ryan, W.B.F, Mountain, G.S., and Twichell, D.C., 1994. Submarine canyon initiation by downslope-eroding sediment flows; evidence in late Cenozoic strata on the New Jersey continental slope. *Geological Society of America Bulletin*, **106**, pp. 395-412.

Praston, L.F., Nittrouer, C.A., Wilberg, P.L., Steckler, M.S., Swenson, J.B., Cacchione, D.A., Karson, J.A., Murray, B., Wolinsky, M.A., Gerber, T.P., Mullenbach, B.L., Spinelli, G.A., Fulthorpe, C.S., O'Grady, D.B., Parker, G., Driscoll, N.W., Burger, R.L., Paola, C., Orange, D.L., Field, M.E., Friedrichs, C.T., Fedele, J.J., 2007. Seascapes evolution on clastic continental shelves and slopes. In, C.A. Nittrouer, J.A. Austin, M.E. Field, J.H. Kravitz, J.P.M. Syvitski, P.L. Wiberg (Eds.), *Continental margin sedimentation: from sediment transport to sequence stratigraphy*. Special publication 37 of the IAS, pp. 339-380.

Ruffman, A., 1997. Tsunami runup mapping as an emergency preparedness planning tool: the 1929 tsunami in St. Lawrence, Newfoundland. Geomarine Associates, Contract Report for Emergency Preparedness Canada (EPC), Ottawa, Ontario, Vol. 1, 107 pp.

Sangree, J.B., and Widmier, J.M., 1977. Seismic stratigraphy and global changes of sea level; Part 9, Seismic interpretation of clastic depositional facies. In, C.E. Payton (Eds.),

Seismic stratigraphy; applications to hydrocarbon exploration. AAPG Memoir no. 26, Tulsa, Ok, pp165-184.

Sangree, J.B., and Widmier, J.M., 1979. Interpretation of depositional facies from seismic data. *Geophysics*, **44**, pp. 131-160.

Schwab, W.C., and Lee, H.J., 1988. Causes of two slope-failure types in continental-shelf sediment, northeastern Gulf of Alaska. *Journal of Sedimentary Petrology*, **58**, pp 1-11.

Shaw, J., Gareau, P., and Courtney, R.C., 2002. Palaeogeography of Atlantic Canada 1-0 ka. *Quaternary Science Reviews*, **21**, pp. 1863-1880.

Shaw, J., Piper, D.J.W., Fader, G.B.J., King, E.L., Todd, T., Bell, T., Batterson, M.J., and Liverman, D.G.E., 2006. A conceptual model of the deglaciation of Atlantic Canada. *Quaternary Science Reviews*, **25**, pp. 2059-2081.

Sheriff, R.E., and Geldart, L.P., 1995. *Exploration Seismology*. Cambridge University Press, Cambridge.

Sheriff, R.E., 2002. *Encyclopaedic Dictionary of Exploration Geophysics*, 4th edition. SEG, Tulsa, 376p.

Shimeld, J., 2004. A comparison of salt tectonic subprovinces beneath the Scotian Slope and Laurentian Fan. In, *Salt-Sediment Interactions and Hydrocarbon Prospectivity: Concepts, Applications, and Case Studies for the 21st Century*. Gulf Coast Section of the Society of Economic Paleontologists and Mineralogists, 24th Annual Bob F. Perkins Research Conference, extended abstracts volume, Houston.

Shimeld, J.W., Warren, S.N., Mosher, D.C., and MacRae, R.A., 2003. Tertiary-aged megaslumps under the Scotian Slope, south of the LaHave Platform, offshore Nova Scotia. In: *Joint Meet, Program with Abstr., Geol Soc Am (NE Sect) and the Atl. Geosci. Soc.*, Halifax, Nova Scotia.

Shipp, R.C., and Gibson, J.L., 2009. Impact of Submarine Mass Movement on Deepwater Operations and Development Infrastructure in the Offshore Energy Industry: What Really Are the Issues?. *4th International Symposium on Submarine Mass Movements and Their Consequences*. Austin, Texas, Nov. 11-14.

Skene, K.I., 1998. Architecture of submarine channel levees. Unpublished Ph.D. thesis, Dalhousie University, Halifax, Nova Scotia, pp. 365.

Skene K.I., and Piper D.J.W., 2003. Late Quaternary stratigraphy of Laurentian Fan: a record of events off the eastern Canadian continental margin during the last deglacial period. *Quaternary International*, **99-100**, pp. 135-152.

- Skene, K.I., and Piper, D.J.W., 2006. Late Cenozoic evolution of Laurentian Fan: Development of a glacially fed submarine fan. *Marine Geology*, **227**, pp. 67-92.
- Stoker, M.S., Pheasant, J.B., and Josenans, H., 1997. Seismic methods and interpretation. In, T.A. Davies, T. Bell, A.K. Cooper, H. Josenans, L. Polyak, A. Solheim, M.S. Stoker, J.A. Stravers (Eds.), *Glaciated Continental margins: An atlas of acoustic images*, pp. 9-19.
- Sultan, N., Cochonat, P., Canals, M., Cattaneo, A., Dennielou, B., Haflidason, H., Laberg, J.S., Long, D., Mienert, J., Trincardi, F., Urgeles, R., Vorren, T., and Wilson, C., 2004. Triggering mechanisms of slope instability processes and sediment failures on continental margins: a geotechnical approach. *Marine Geology*, **213**, pp. 291– 321.
- Tuttle, M.P., Ruffman, A., Anderson, T., and Jeter, H., 2004. Distinguishing Tsunami from Storm Deposits in Eastern North America: The 1929 Grand Banks Tsunami versus the 1991 Halloween Storm. *Seismological Research Letters*, **75**, pp. 117-131.
- Uchupi, E., and Austin, J., 1979. The stratigraphy and structure of the Laurentian cone region. *Canadian Journal of Earth Sciences*, **16**, pp. 1726-1752.
- Vail, P.R., Mitchum, R.M., Todd, Jr., R.G., Widmier, J.M., Thompson, S., III, and Sangree, J.B. 1977. Seismic stratigraphy and global changes of sea level. In, C.E. Payton (Eds.). *Seismic stratigraphy-applications to hydrocarbon exploration*, American Association of Petroleum Geologist Memoir 26, pp. 49–212 Tulsa.
- Vanneste, M., Mienert, J., and Bünz, S., 2006. The Hinlopen Slide: A giant, submarine slope failure on the northern Svalbard margin, Arctic Ocean. *Earth and Planetary Sciences Letters*, **245**, pp. 373-388.
- Veeken, P.C.H., 2007. Seismic Stratigraphy, basin analysis and reservoir characterization. In, K. Helbig and S. Treitel (Eds.), *Handbook of geophysical exploration*, **37**, 487p.
- Verhoef, J. and Jackson, H.R., 1991. Admittance signatures of rifted and transform margins: examples from eastern Canada. *Geophysical Journal International*, **105**, pp. 229-39.
- Wade, J.A. and MacLean, B.C., 1990. The Geology of the Southeastern Margin of Canada. In, M.J. Keen and G.L. Williams (Eds.), *Geology of the Continental Margin of Eastern Canada*, Geological Survey of Canada, *Geology of Canada*, no. 2, pp. 190-238.
- Wade, J.A., MacLean, B.C., and Williams, G.L., 1995. Mesozoic and Cenozoic stratigraphy, eastern Scotian Shelf: new interpretations. *Canadian Journal of Earth Sciences*, **32**, pp. 1462-1473.

Weimer, P., and Slatt, R.M, 2006. Introduction to the petroleum geology of deepwater settings. AAPG Studies in Geology, **57**, pp. 781.

Wielens, H.J.B.W., Jauer ,C., and Williams, G.L., 2004. Is there a viable petroleum system in the Carson and Salar basins, offshore Newfoundland?. Journal of Petroleum Geology, **29** (4), pp. 303–326.

Wright, S.G., and Rathje, E.M., 2003. Triggering Mechanisms of Slope Instability and their Relationship to Earthquakes and Tsunamis. Pure Applied Geophysics, **160**, pp. 1865-1877.

Yilmaz O., 1987. Seismic Data Processing, Society of Exploration Geophysicists, Investigations in geophysics No. 2, Tulsa, Society of Exploration Geophysicists, 529p.

Yilmaz, O., 2001. Seismic Data Analysis, Volumes 1 and 2. Society of Exploration Geophysicists, Investigations in geophysics No. 10, Tulsa, Society of Exploration Geophysicists, 2027p.

Zachos, J.C., Pagani, M., Sloan, L., Thomas, E., and Billups, K., 2001. Trends, rhythms, and abbreviations in global climate 65 Ma to present. Science, **292**, pp. 686-693.

